ELECTROKINETIC PROPERTIES AND CONDUCTANCE RELAXATION OF POLYSTYRENE AND SILVER IODIDE PLUGS

Promotor: dr. B.H. Bijsterbosch,
hoogleraar in de fysische en kolloïdchemie.

Th.J.J. van den Hoven

ELECTROKINETIC PROPERTIES AND CONDUCTANCE RELAXATION OF POLYSTYRENE AND SILVER IODIDE PLUGS

Proefschrift
ter verkrijging van de graad van
doctor in de landbouwwetenschappen,
op gezag van de rector magnificus,
dr. C.C. Oosterlee,
in het openbaar te verdedigen
op woensdag 7 november 1984
des namiddags te vier uur in de aula
van de Landbouwhogeschool te Wageningen

STELLINGEN

1. Ten onrechte is in Nederland tot nog toe voorbijgegaan aan de mogelijkheid van fosfaatdosering om de opname van metalen in drinkwater vanuit het leidingnet terug te dringen.

2. De normstelling die in het Waterleidingbesluit is vastgelegd voor het loodgehalte van drinkwater is, gezien de voorgeschreven bemonsteringsprocedure, als toetssteen voor de kwaliteit van drinkwater van twijfelachtige betekenis.

   Waterleidingbesluit, Stb. 1984, 220.

3. De chloordosis die de VEWIN aanbeveelt voor de ontsmetting van nieuw gelegde en gerepareerde drinkwaterleidingen kan aanzienlijk verlaagd worden door ook de pH en het bufferend vermogen van de ontsmettingsvloeistof voor te schrijven; op deze wijze kan een onnodige belasting van het milieu met chloor worden voorkomen.

   VEWIN Aanbevelingen 1960.

4. Elektrokinetische metingen aan geconcentreerde systemen kunnen aanzienlijk beïnvloed worden door polarisatieprocessen aan de meetelektroden en in het onderzochte systeem. Een vier-elektroden cel, waarin platina zwart elektroden zijn opgenomen, is uitermate geschikt om voor deze invloeden te corrigeren.

   Dit proefschrift, hoofdstuk 3.

5. Elektrokinetische en elektrische metingen aan geconcentreerde dispersies van polymeerkolloïden verschaffen niet alleen informatie over de elektrische dubbellaag aan het vast-vloeistof grensvlak, maar ook over de oppervlaktestructuur van de vaste fase.

   Dit proefschrift, hoofdstuk 5 en 6.

6. Het oppervlak van in water gesuspendeerde polystyreendeeltjes is "harig". De harigheid wordt onderdrukt door adsorptie van tetraalkylammonium ionen en laagmoleculair polylysine.

Dit proefschrift, hoofdstuk 6.
Van den Hoven, Th.J.J., niet gepubliceerde resultaten.

7. De onzekerheden rondom het specifiek oppervlak van zilverjodide zijn een modelsysteem onwaardig.

8. Omdat Greenstock en Ruddock zich er niet van bewust zijn dat methylviologeen en paraquat verschillende benamingen voor dezelfde stof zijn, bieden zij de lezer de uitzonderlijke mogelijkheid om de door hen opgegeven nauwkeurigheid van hun experimenten te verifiëren; er blijkt van een ruime overschatting sprake te zijn.

Greenstock, C.L. en Ruddock, G.W., Biochim. Biophys. Acta 383, 464 (1975).

9. De aannamen van Trivedi et al. bij de polarografische bepaling van de fractie gebonden cadmium ionen in cadmiumcarboxymethylcellulose, dat alleen de vrije cadmium ionen bijdragen aan de diffusiestroom én dat de evenwichtsinstelling snel is, zijn strijdig.

Trivedi, H.C., Patel, C.P., Patel, C.K. en Patel, R.D., Angew. Makromol. Chemie 70, 39 (1978).

10. De veronderstelling van Detellier en Villemure dat de maximale adsorptie van methylviologeen op montmorilloniet klei bepaald wordt door geometrische factoren, is onjuist.

Detellier, C. en Villemure, G., Inorg. Chim. Acta 86, L19 (1984).
Hayes, M.H.B., Pick, M.E. en Toms, B.A., J. Colloid Interface Sci. 65, 254 (1978).

11. Gewetensbezwaarden die voor hun tewerkstelling een baan in het verlengde van hun opleiding accepteren, maken zich schuldig aan concurrentievervalsing op de arbeidsmarkt en zouden daarom een bezwaard geweten moeten krijgen.

12. Het behoort tot de taak van de inspectie van het onderwijs erop toe te zien dat in de toekomstige basisschool de verworvenheden van het kleuteronderwijs behouden blijven.

Projectgroep Leerplanontwikkeling Basisschool,
Kleuteronderwijs: Een Overzicht, SLO Enschede, 1981.

Proefschrift Th.J.J. van den Hoven
Electrokinetic properties and conductance relaxation of polystyrene and silver iodide plugs.
Wageningen, 7 november 1984.

Voor mijn ouders
Voor Elly

CONTENTS

CHAPTER 1

INTRODUCTION

1.1 GENERAL BACKGROUND AND PURPOSE OF THIS STUDY

Electrokinetics is the domain of science that deals with those transport phenomena in which two phases are displaced with respect to each other. In general, one phase is a fluid and the other a solid. It is essential that their interface is electrified. The displacement may arise either from the application of an electrical or of a mechanical force. An example of the first kind is electrophoresis, which is the movement of charged particles through a stationary solution due to an imposed electrical field; a representative of the second group is the streaming potential which develops when a fluid is forced through a charged capillary or porous medium by an external pressure difference.

In technology (1,2) as well as in fundamental sciences (2,3) electrokinetic phenomena have received considerable attention. They find their application in e.g. painting processes, in the isolation of biological materials, in the drying of concrete and in the dewatering of clays. In colloid science electrokinetic techniques are frequently made use of to investigate the electrical state of solid-liquid interfaces. More often than not, such an interface is the site of an electrical double layer, consisting of a layer of charged species at the solid surface and a layer of diffusely distributed ionic charges in the solution. For the understanding of the behaviour of many model as well as practical systems, knowledge about the details of such an electrical double layer is of major importance. Merely the sign of the charge, e.g., may determine whether or not dissolved charged species adsorb onto the solid phase. The charge on the particles in a dispersion is also one of the major factors determining the interaction between the particles and, consequently, their stability against aggregation. Both aspects play a role in water purification processes, where chemicals are used to promote the coagulation of finely dispersed matter like algae and clay particles. In some cases electrokinetic techniques have proved to be useful in the control of the dosage of these

chemicals (4).

An important concept in the analysis of electrokinetic phenomena is the slipping plane, being the imaginary dividing plane between the liquid firmly adhering to the solid surface and the "free-flowing" bulk solution. Determinative for electrokinetic effects is the charge density or the electrical potential at this slipping plane. This potential is called the zeta potential. In general, the electrokinetic and surface charge density are not identical, because the slipping plane does not coincide with the solid surface. On surveying the literature, it is found that large uncertainties exist as to the exact position of the slipping plane and, consequently, about the significance of the zeta potential. The fact that many studies have been carried out with ill-defined systems and/or improper measuring techniques has contributed to this confusion.

Because of the presence of the electrical double layer, the electrolyte solution near the solid has a composition different from that beyond the double layer region. As a consequence its electrical conductance is different (usually higher). This peculiar phenomenon is referred to as surface conductance. If the slipping plane and the solid surface do not coincide, the interjacent immobile solvent layer may also contribute to this phenomenon. This does not necessarily imply a negative contribution. It is conceivable, e.g., that the ions in this hydrodynamically immobile layer retain their electrical mobility. If so, surface conductance measurements may give an indication of the structure of this part of the double layer. Therefore the combination of electrokinetic and conductance measurements enables information to be obtained on the charge distribution across the entire interfacial region and on the location of the slipping plane. Clarification of this approach is the main purpose of this thesis.

The most widely used technique for measuring zeta potentials is electrophoresis. This technique is easily applicable, particularly so because measuring devices are commercially available. A serious drawback of electrophoresis, however, is that the material under investigation must be present as a stable, rather dilute disper-

sion. This requirement precludes application to numerous important systems, like membranes, fibres and colloidal dispersions close to conditions of coagulation (e.g. near the point of zero charge or at high salt concentrations). In those cases measurements on condensed systems have to be performed, calling for the streaming potential and streaming current technique. Clarifying the advantages of these electrokinetic methods is also essential in this work.

In practice there are a number of complications associated with electrokinetic and conductance measurements on concentrated systems, that, if ignored, may easily lead to erroneous zeta potentials and surface conductivities. The best known example is electrode polarization and several procedures have been suggested to correct for its interference in conductance measurements (5). One of these correction methods, the four electrode technique, has recently been introduced by Van der Put and Bijsterbosch (6) to eliminate electrode polarization effects in streaming current experiments. This technique also enables correction for the influence of polarization phenomena occurring in the studied system itself. These so-called intrinsic polarizations have rarely been referred to in existing literature.

The purpose of the present work is

(i) to study the characteristics of the four electrode cell for different types of electrodes, in order to devise optimum experimental procedures that account for phenomena which may interfere in electrokinetic measurements on condensed systems.

(ii) To study the intrinsic polarizations by measuring the variation of the conductance in the low frequency range.

(iii) To investigate the double layer structure of a number of well-defined colloidal systems by applying the now well-established electrokinetic and electrical techniques.

In the course of this study, it became apparent that the intrinsic polarization phenomena provide insight into the surface structure of polymer colloids. This feature led us to investigate the impact of adsorbing species on this structure, since in literature minimal attention has been paid to this aspect.

1.2 SYSTEMS USED AND OUTLINE OF THE INVESTIGATION

For the present study we chose concentrated polystyrene and silver iodide dispersions as the model systems to be investigated. These substances represent two widely used, but strongly differing groups of colloidal systems.

Polystyrene latices belong to the class of polymer colloids. An attractive feature of these colloids is that dispersions of spherical, monodisperse particles can be readily obtained. These properties are very convenient in the theoretical analysis of electrokinetic and electroconduction data, because the most sophisticated theories have been formulated for this geometry. Another important advantage is, that the density of the charged groups at the surface is independent of ionic strength. A drawback is that uncertainties exist about their chemical surface properties (7). Therefore we decided to pay special attention to this aspect.

Silver iodide is an inorganic colloid, that has been extensively studied. As a consequence, its surface properties are known in great detail (8). An important advantage of the silver iodide system is that the surface potential and, for that matter, the surface charge density can be readily varied over a large range of both positive and negative values. A drawback is that in general the particles are not spherical and the dispersions heterodisperse.

Tetraalkylammonium ions were chosen as the substances to be adsorbed in the adsorption experiments. The motives for this choice are discussed in chapter 6.

The study was initiated with the preparation and characterization of polystyrene latices. Attention was focussed on the influence purification procedures, electrokinetic experiments and storage may exert on their surface characteristics. This matter is dealt with in chapter 2. Chapter 3 reports the experiments with the four electrode cell. The numerous disturbing phenomena that may occur in electrokinetic and conductance measurements on condensed systems are discussed and a generally applicable method to correct for their effect is presented. Chapter 4 concerns the theoretical models that have been used for the calculation of zeta potentials

and surface conductivities. Chapters 5 and 6 describe the experiments with the polystyrene plugs. In chapter 5 special attention is paid to the intrinsic polarization phenomena. The results are interpreted in terms of a special structure of the polystyrene surface. In chapter 6 the influence of adsorbed tetraalkylammonium ions on the surface structure is examined. This comprises electrokinetic, a.c. conductance and adsorption measurements. Chapter 7 deals with the experiments on silver iodide plugs. The results demonstrate the general applicability of the techniques developed in this work. Moreover, they reveal a number of peculiar features of the silver iodide-aqueous solution interface.

1.3 REFERENCES

1. See e.g. Kaden, H. and Jacobasch, H.J., Wissenschaft und fortschritt 29, 178 (1979).
2. Hunter, R.J. in "Colloid Science" (R.H. Ottewill and R.L. Rowell, Eds.), Vol. 2, Academic Press, London, 1981.
3. Dukhin, S.S. and Derjaguin, B.V. in "Surface and Colloid Science" (E. Matijević, Ed.), Vol. 7, Wiley, New York, 1974.
4. Converse, C.W. and Colas, E., Eau, Industrie, Nuisances 73, 33 (1983).
5. Schwan, H.P., Biophysik 3, 181 (1966).
6. Van der Put, A.G. and Bijsterbosch, B.H., Acta Polym. 32, 311 (1981).
7. Hearn, J., Wilkinson, M.C. and Goodall, A.R., Adv. Colloid Interface Sci. 14, 173 (1981).
8. Bijsterbosch, B.H. and Lyklema, J. Adv. Colloid Interface Sci. 9, 147 (1978).

CHAPTER 2

ADVANTAGES AND DISADVANTAGES OF POLYSTYRENE LATEX AS A MODEL COLLOID

2.1 INTRODUCTION

The use of monodisperse spherical polystyrene latices as model colloids in electrokinetic investigations is very appealing. Their geometry, e.g., enables the application of models, that describe the influence of various types of polarization on the electrokinetic parameters in great detail (chapter 4).

Since recipes for the preparation of homodisperse polymer latices have been available for over twenty years, their use as colloidal systems was promoted in many divergent studies. In effect, they quantitatively outstripped the classical sols (like silver iodide), which are usually not monodisperse and not made up of spherical particles (1,2,3). Despite much fundamental research, however, the surface characteristics of polystyrene latices have proven to be much more difficult to control than in the classical systems. For instance, different investigators, although using similar recipes, have observed the occurrence of different surface groups (4). In addition, changes in the number and the nature of those groups upon cleaning and storage have been reported. An excellent review concerning these issues has recently been published by Hearn et al. (2).

The major part of the electrokinetic study described in this thesis was carried out with polystyrene latices prepared according to the emulsifier-free recipe of Furusawa et al. (5). It is the purpose of this chapter to investigate the reproducibility of preparing these latices and to assess possible effects of cleaning methods, storage and electrokinetic experiments on their properties. In particular attention is paid to the effect of contacting these latices with a solution of high ionic strength. In agreement with the observations of Van der Put (6) preliminary electrokinetic experiments indicated that such a treatment causes the surface charge density to increase. Following these investigations methods are developed so as to minimize the effects of "non-idealities" on

the electrokinetic experiments.

2.2 EXPERIMENTAL

2.2.1 PREPARATION

Emulsifier-free polystyrene latices were prepared according to the method of Furusawa et al. (5). Essentially a portion of the styrene monomer, distilled under nitrogen just prior to use, and an aqueous buffer ($KHCO_3$ or KH_2PO_4) solution were mixed and saturated with nitrogen in a bottle at 70 °C. The buffer was added in order to suppress the formation of surface hydroxyl groups during the polymerization (2). The reaction was subsequently started by adding a nitrogen-saturated $K_2S_2O_8$ solution. A more detailed description of the Furusawa method has been given by Norde (7).

Within each run four batches of about 0.2 l were prepared simultaneously. Batches with particles differing less than circa 1 % in diameter (as inferred from electronmicroscopy) were mixed prior to purification.

2.2.2 PURIFICATION

In order to remove unreacted monomer, impurities formed during the polymerization and electrolytes, the latices have been steam stripped and subsequently ion exchanged. Dialysis (7) was not efficient enough as became apparent from the results of adsorption measurements (chapter 6). In the course of these measurements, blank experiments were performed, in which a dye was added to the filtrate of dialyzed samples. Chloroform extraction of these solutions revealed the presence of impurities, complexing with the dye (for more information see section 6.2.2.1). Such impurities were absent in the filtrate of steam stripped latices. The inefficiency of the dialysis could also be inferred from the typical styrene-like odour, which was retained in the latices even after dialysis periods of months. Freshly steam stripped latices were always odourless. Incomplete removal of reactants and by-products by dialysis has also been reported by others (8,9,10). These publications provide strong evidence that steam stripping is much more

effective, in agreement with our observations.

Another drawback of dialysis may be that protracted periods of contact with the dialysis tubing can cause contamination of the latex (e.g. 11).

Steam stripping was performed at reduced pressure (ca 2.5 kPa) and temperature (ca 40 °C) in order to minimize the rate of hydrolysis of sulfate groups, which strongly increases with increasing temperature (8,12). The steam stripping was continued until the distillate did not show U.V. absorption in the range 150-200 nm any more and the latex had become odourless. Usually a twenty-fold excess of water was needed.

Generally, after storing a steam stripped latex for a few months, styrene could be smelled again. Probably this stems from monomer occluded by the inner core of the particles and diffusing slowly into the aqueous phase. Therefore, all samples were steam stripped shortly before use.

Ion exchange was performed with a mixed bed, consisting of a Dowex 50W-X4 cation resin and a Dowex 1-X4 anion resin. Prior to use each resin was extensively purified according to the method of Van den Hul and Vanderhoff (13). The efficiency of this purification method was checked by measuring the conductance, surface tension and U.V. absorption of the water equilibrated with the resins. All latex samples were ion exchanged three times with a more than three fold excess of mixed resin.

2.2.3 CHARACTERIZATION

Analysis of the number and type of surface groups was performed by conductometric titration of 20 ml of the latex samples in the H^+-form (solid content 1-7 % w/w) in a nitrogen atmosphere. A double-walled cell, thermostated at 20 °C, was used. Standardized NaOH solution was added with an Agla micrometer syringe. The conductivity was measured with a Philips conductance cell, PW 9501, using a Wayne-Kerr universal bridge, B224 (at 1592 Hz).

Particle sizes were determined by transmission electron microscopy with a Philips EM 300 apparatus. Each series of fotographs at a certain magnification included a carbon grating with exactly known dimensions, serving as a reference. On average about thirty

particles were measured per sample.

2.2.4 SURVEY OF EXPERIMENTS

1. Attention was paid to the reproducibility of latex preparation with respect to number and nature of the surface groups and the particle size. Variations between as well as within runs were considered.
2. It was investigated whether the employed purification methods affected the number and nature of the surface groups and the particle dimensions.
3. Electrokinetic studies on condensed systems include the determination of the conductometric cell constant (chapter 4), an investigation requiring a high ionic strength. Preliminary electrokinetic experiments showed an irreversible increase of the surface conductivity and, to a lesser extent, the zeta potential upon first contact of a polystyrene plug with a solution of high salt content (10^{-1} M). Similar observations have been made by Van der Put (6). These phenomena suggest an irreversible increase of the number of surface groups. Obviously, the best way to verify this hypothesis is by conductometric titration. This was accomplished according to the following experimental scheme

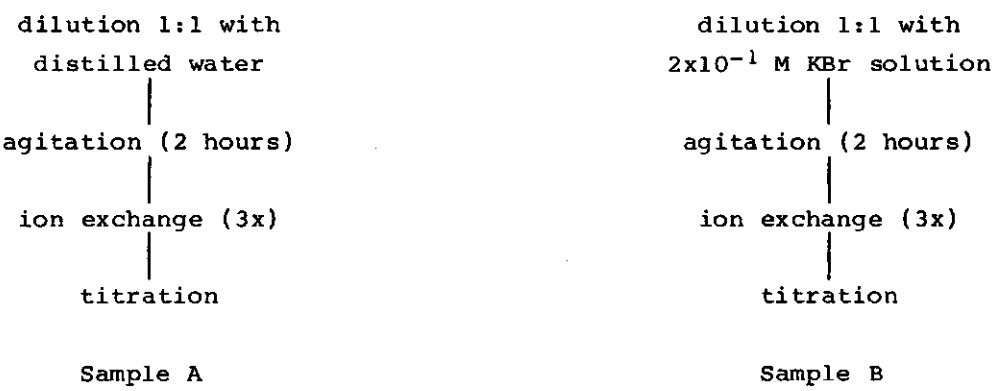

The polystyrene sample N was prepared according to the B1 recipe mentioned in reference 5.

Both samples were diluted to an equal extent in order to avoid any effect of differences in solid content on the shape of the titration curves (10).

4. Electrokinetic experiments are rather time-consuming. Therefore constancy of latex properties over periods of several months is required. Attention was paid to this requirement and some efforts have been made to specify the optimum conditions of storage.

2.3 RESULTS AND DISCUSSION

2.3.1 REPRODUCIBILITY OF PREPARATION

Although Norde (7) reported that the Furusawa method yields reproducible latices, we observed that repeated application of the same recipe did not produce latices with the same characteristics. In particular, rather large variations were observed in the number of surface groups per unit area. By way of illustration the characteristics of four batches, prepared simultaneously within one run according to the B1 recipe of Furusawa et al. (5) are given in table 2.1. The titration curves of all samples indicated the presence of only strong acidic groups.

Table 2.1 - Characteristics of four latex samples, prepared simultaneously within one run.

Sample code	σ_0*(mC/m^2)	d (nm)	
		before i.e.	after i.e.
M_1	29.9	591 ± 1	578 ± 2
M_2	21.7	581 ± 1	540 ± 2
M_3	62.1	591 ± 1	582 ± 3
M_4	58.8	613 ± 2	596 ± 2

* Only strong acidic groups.

With regard to the particle diameter d, the batches coincide much better than with respect to their charge density σ_0. Nevertheless it follows from table 2.1 that mixing the four batches of one run may lower the degree of monodispersity. The variations among different runs showed a similar trend.

Additional experiments showed that neither the number of ion exchange treatments nor the steam stripping process affected σ_0 significantly. Since, moreover, the titrations appeared to be reproducible (better than about 95 %), the observed variations can probably be ascribed to subtle differences in the preparation procedure. Standardization of the addition of the reactants may possibly lead to improvements.

In conclusion it must be stated, that assessment of the surface charge density solely on the basis of the employed recipe is not possible.

2.3.2 *EFFECT OF ION EXCHANGE ON THE PARTICLE SIZE*

Ion exchange resulted in a small but significant decrease in the mean particle diameter, as shown in table 2.1. Over all studied samples the decrease varied from 1 to 7 %, the mean reduction being 3.9 %. Several explanations for this observation can be suggested:

1. preferential adsorption of the bigger particles onto the resins (fractionation). In view of the high degree of monodispersity, however, this supposition is not very likely.
2. Shrinkage of the particles during exposure to the electron beam. Although this cannot be entirely excluded, it is unlikely that ion exchange enhances the susceptibility of the latices to deformation by the electron beam.
3. Diffusion of unreacted monomer out of the particles as a result of osmotic suction by the resins. This possibility finds support in the observation of Goodwin et al. (9) that ion exchanged latices swell considerably when contacting them with their own monomer.
4. Rearrangement of polystyrene chains in the surface region, induced by the resins and leading to a more compact structure of the particles.
5. Desorption of material from the surface of the polystyrene

particles. This phenomenon was suggested by Furusawa et al. (5) in order to explain the decrease in sulfur content upon ion exchange. This loss of sulfur was determined by X-ray fluorescens and varied from about 15 to 30 %. Assuming a homogeneous distribution of sulfate groups over the core of the particles, these losses would correspond to a reduction in the particle diameter of 5 to 11 %. In reality, however, the reduction will be less, as the sulfates will be predominantly located close to the surface, due to their hydrophilic character. Moreover, the loss of sulfur may also result from hydrolysis of the sulfate groups (see section 2.3.3).

As it is beyond the scope of this thesis, gaining further insight into the mechanism of particle size reduction has not been further pursued.

According to Bonekamp (14), ion exchange does not have an appreciable effect on the surface charge density. He arrived at this conclusion from the observation that the adsorption of polylysine onto polystyrene latex, being sensitive to σ_0, did not change by ion exchanging the latex.

The steam stripping process employed did not affect either the particle dimensions or the number and type of surface groups.

2.3.3 EFFECT OF ELECTROLYTE TREATMENT; CHARGING PHENOMENON

The conductometric titration curves of the untreated and treated sample are shown in Fig. 2.1 (curves A and B, respectively). The solid content of sample A was 2.82 % w/w, that of sample B 2.56 % w/w. From the rater low initial specific conductance of sample B it can be inferred that ion exchange has been sufficiently effective in removing the added salt. Both curves indicate the presence of only strong acidic groups. The surface charge density amounts to 25.6 mC/m^2 and 39.5 mC/m^2, respectively, as inferred from the equivalence points and the specific surface area (10.8 m^2/g, calculated from the particle diameter (529 nm) and the density of polystyrene (1.05 kg/l)). Thus these experiments unequivocally prove the charging of polystyrene latex upon contact with a solution of high ionic strength. Although one can only

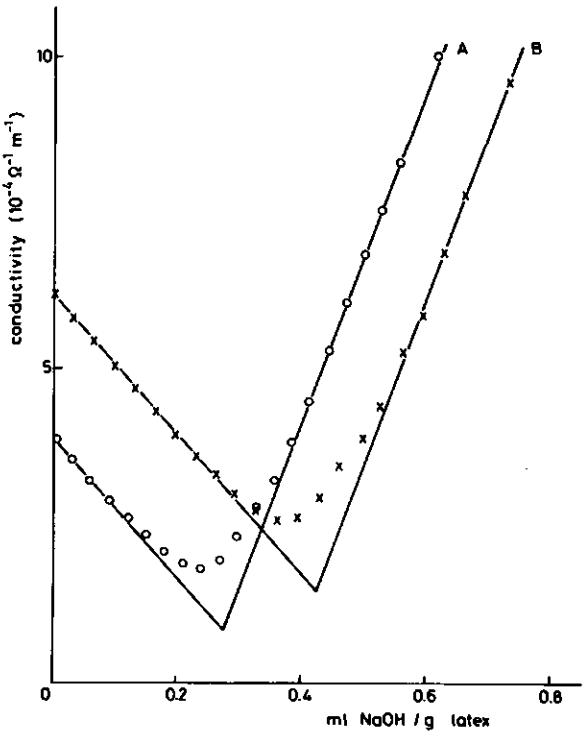

Fig. 2.1 - Conductivity of samples A and B as a function of the added volume 1.038×10^{-2} M NaOH.

A: sample N diluted 1:1 with distilled water and subsequently ion exchanged.

B: sample N diluted 1:1 with 2×10^{-1} M KBr and subsequently ion exchanged.

speculate as to the mechanism causing this charging phenomenon, it seems likely to be connected with the polyelectrolyte character of the surface (chapter 5). Recently Van der Put (6), observing an irreversible increase of electrokinetic signals upon contact of polystyrene plugs with a 10^{-1} M solution of KCL, suggested the following mechanism: at high ionic strength the polystyrene chains collapse at the surface, thereby activating subsurface groups to exposure upon subsequent dilution.

In order to check the ion exchange and characterization procedure, the titrated samples A and B have been ion exchanged and titrated again. The results of these experiments confirmed the

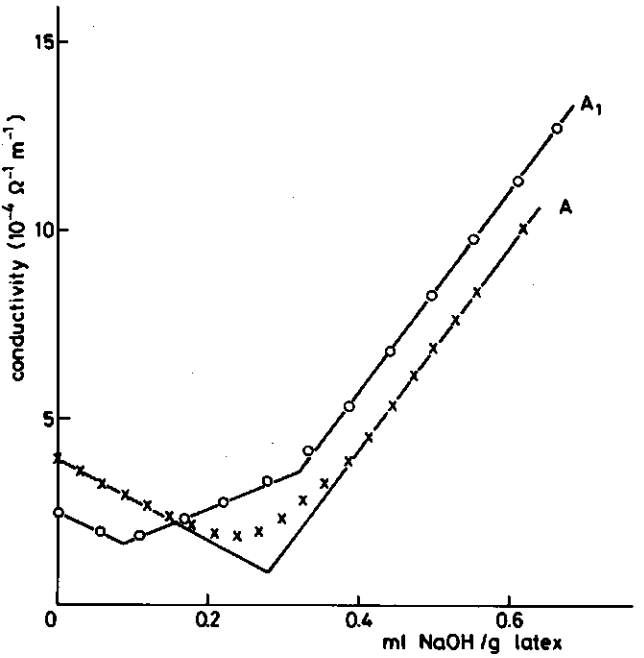

Fig. 2.2 - Effect of titration and subsequent ion exchange of sample A on the plot of conductivity versus added volume 1.038×10^{-2} M NaOH.

A : as Fig. 2.1, curve A.

A_1: sample A after first titration and subsequent second ion exchange.

charging, observed in the first run, almost quantitatively. Surprisingly, however, the conductometric titration curves of both samples contained two, in stead of one, distinct kinks, as shown in Fig. 2.2 (curve A_1) and Fig. 2.3 (curve B_1) for samples A and B respectively. For comparison the curves obtained after the first ion exchange treatment have been included. The occurrence of two kinks points to the presence of two types of acidic groups. Besides sulfate groups these are presumably carboxyls. The number of sulfate groups can be inferred from the first equivalence point, that of the carboxyls from the difference between the first and second one. Thus from Fig. 2.2 (curve A and A_1) and Fig. 2.3 (curve

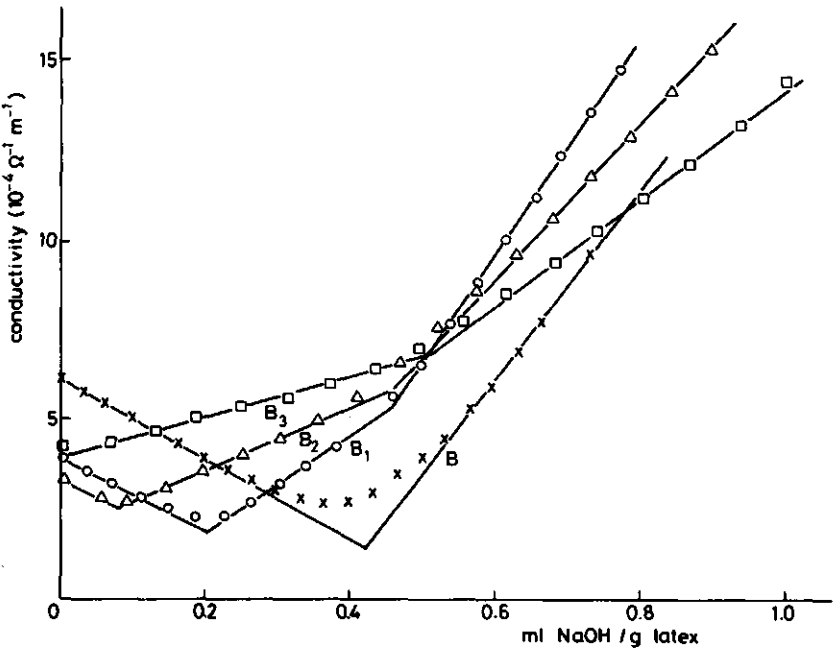

Fig. 2.3 - Effect of consecutive cycles of titration and subsequent ion exchange on the conductometric titration curves of sample B (1.038×10^{-2} M NaOH).

B : as Fig. 2.1, curve B.

B_1: sample B after first titration and subsequent ion exchange.

B_2: sample B after second titration and subsequent ion exchange.

B_3: sample B after third titration and subsequent ion exchange.

B and B_1) it is seen that, whilst the total number of surface groups remains about constant, part of the sulfates is converted into carboxyls due to a titration followed by ion exchange.

Fig. 2.3 shows that a subsequent, but identical treatment of sample B leads to a further substitution of strong by weak acidic groups (curve B_2) until after four runs only weak acidic groups are present (curve B_3).

It is stressed that only a combination of titration and subsequent ion exchange led to the loss of sulfate groups. In agreement with the findings of others (7,14) the number of ion

exchanges without intermittent titration appeared not to influence number and nature of the surface groups.

McCarvill and Fitch (12) also report a decrease in the sulfate content upon successive ion exchanges. Unfortunately, their paper does not elucidate whether one sample has been subjected to successive cycles of titration and ion exchange (as in our case) or that various samples, differing only in the number of applied ion exchanges, have been titrated. In the first case their results would fit in with ours, in the second their observations would be contradictory to those of Norde (7), Bonekamp (14) and ourselves.

The chemical instability of polystyrene latices, prepared with $K_2S_2O_8$ as the initiator has also become apparent from other studies (2). For instance, these latices may loose their sulfate groups upon storage (see also next section). This loss is presumably caused by hydrolysis according to

$$\text{— O — } \overset{\overset{O}{\|}}{\underset{\underset{O}{\|}}{S}} \text{ — } O^- + H_2O \rightarrow \text{ — OH} + HSO_4^-$$

Subsequent oxidation of hydroxyl to carboxyl groups might explain the loss of strong acidic and the production of weak acidic groups. It is likely that the hydrolysis is related to the titration and the oxidation to the ion exchange treatment. After completion of the titration the sample is at a relatively high pH (about 10), a condition which is known to catalyze the hydrolysis of alkylsulfates (15). Ion exchange goes along with strong agitation of the latices, which promotes the supply of the required oxygen.

A small increase in the total number of surface groups is observed after the fourth treatment of sample B (see Fig. 2.3). This might be attributed to oxidation of hydroxyl groups, that were already introduced during the polymerization.

One might wonder whether a second contact of latex with a 10^{-1} M KBr solution would lead to an even more extensive charging process. Electrokinetic experiments indicated that, in all probability, this will not be the case. Therefore the effect of subsequent electrolyte treatments has not been studied, since the required process is rather laborious.

2.3.4 HYDROLYSIS OF SURFACE GROUPS UPON STORAGE

Characterization of latices that, after dialysis and ion exchange, had been stored for a few years, revealed considerable aging effects. Both the number and the nature of the surface groups appeared to have changed. By way of example the conductometric titration curves of sample M_3 (see table 2.1) measured shortly after preparation (curve a) and after two years of storage in the H^+-form (curve b) are shown in Fig. 2.4. The loss of strong acidic groups upon storage is obvious. This is presumably due to hydrolysis of the sulfate groups. Inference of the hydrolysis rate from Fig. 2.4 depends on the interpretation of curve b. Whilst curve a indicates the presence of only strong acidic groups, curve b is somewhat ambiguous. Interpreted in terms of only strong acidic groups (drawn line), the rate of hydrolysis would amount to about

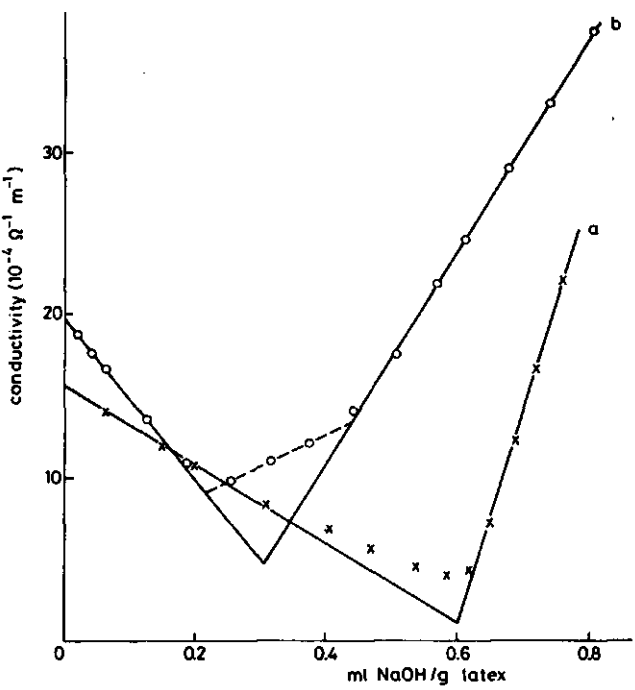

Fig. 2.4 - Conductometric titration curves of sample M_3 immediately after preparation and cleaning (curve a) and after two years of storage in the ion exchanged (acidic) form (curve b).

25 % per year. Assuming the surface of the aged latex to bear both strong and weak acidic groups (dotted line) this becomes about 70 % per year. However, these figures are not typical: one latex even showed no surface charge at all after storage over a period of a few years. Nevertheless this latex was stable, indicating that the particles are probably sterically stabilized.

The weak acidic groups, possibly present in sample M_3 after storage, might be produced by oxidation of hydroxyls (see previous section). The major part of the produced hydroxyls has not been converted into carboxyl groups, as can be inferred from Fig. 2.4. Apparently the supply of oxygen during storage and ion exchange has not been sufficient. It is noted that the weak acidic groups might also be introduced by retarded reactions of residual monomers or by microbial contamination (2).

Hydrolysis of sulfate groups upon storage is reported by several authors (2). The rate of hydrolysis appears to vary widely. Goodall et al. (8), e.g., found rates of hydrolysis varying from 2 to 37 % per month (at 25 °C), whereas Vanderhoff (16) reports the complete loss of sulfate groups of an ion exchanged latex within fourteen days. Most reports only mention the removal of sulfates upon storage as a result of hydrolysis. Only Vanderhoff (16) and Goodall et al. (8) observed also the appearance of weak acidic groups.

The hydrolysis of alkyl sulfates is known to be catalyzed by hydrogen and hydroxide ions (15). At neutral pH the reaction rate is minimal. Therefore it may be expected that aging effects can be suppressed by storing the latices at neutral pH. This supposition is supported by the observation that a latex sample, titrated just up to the equivalence point straight after steam stripping and ion exchange, retained all its sulfate groups for at least half a year.

It seems worthwhile exploring the possible use of latices, that are stabilized by sulfonate groups, since these seem to be much more resistant to hydrolysis (2).

2.4 CONCLUDING REMARKS

The surface properties of polystyrene latices are far from controllable and constant. The number and nature of the surface

groups may change considerably upon storage as well as a result of titration and subsequent ion exchange. Treatment with a solution of high salt content leads to an additional charging of the surface.

In order to minimize the occurrence of the observed non-idealities and thus of their influence on the electrokinetic investigations described in this thesis, after their preparation the polystyrene latices should be and have been handled as follows:

1. Determination of the particle radius per batch and subsequent mixing of batches with particle sizes corresponding within narrow limits.
2. Treatment with a solution of high ionic strength ($> 10^{-1}$ M). Removal of salt by ion exchange.
3. Purification by steam stripping (at low temperature) and subsequent ion exchange.
4. Storage at neutral pH.
   Comparative experiments should be performed within a few months.
5. Characterization immediately prior to use.

2.5 REFERENCES

1. Vanderhoff, J.W., Van den Hul, H.J., Tausk, R.J.M. and Overbeek, J.Th.G. in "Clean Surfaces: Their Preparation and Characterization for Interfacial Studies" (G. Goldfinger, Ed.), Marcel Dekker, New York, 1970.
2. Hearn, J., Wilkinson, M.C. and Goodall, A.R., Adv. Colloid Interface Sci. 14, 173 (1981).
3. Bijsterbosch, B.H. and Lyklema, J., Adv. Colloid Interface Sci. 9, 147 (1978).
4. Yates, D.E., Ottewill, R.H. and Goodwin, J.W., J. Colloid Interface Sci. 62, 356 (1977).
5. Furusawa, K., Norde, W. and Lyklema, J., Kolloid Z.Z. Polymere 250, 908 (1972).
6. Van der Put, A.G., Thesis, Agricultural University, Wageningen (1980).
7. Norde, W., Thesis, Agricultural University, Wageningen (1976).
8. Goodall, A.R., Hearn, J. and Wilkinson, M.C., J. Polym. Sci. Polym. Chem. Ed. 17, 1019 (1979).
9. Goodwin, J.W., Ottewill, R.H., Harris, N.M. and Tabony, J., J.

Colloid Interface Sci. 78, 253 (1980).
10. Everett, D.H., Gültepe, M.E. and Wilkinson, M.C., J. Colloid Interface Sci. 71, 336 (1979).
11. Wilkinson, M.C., Hearn, J., Cope, P. and Goodall, A.R., J. Colloid Interface Sci. 77, 566 (1980).
12. McCarvill, W.T. and Fitch, R.M., J. Colloid Interface Sci. 67, 204 (1978).
13. Van den Hul, H.J. and Vanderhoff, J.W., J. Colloid Interface Sci. 28, 336 (1968).
14. Bonekamp, B.C., Thesis, Agricultural University, Wageningen (1984).
15. Kurz, J.L, J. Phys. Chem. 66, 2239 (1962).
16. Vanderhoff, J.W., Pure Appl. Chem. 52, 1263 (1980).

CHAPTER 3

A GENERALLY APPLICABLE METHOD FOR THE ASSESSMENT OF ELECTRODE AND INTRINSIC POLARIZATIONS IN THE EVALUATION OF STREAMING CURRENTS AND STREAMING POTENTIALS

3.1 INTRODUCTION

Streaming potential and streaming current measurements belong to the collection of electrokinetic techniques that glory in a long tradition of contributing to the elucidation of electrical double layer structures at solid-liquid interfaces (1,2). Both phenomena occur upon displacement of a liquid with respect to a charged solid phase, which is usually present as a plug or a capillary. A streaming current I_s appears when using short-circuited electrodes; a streaming potential V_s develops when connecting the electrodes by a high impedance voltmeter.

I_s and V_s are a measure of the potential drop ζ across the hydrodynamically mobile layer. Under conditions of laminar flow and a double layer thickness small as compared to the radius of curvature of the surface, the quantitative relations read (2):

$$\frac{I_s}{\Delta P} = \frac{\varepsilon \zeta}{\eta C_p} \qquad [3.1]$$

$$\frac{V_s}{\Delta P} = \frac{\varepsilon \zeta}{\eta C_p K} \qquad [3.2]$$

where ΔP is the pressure drop across the dispersed phase, C_p the conductometric cell constant, K the conductance of the assembly and ε and η are the permittivity and the viscosity of the solution, respectively. Since K represents the overall conductance, it includes any contribution of surface conductance. Eqs. 3.1 and 3.2 are the well-known Helmholtz-Smoluchowski formulae. These model equations illustrate that determination of the streaming current should render the same result as a combined measurement of the streaming potential and the plug conductance. This theoretical requirement can be proven more generally by application of the theory of irreversible thermodynamics (3). Experimentally, the

equivalency of both methods is usually confirmed (4,5,6), although some authors report a discrepancy (7,8).

In practice, the application of both the streaming current and streaming potential method is complicated by polarization phenomena taking place at the measuring electrodes. Generally one is aware of this complication. Less well recognized, however, is that polarizations may also occur in the studied system itself (6), a phenomenon interfering with the conductance and current measurements. The experiments to be described in this thesis indicate that such intrinsic polarization phenomena occur rather generally and in fact we observed them in plugs of organic (polystyrene) as well as of inorganic (silver iodide) material.

In this chapter we will describe the influence of electrode and intrinsic polarizations on the experimental signals in electrokinetic investigations and present a generally applicable method to assess their effects. We start with a treatment of the principles of this method, which is partially based on a recent discourse (9).

3.2 PRINCIPLES OF THE METHOD

3.2.1 STREAMING POTENTIAL METHOD

Determination of the electrokinetic potential ζ by means of the streaming potential method implies measuring the streaming potential V_s, and the conductance K and the cell constant C_p of the system under investigation, as can be inferred from equation 3.2. V_s can be obtained relatively simply, among other things because it does not depend on the material or the dimensions of the electrodes, nor on the distance between the plug and the electrodes (section 3.5.2.1). This is probably the main reason why this method has been preferred in many electrokinetic studies.

Determination of K or, for that matter, the reciprocal resistance is more complicated, because the measured resistance always includes a contribution of the electrode-solution interface. This contribution (electrode polarization) is related to the rate of transport and (dis)charge of the reacting species. It generally decreases with increasing frequency and is usually eliminated by

employing an R-C bridge in the kiloherz range (e.g. 5,10,11,12). The resulting a.c. conductance is subsequently substituted in equation 3.2. However, during streaming potential measurements a direct field is generated, so that actually a d.c. conductance is operative. Consequently, it is only justified to substitute said a.c. value in the Helmholtz-Smoluchowski equation, when the conductance of the medium itself shows no frequency dependence towards the low frequency range. Low frequency dispersions were observed, however, in plugs of both materials studied in this work, i.e. polystyrene (chapters 5 and 6) and silver iodide (chapter 7). An example, to be discussed below, is presented in Fig. 3.1, where the a.c. conductance (admittance) of a polystyrene plug not influenced by elec-

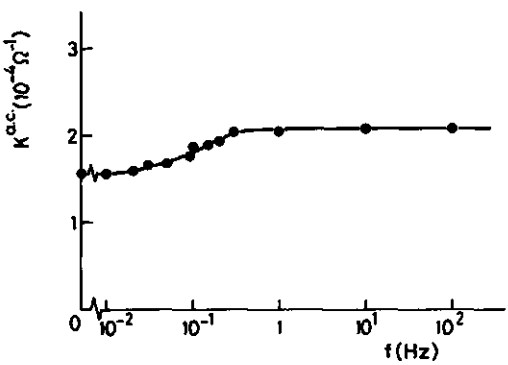

Fig. 3.1 - A.c. conductance (admittance) of a polystyrene plug as a function of frequency. Electrolyte: $5x10^{-3}$ M KCl.

trode polarization, is plotted as a function of the frequency. This is an indication for the occurrence of intrinsic polarizations. Apparently some of the charge carriers that participate in the conduction current in the plug at high frequencies, are immobilized at lower ones. A detailed study of this phenomenon will be presented in chapter 5. Similar low frequency dispersions have been reported previously for quartz fibres (13), cellulose fibres (14), ion exchange membranes (15) and thorium oxide plugs (16). It must be concluded that serious errors can be made by simply substituting a.c. conductances in the Helmholtz-Smoluchowski equation.

As an alternative for the bridge method one sometimes employs the shunt method introduced by Eversole and Boardman (17). Generally, in addition to the normal streaming potential V_s one then measures the "streaming potential" V_s' as it occurs when a known shunt resistance R_s is placed between the electrodes (see e.g. 12,18,19). The plug resistance R_p is calculated from

$$R_p = \left(\frac{V_s}{V_s'} - 1\right) R_s \qquad [3.3]$$

However, the value of R_p thus obtained comprises a component due to the electrode polarization originating from the current flowing through the measuring electrodes during the shunting. This component may considerably contribute to R_p, especially at high salt concentration. On the other hand, the shunt method is not sensitive to intrinsic polarizations since it yields a d.c. resistance.

In our investigations the effect of electrode polarization has been eliminated by applying the four electrode technique suggested by Schwan (20). The results given in Fig. 3.1 were obtained with this method. In this approach, beyond the electrodes 2 and 2' making contact with the plug (Fig. 3.2) two auxiliary electrodes 1 and 1' are introduced through which a constant current is applied.

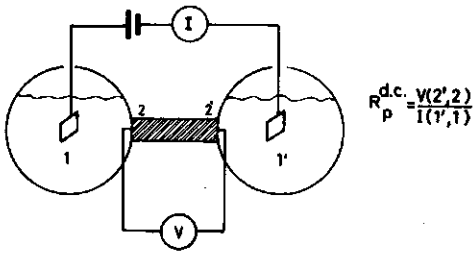

Fig. 3.2 - Schematic representation of the four electrode technique for measuring plug resistances.

Simultaneously, the resulting potential drop across the plug is measured with the inner electrodes. This potential difference contains no contribution of the electrode-solution interface, because

only a negligible current passes through the inner electrodes. Through Ohm's law, the resistance of the plug is obtained as the ratio between this potential drop and the externally applied current. The plug conductance thus measured under d.c. conditions, can rightly be substituted in the Helmholtz-Smoluchowski equation.

The cell constant C_p in eq. 3.2 is obtained from the ratio between the bulk conductivity and the plug conductance at high ionic strength.

In conclusion, the four electrode cell permits the proper determination of the plug conductance and, consequently, the zeta potential, eliminating any influences of electrode and intrinsic polarization phenomena.

3.2.2 STREAMING CURRENT METHOD

Electrode polarization is a serious complication in the streaming current method too. In this approach a convection current is generated, that has to be measured by short-circuited electrodes placed against the matrix. In order to obtain the real streaming current the charge transfer processes at these electrodes should be fast enough to process the convected charge in such a way as to avoid electrode polarization (Fig. 3.3a). However, it appears that in our experiments this condition can never be met. For reversible as well as irreversible electrodes application of a pressure drop across the matrix always gives rise to a retardation of the current (Fig. 3.3b). The initial (maximum) value that is measured, appears to depend on such experimental conditions as reaction time of the recording instrument and speed of pressure change. So determination of the streaming current in this direct way is usually not possible.

Remarkably few explicit reports on this retardation phenomenon have been published, though sometimes rather vague remarks indicate that there was an awareness of its occurrence (21). Results of yet other investigations clearly show the retardation (references 7 and 22, figures 3 and 6, respectively), although it is not explicitly noticed. Only Van der Put recently paid attention to this phenomenon (6). He showed that during the current retardation a potential drop develops across the plug which can be measured with the two

auxiliary electrodes discussed in section 3.2.1 (see Fig. 3.3c). This potential drop is caused by the hampered processing at the electrodes, which causes part of the convected charge to remain in

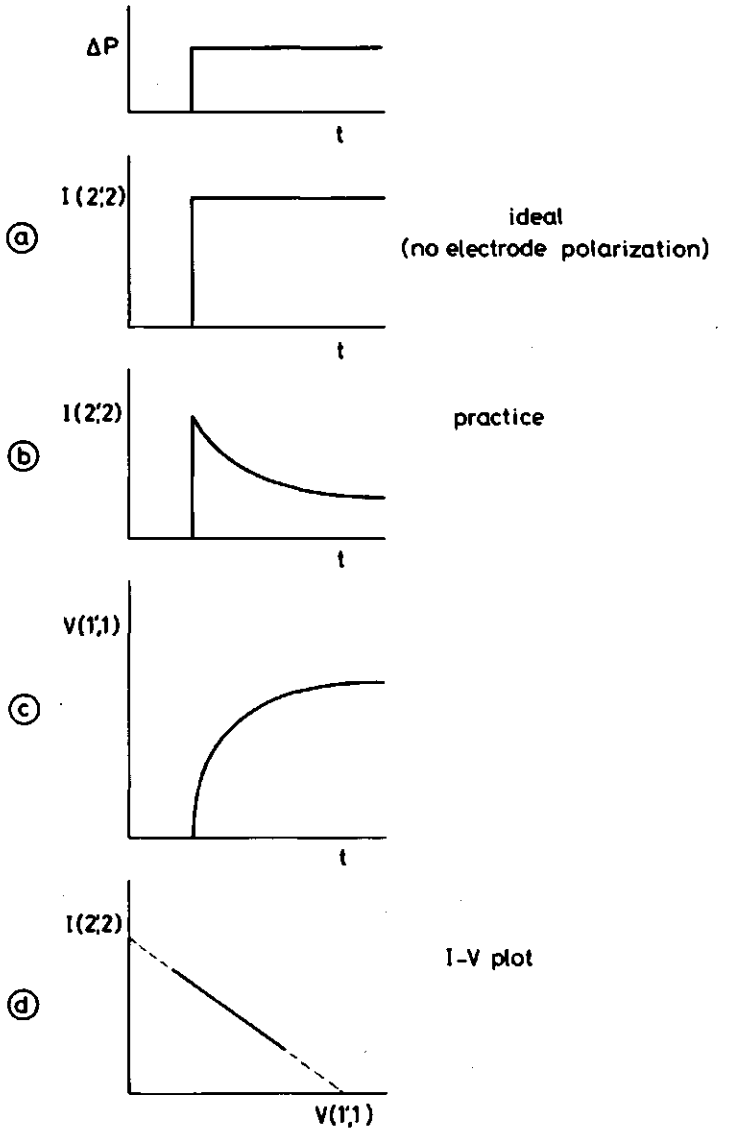

Fig. 3.3 - Elucidation of the I-V plot method for the determination of streaming currents. Explanation given in the text.

the electrode regions at both sides of the plug. Plotting the retarding current I(2',2) against the increasing potential drop V(1',1) provides a straight line (Fig. 3.3d). This enables the determination of the real streaming current, not influenced by electrode polarization, by extrapolating the linear I-V plot to V(1',1) = 0.

Intrinsic polarizations will contribute to the measured current when their time constants exceed those of the pressure application and/or recording device. In section 3.5.2.2 it will be shown that the I-V plot is extremely suitable for elimination of these contributions.

3.3 OUTLINE OF THE EXPERIMENTS

The usefulness of the four electrode technique in streaming current as well as streaming potential and resistance measurements has been investigated in further detail, employing polystyrene latex as the plug material. This model colloid was chosen since its electrokinetic properties are the subject of investigation in the major part of this thesis.

Different types of electrodes have been tested for their usefulness: silver-silver chloride, silver-silver iodide and platinum. Silver-silver chloride electrodes are the most popular ones in electrokinetic investigations, but they lack reversibility in solutions that do not contain chloride ions. As part of the experiments described in this thesis required an iodide medium, the silver-silver iodide electrode was introduced. Platinum was chosen as representative of the class of irreversible electrodes.

During the electrokinetic measurements it appeared necessary to gain more insight into the processes taking place at the platinum electrode. To that end a few electrode kinetic experiments were carried out.

In the following sections attention is focussed on the characteristics of the four electrode technique itself. The electrokinetic properties of the model system will be treated in chapters 5 and 6.

3.4 EXPERIMENTAL

3.4.1 ELECTROKINETIC EQUIPMENT

A schematic diagram of the electrokinetic equipment is shown in Fig. 3.4. Basically it is the same as that described by Van der Put (6), but a few modifications were introduced to improve and facilitate the experiments. Therefore the set-up will be discussed in detail, except for the plugholder section, which has not been changed.

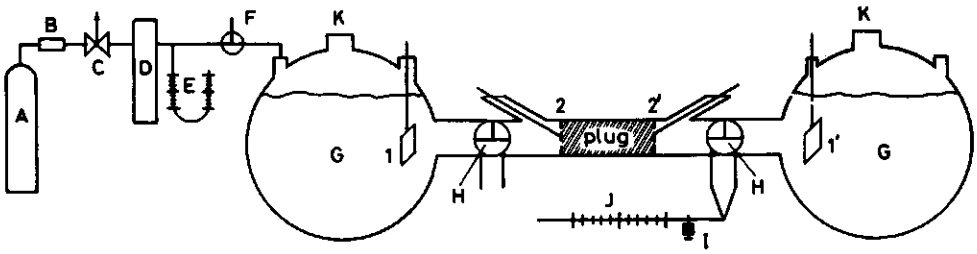

Fig. 3.4 - Experimental set-up for the electrokinetic and hydrodynamic measurements. Details described in the text.

The *pressurizing system* consisted of a nitrogen tank A (Hoek-Loos, typical N_2 vol. perc. 99.995), with pressure valve B and regulator C to generate the desired pressure difference. This arrangement was connected to a pressure vessel D with five outlets, one for a mercury manometer E (0-40 cm Hg*, accuracy 0.07 cm Hg) and four connectable to independent electrokinetic cells. In this way four cells could be pressurized simultaneously. The connection between the pressure vessel and each individual cell contained an aircock F, by which (de)pressurization could be achieved within about 0.2 seconds.

The *electrokinetic cell* encompassed two electrolyte reservoirs G, between which the plugholder section, with perforated

* 1 cm Hg corresponds to 1.33 kPa.

electrodes firmly screwed against the plug, was fastened by means of Sovirel caps. Between the plugholder and each reservoir a three-way cock H was inserted, permitting the flow direction to be either towards the electrolyte reservoir or towards a flow-measuring device. This arrangement was incorporated in order to perform permeability measurements. The flow-measuring device consisted of a calibrated capillary tube J, with a piston I to adjust the initial meniscus position in the capillary.

In each of the electrolyte reservoirs an opening K was constructed for insertion of a conductivity cell that enables the determination of the bulk conductance in the reservoirs.

The plug (2,2')- and reservoir (1,1') electrodes were connected to an *electrical measuring device* that has been described elsewhere (reference 6, page 46). Between the potential measuring electrodes and the recording instrument a d.c. Volt compensator was introduced in order to nullify the no-flow-potential that occurs when using platinum electrodes (see section 3.5.2.1). This arrangement enabled a sensitive recording. All shields were connected to just one earth point. When using separate connections to earth, sometimes leakage currents in the shields were generated, influencing the potential readings.

Apart from obtaining them by the four electrode technique, plug resistances were also measured directly by connecting the inner electrodes with a Wayne Kerr Universal Bridge B224 (internal frequency 1592 Hz).

The electrokinetic cells were placed in a cabinet, that was thermostated by a combination of a cooling thermostat and heating lamps connected with an electronic temperature regulator (temperature sensitive diode). In this way temperature fluctuations in the cabinet could be kept within 0.1 °C and in the reservoirs within 0.05 °C.

3.4.2 PREPARATION OF ELECTRODES

The silver-silver halide electrodes were prepared by electrolytically depositing a silver layer on a bare platinum electrode, followed by partial conversion of this layer into the required silver halide (23). The experimental details have been described by

de Keizer (24). The electrodes were aged for three days at 80 °C in a solution of 10^{-4} M chloride or iodide. Bias potentials were usually less than 1 mV.

During the electrokinetic experiments with bright Pt electrodes it appeared necessary to platinize them. This was accomplished by the "lead procedure" described in reference 25 with some minor modifications. After treatment of the bare platinum with hot HNO_3 (60 %) for 15 minutes and rinsing with distilled water, the substrate was further cleaned by cathodic electrolysis in a dilute H_2SO_4 solution, using a platinum counter-electrode in order to avoid contamination of the solution. Thereafter the electrodes were immediately platinized by electrolysis in a 2 percent solution of chloroplatinic acid, containing 0.02 percent lead acetate, at 300 A/m^2. The electrolysis was stopped when a uniform, deep black coating appeared. Usually 1 to $2x10^5$ C/m^2 was needed. Although Schwan (20) reports a minimal polarization impedance at a somewhat more extended coating, further electrolysis did not improve the results of our electrokinetic measurements. The electrodes were stored in distilled water until use.

The plug electrodes (2,2') consisted of circular disks, with the same cross-section as the plug, perforated with 0.4 mm diameter holes in a staggered pattern. The area available to flow was chosen such that its hydrodynamic resistance was negligible as compared to that of the plug. The reservoir electrodes (1,1') consisted of rectangular plates (about 4 cm^2). To each electrode a platinum wire, partially sealed in a glass tube, was welded for connection to the electrical system.

3.4.3 ELECTROKINETIC EXPERIMENTS

The electrokinetic experiments have been conducted with polystyrene plugs, which were prepared by centrifugating the latex. To enable a comparison of the different types of electrodes, the experiments had to be performed with the same plug for each ionic strength. This required a frequent unscrewing of the plugholder section in order to interchange the electrodes making contact with the plug. Obviously this might damage the plug and thus invalidate the experiments. In order to check for possible crumbling of the

plug, after each experimental run the originately mounted electrodes were assembled again. Only in the case of complete agreement between the results of the first and last experiment were the results of that particular run retained. In table 3.1 a survey is given of the experimental runs meeting this requirement. After interchanging the electrodes the plug was permeated until equilibrium was attained. As criteria the constancy of the I-V plot and of the plug conductance at 1592 Hz was used.

All measurements were carried out at 25.0 °C.

Table 3.1 - Survey of experiments in testing the various electrodes.

Plug	Electrolyte (M)	Tested electrodes
I	10^{-1} and $5x10^{-3}$ KCL	Ag/AgCL, bright Pt, black Pt
II	$7x10^{-4}$ KCL	Ag/AgCL, bright Pt, black Pt
III	10^{-1},10^{-2},10^{-3} and 10^{-4} KI	Ag/AgI

3.4.4 ELECTRODE KINETIC EXPERIMENTS

In order to study the processes occurring at a platinum electrode two perturbation experiments were performed. In the first (galvanostatic method) the potential change of the electrode was recorded during the passage of a constant current. In the second (potentiodynamic method) the electrode current was measured during a sweep of the potential from the hydrogen potential in anodic direction and back. Both experiments were carried out in a thermostated Pyrex cell with perspex cover, with a three electrode system, i.e. a reference-(saturated calomel), counter-(reversible silver-silver halide) and a working-electrode. The current flows through the circuit encompassing the counter- and working-electrode. The potential of the latter was determined by combining it with the reference-electrode.

In the galvanostatic experiment the constant current source of the electrokinetic set-up was used. The potential was recorded with a digital electrometer (Keithley 616). This method was applied to a

platinum bright, a platinum black and, for comparison, a silver-silver chloride electrode in 10^{-3} M KCL, which is within the concentration range of the electrokinetic experiments. The platinum electrodes were equilibrated several hours in advance, until their potential drift was negligible.

The potentiodynamic experiment was carried out with a PAR polarograph (model 174A). In applying this method the resistance of the counter-electrode and that of the solution must be negligible with respect to that of the working-electrode. Therefore only a platinum bright (wire) electrode at high ionic strength was studied.

All experiments were conducted with de-aerated solutions under nitrogen atmosphere.

3.5 RESULTS AND DISCUSSION

3.5.1 ELECTRODE KINETICS

Results of the galvanostatic experiments with bright platinum, platinized platinum and silver-silver chloride electrodes in 10^{-3} M KCL for stirring and non-stirring conditions are shown in Fig. 3.5.

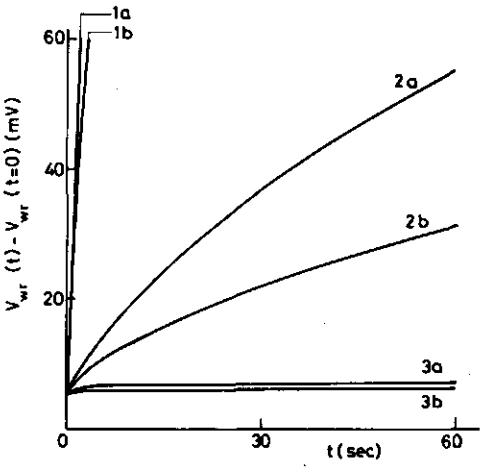

Fig. 3.5 - Polarization of a bright Pt (1), a black Pt (2) and a Ag/AgCL (3) electrode during current passage (I = 20 mA/m^2) for stirring (b) and non-stirring (a) conditions. Electrolyte: 10^{-3} M KCL. V_{wr} = potential difference between working and reference electrode.

In all cases switching on the current creates an instantaneous potential rise, representing the IR drop through the electrolyte solution between the working- and reference-electrode.

The reversible silver-silver chloride electrode polarizes only slightly during current passage, as expected. The observed small polarization is almost completely suppressed by stirring the solution. Apparently only the generation of concentration gradients in the electrode regions gives rise to polarization. Activation polarization does not occur on the time scale of seconds.

The noble metal platinum is polarized drastically, the more so the smaller the surface area. The polarization is considerably reduced in a stirred solution, which points to the participation of a process controlled by mass transfer in the solution. Apparently, both interfacial activation polarization and concentration polarization occur during passage of a current through the platinum electrode-solution interface.

More insight into this mass transfer controlled process can be obtained from the results of the potentiodynamic experiments shown in Fig. 3.6. The presented voltammogram refers to a solution of 1 M $HClO_4$ and 10^{-3} M KCl. Preliminary experiments showed this solution to give more reproducible results than solutions of 1 M KCl or 1 M HCl, probably due to a lower impurity level. As only qualitative information was needed, no attempts were made to improve the results by purifying the solution. Nevertheless, the presented voltammogram closely resembles those obtained in sulfuric acid (e.g. 26) and perchloric acid (27) solutions in more elaborate investigations. In agreement with these reports, four stages can be distinguished in the anodic profile, viz. hydrogen oxidation at potentials below 0.4 V, double layer charging in the region from 0.4 V to about 0.8 V, oxidation of water above 1.2 V and, most striking, a wave pointing to the oxidation of the platinum surface between about 0.8 V and 1.2 V.

In all solutions used in the electrokinetic experiments, the open-circuit potential of the platinum electrode appeared to drift slowly towards a value around 0.9 V, which is in the oxide layer region.

From these results it may be concluded that during current passage the following overall oxidation-reduction reactions occur:

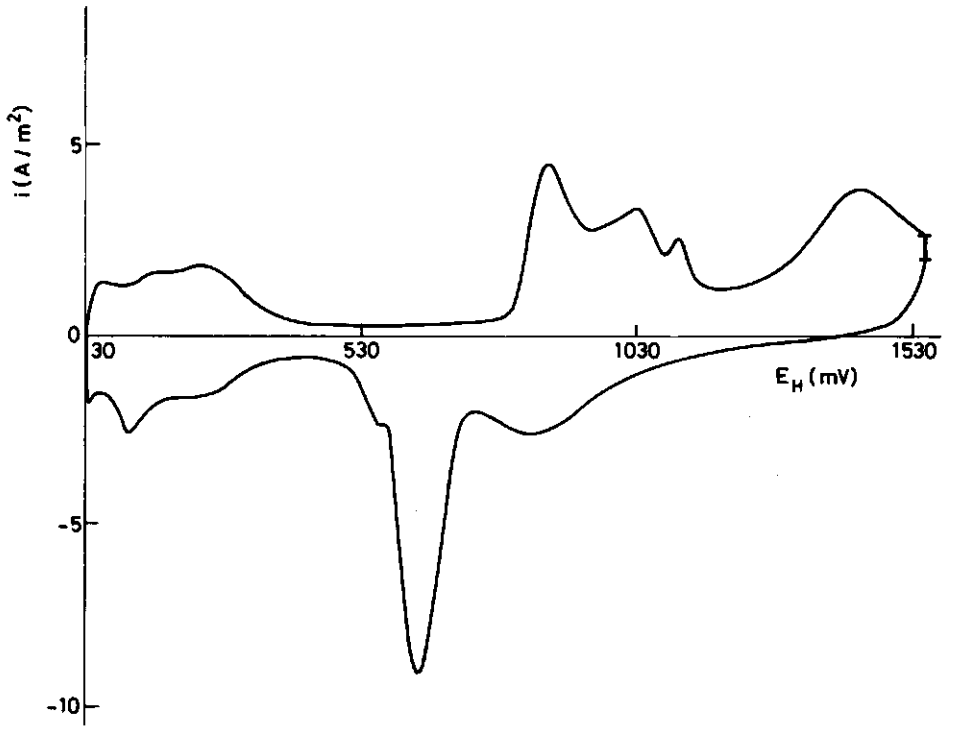

Fig. 3.6 - Potendiodynamic I-V profile of a Pt wire in a solution containing 1 M $HClO_4$ and 10^{-3} M KCL. The electrode potentials are referred to the hydrogen electrode in the same solution. Sweep rate: 0.1 V/sec.

$$Pt + xH_2O \rightarrow PtO_x + 2xH^+ + 2xe^-$$

Fig. 3.6 also illustrates that in the cathodic wave the oxide layer is reduced at potentials that are lower than those at which it was formed in the anodic one. Apparently the oxidation process is irreversible. Angerstein-Kozlowska et al. (26) showed that the irreversibility of the platinum oxide formation increases as coverage and potential increase.

3.5.2 ELECTROKINETICS

3.5.2.1 STREAMING POTENTIAL METHOD

Electrode potential drift and asymmetry

Whilst the reversible Ag/AgCl and Ag/AgI electrodes have constant and very low asymmetry potentials (less than 1 mV), it has often been reported that Pt electrodes show large potential drifts and high asymmetry potentials. Korpi and de Bruyn (28) and Ardizzone and Formaro (5) pointed out that the corresponding polarization effects may obscure the potential measurements in an unpredictable way. We did indeed find that the Pt electrode potential under no-flow and no-current conditions could change rapidly with time. Obviously, this drift is related to the formation and dissolution of the oxide layer discussed in the previous section. However, this potential drift occurred mainly during the first hours after mounting the electrodes in the equipment. After longer equilibration times (usually a day or more) the drift was alsmost always negligible as compared to the potential response to a pressure change or current pulse, even at high ionic strength. Moreover, platinizing appeared to suppress the potential drift, which is in agreement with observations of Wijga (18). These procedures did not diminish the asymmetry potential, for which values up to 150 mV were observed. However, these were easily taken into account by determining the streaming potential and the d.c. resistance from the change in potential difference between flow and no-flow conditions, and that between current and no-current conditions, respectively. In this way the rather complex procedure of Hunter and Alexander to reduce the asymmetry potential (29) could be avoided. Horn and Onoda (30) nullified the no-flow potentials by compensating them by means of R-C circuits, but this method fails in the case of rapidly changing rest potentials.

Streaming potential

In all cases streaming potentials determined as the instantaneous change in potential difference resulting from a variation

in the applied pressure did not depend either on the material or the dimensions of the electrodes. Moreover, with the plug electrodes the same result was obtained as with the reservoir electrodes. Thus the distance between the plug and the sensing electrodes is irrelevant. Anomalous potential differences were only obtained with Ag/AgI electrodes when these were screwed firmly against the plug.

In the studied pressure range (0 - 30 cm Hg) streaming potential vs. pressure curves were perfectly linear and passed through the origin (Fig. 3.7) for all ionic strengths. For opposite flow

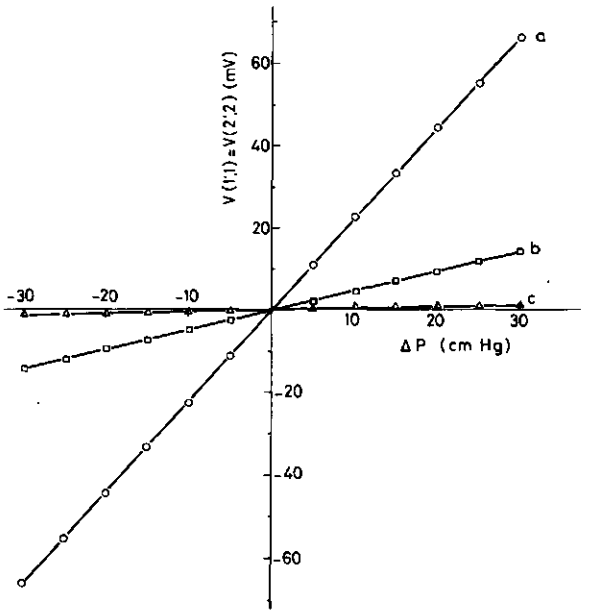

Fig. 3.7 - Streaming potential vs. pressure as obtained for (a) plug II at 7×10^{-4} M KCl, (b) plug I at 5×10^{-3} M KCl, (c) plug I at 10^{-1} M KCl.

directions identical results were obtained.

Streaming potentials measured with Pt electrodes were time-independent for at least one minute for all ionic strengths. With reversible electrodes a small increase in the streaming potential for several minutes was observed for ionic strengths below about

$5x10^{-3}$ M. This increase may be explained as follows: at low ionic strength ion exclusion (Donnan effect) occurs, leading to accumulation and depletion of electrolyte at the high pressure and low pressure side, respectively. When employing electrodes reversible to the excluded ions, this salt sieving process superimposes a concentration potential on the streaming potential (9).

D.c. conductance

In determining d.c. conductances by means of the four electrode method, at concentrations above about $5x10^{-3}$ M application of constant currents through the reservoir electrodes gave rise to an instantaneous readjustment of the potential drop across the plug. This behaviour is schematically depicted in Fig. 3.8a. From such voltage-current characteristics d.c. conductances can be easily determined.

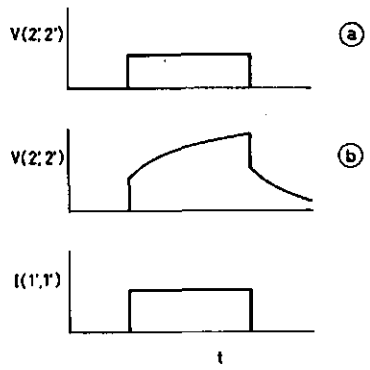

Fig. 3.8 - Response of the potential difference between plug electrodes to a constant current pulse through the plug at salt concentrations above (a) and below (b) about $5x10^{-3}$ M

Below concentrations of about $5x10^{-3}$ M, however, transient potential changes were recorded (Fig. 3.8b) irrespective of the type of sensing electrodes. In principle this time dependence may result from concentration polarization at the plug boundaries, a phenom-

enon that generally occurs when a current passes through an ion excluding medium (31). As a first approximation the contribution of this polarization potential to the overall potential drop can be assessed from the change in the streaming potential under similar conditions, i.e. for equal amounts of displaced salt. As noted in the previous section, for Pt electrodes the streaming potential is constant for at least one minute. This period corresponds to an effective salt displacement of 4×10^{-9} mole at 7×10^{-4} M KCL (plug permeability 10^{-4} ml/sec at 30 cm Hg; we neglect the small decrease of the electrolyte concentration in the pores of the plug owing to the Donnan exclusion). In the conductance measurement (I(1',1) = 2 μA) this amount is displaced only after more than three minutes. Hence, for small currents (a few μA) and short pulse durations (a few minutes) concentration polarization does not lead to observable changes in the potential drop across the plug as measured with Pt electrodes. The same conclusion holds for reversible electrodes, as, here too, for small amounts of displaced salt the increase of the streaming potential is negligible with regard to the change in potential drop during current passage. In all probability the slow increase of the potential drop across the plug upon passage of a time-independent current must be ascribed to intrinsic polarization phenomena.

From the value at which the potential levels off, the d.c. plug conductance can be obtained. D.c. conductances determined in this way are summarized in table 3.2. No significant differences between the various electrode types were observed. To illustrate the remarkable difference with d.c. values, a.c. conductances at 1592 Hz have been included. The latter data, which was obtained with an R-C bridge connected to the plug electrodes, does depend on the electrode material, indicating different contributions of the electrode polarization to the total impedance. Nevertheless, in all cases the d.c. conductance is smaller than its a.c. counterpart, especially at low ionic strength. Thus it is clear that substitution of a.c. conductances in the Helmholtz-Smoluchowski equation would lead to erroneous ζ-potentials.

It was noticed, that when using Ag/AgI inner electrodes, d.c. conductances could only be measured when the electrodes were freshly prepared. After longer periods of contact of these elec-

Table 3.2 - $K^{d.c.}$ and $K^{a.c.}$ of plugs I and II at different KCl concentrations. $K^{d.c.}$ was obtained with the four electrode method. The values were independent of the electrode material. $K^{a.c.}$ was obtained with an R-C bridge connected to the plug electrodes.

Plug	KCl conc. (M)	$K^{d.c.}$ (Ω^{-1})	$K^{a.c.}$ (at 1592 Hz) (Ω^{-1})		
			bright Pt	black Pt	Ag/AgCl
I	10^{-1}	1.73×10^{-3}	1.98×10^{-3}	1.91×10^{-3}	1.76×10^{-3}
I	5×10^{-3}	2.13×10^{-4}	2.51×10^{-4}	2.52×10^{-4}	2.35×10^{-4}
II	7×10^{-4}	2.47×10^{-5}	-	3.15×10^{-5}	2.81×10^{-5}

trodes with the plug (some weeks), the potential drop across the plug during current passage showed an enormous, irregular time dependence and its actual value could thus not be established. Therefore, results of conductance measurements with plug III are not considered.

3.5.2.2 STREAMING CURRENT METHOD

Ag/AgCl electrodes

Fig. 3.9 presents the streaming current retardations together with the corresponding I-V plots as obtained with Ag/AgCl electrodes* for a number of KCl concentrations. The results refer to a pressure drop of 30 cm Hg. In the I-V plots the independently measured streaming potentials have also been indicated. The following striking features are observed:

(i) Especially at high ionic strength the retardation is very pronounced. At 10^{-1} M KCL the streaming current obtained by

* These are the electrodes making contact with the plug. In all cases the material of the potential sensing electrodes (1,1') appeared to be irrelevant.

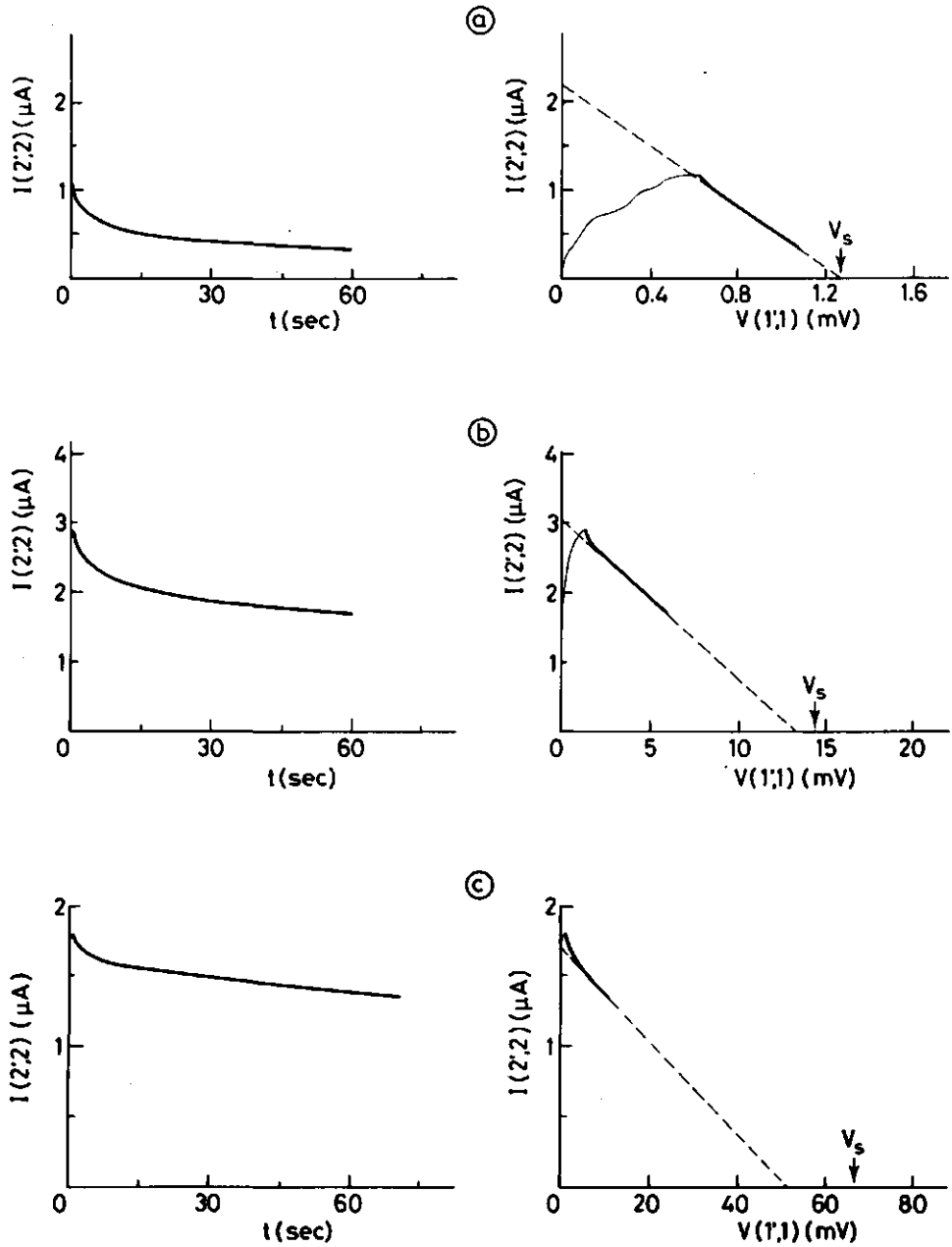

Fig. 3.9 - Current retardation and corresponding I-V plots as obtained with Ag/AgCl plug electrodes (ΔP 0 → 30 cm Hg). a,b = plug I at 10^{-1} M and $5x10^{-3}$ M KCl, respectively; c = plug II at $7x10^{-4}$ M KCl. The independently determined streaming potentials are indicated as V_s.

extrapolation of the I-V plot considerably exceeds the initial value. Identifying the latter with the streaming current leads to a serious underestimation. Fig. 3.9a clearly demonstrates that even fast measurements (21) may yield erroneous streaming currents.

(ii) At low ionic strength (Fig. 3.9c) the initial current exceeds the value obtained by extrapolating the I-V curve. This points to an intrinsic charge displacement in addition to the electrokinetic one, contributing to the current in the external circuit during the first seconds following pressure application. Detailed information on these intrinsic processes will be presented in chapter 5. It will be shown that at lower ionic strengths these processes are so slow that their effect becomes visible in the I-V plots.
Fig. 3.9c illustrates again that by identifying the initial current value with the streaming current, erroneous results are obtained.
It is appropriate to remark that plug II had been used earlier in experiments with solutions of tetraamylammonium ions. These ions do not desorb completely when permeating the plug with aqueous solutions. Even at small surface coverages, tetramylammonium ions considerably lower the contribution of the intrinsic processes (chapter 6). For plugs of bare latex the difference between the extrapolated and the maximum current value at low ionic strength is usually much larger than in Fig. 3.9c (see chapter 5).

(iii) Extrapolation of the I-V curves to $I(2',2) = 0$ at 0.1 M yields the independently measured streaming potential (Fig. 3.9a). Below concentrations of about 5×10^{-3} M, however, the potential obtained by extrapolating the I-V curve deviates from V_s (Figs. 3.9b and 3.9c).

The last observation can be explained by considering the transport and charge transfer processes during a streaming current experiment in more detail. To that end we consider the (negatively charged) polystyrene plug as a bundle of capillaries filled with a KCl solution and encompassed between short circuited Ag/AgCl electrodes (Fig. 3.10a). Application of a pressure gradient forces an excess

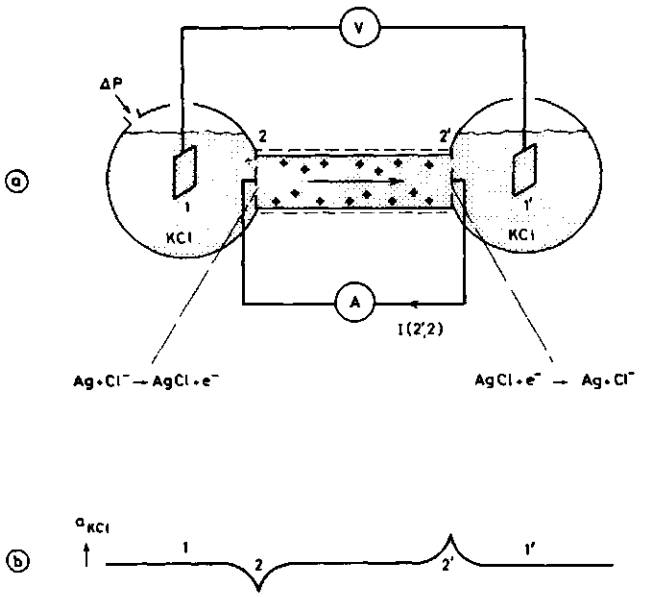

Fig. 3.10 - Reactions at the Ag/AgCl electrodes in streaming current measurements (a) and the resulting schematic profile of the KCL concentrations (b).

of positive K^+ ions to flow to the low pressure side, where the resulting charge is counterbalanced by the following electrochemical reaction:

$$AgCL + e^- \rightarrow Ag + Cl^-$$

At the high pressure side K^+ ions are removed by convection into the plug and Cl^- ions by the electrode reaction

$$Ag + Cl^- \rightarrow AgCl + e^-$$

Thus the streaming current experiment leads to accumulation and depletion of salt in the electrode regions at the low and high

pressure side, respectively (Fig. 3.10b). As a result of these concentration gradients the following diffusion potentials V_d originate across the streaming current cell.

$$V_d(2',1) = (2\ t_+ - 1)\ \frac{RT}{F}\ \ln\ \frac{a_2'}{a_1'} \qquad [3.4a]$$

$$V_d(2,2') = (2\ \tilde{t}_+ - 1)\ \frac{RT}{F}\ \ln\ \frac{a_2}{a_2'} \qquad [3.4b]$$

$$V_d(1,2) = (2\ t_+ - 1)\ \frac{RT}{F}\ \ln\ \frac{a_1}{a_2} \qquad [3.4c]$$

where t_+ and $\tilde{t}_+$ are the transport numbers of the K^+ ion in the bulk and inside the plug, respectively. a_i' refers to the KCL activity in the region of electrode i at the low pressure side, a_i to that at the high pressure side. The other symbols have their usual meaning. Adding up these contributions and equating a_1 and a_1' yields the following overall diffusion potential across the plug:

$$V_d(1,1') = (2\ t_+ - 2\ \tilde{t}_+)\ \frac{RT}{F}\ \ln\ \frac{a_2'}{a_2} \qquad [3.5]$$

This equation demonstrates that the various diffusion potentials cancel when t_+ equals $\tilde{t}_+$, which is the case at high ionic strength, where the double layer thickness κ^{-1} is small compared to the mean pore radius a (at 10^{-1} M 1-1 electrolyte, e.g., $\kappa a > 100$ for plugs I and II). With decreasing ionic strength, however, the shielding of the plug charge is diminished, which favours the transport of the counterions (K^+) over that of the co-ions (CL^-). As a result at low salt content $\tilde{t}_+$ exceeds t_+ and according to eq. 3.5 a diffusion potential is established, which, of course, is measurable with the reservoir (1,1') electrodes.

In effect, when ion exclusion occurs, the potential difference across the plug developed during a streaming current retardation contains two components:

1. an electrical potential due to electrode polarization (section 3.2.2). In case of complete blocking of the electrode current, this potential equals the streaming potential. The same condition is than created as during a streaming potential measurement, where a high impedance is included in the external circuit.

2. a diffusion potential given by equation 3.5. It can easily be shown that this potential counteracts the electrical potential.

In conclusion the deviation, at low ionic strength, between the streaming potential obtained by extrapolating the I-V plot to I(2',2) = 0 must be ascribed to the diffusion potentials generated by the electrolysis processes at the electrodes neighbouring the boundaries of the plug.

Ag/AgI electrodes

Despite the chemical similarity between AgCL and AgI, the behaviour of Ag/AgI electrodes was very irregular and completely different from that of Ag/AgCL electrodes. We mentioned this anomalous behaviour previously in relation to the streaming potential method (section 3.5.2.1) and observed it also in the streaming current experiments. In most cases the I-V plot was not linear, a typical example being shown in Fig. 3.11. It is clear that a

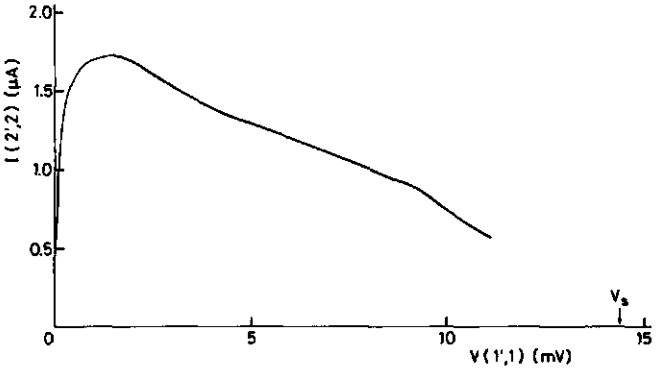

Fig. 3.11 - Typical example of an I-V plot obtained with Ag/AgI electrodes.

reliable determination of the relevant electrokinetic quantities is not possible in this case. Therefore, Ag/AgI electrodes were not used any further.

Despite these irregularities, which we observed for several series of electrodes, the Ag/AgI electrodes did show Nernstian behaviour and their potentials differed mutually less than a few mV. Possibly, these electrodes are mechanically not stable enough to be used in this particular electrokinetic equipment.

Platinum electrodes

With bright Pt electrodes the streaming current could only be measured at low ionic strength. Above concentrations of about 10^{-2} M these electrodes became completely polarized within the response time of the recorder. Hence, construction of an I-V plot was ineffective.

The enhanced sensitivity to polarization at high ionic strength is caused by the low plug resistance, as can be illustrated with a schematic picture of the streaming current cell (Fig. 3.12).

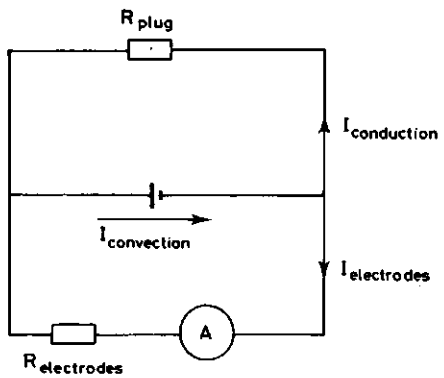

Fig. 3.12 - Schematic picture of the competing processes taking place when measuring streaming currents.

The hydrodynamically generated convection current can either be digested by the electrodes, or the charge - excess can be transported backwards through the plug as a conduction current, their ratio being dependent on the ratio of the resistances of the plug

and the electrode. The former decreases with increasing ionic strength, which promotes the conduction current. Thus, to enable the determination of the streaming current at high electrolyte concentration, the electrode resistance has to be reduced. This can be achieved by electrolytically enhancing the surface area, a process known as platinizing.

The effect of platinizing becomes obvious in Fig. 3.13a, where the retardation as well as the corresponding I-V plot for 10^{-1} M KCl is displayed. Patinizing enlarges the current through the electrodes drastically, as can be seen from the comparison with the bright Pt electrodes. Hence a meaningful I-V curve can be constructed from which the streaming current can be inferred.

Upon decreasing the ionic strength the retardation of the current through the bright Pt electrode becomes much slower, as can be seen at the left side of Figs. 3.13b and 3.13c. Useful I-V plots can easily be obtained, in which the linear parts coincide with parts of the linear I-V curves for Pt black. Therefore, the extrapolation method yields the same streaming current for both types of electrodes.

Just as with the Ag/AgCl electrodes (Fig. 3.9), extrapolation of the linear I-V curves in Fig. 3.13 to V(1',1) = 0 yields a current value that deviates from the initial one, both at low and at high ionic strength. At 10^{-1} M KCl this deviation is much less for Pt black than for Ag/AgCL electrodes (compare Figs. 3.13a and 3.9a). Nevertheless, it must be concluded that also when using Pt black electrodes it is a mistake to consider the initial current value to be the streaming current.

It is also worth mentioning that for low ionic strength the instrinsic polarization phenomena manifest themselves again clearly.

In comparing I-V curves related to Pt black and Ag/AgCl electrodes it is observed that

(i) within experimentel error, the extrapolation method yields the same streaming current for both types of electrodes, despite their strongly different electrochemical behaviour. This confirms the reliability of the method discussed.

(ii) In all cases, but especially so at low salt content, the difference between initial and final current is much bigger

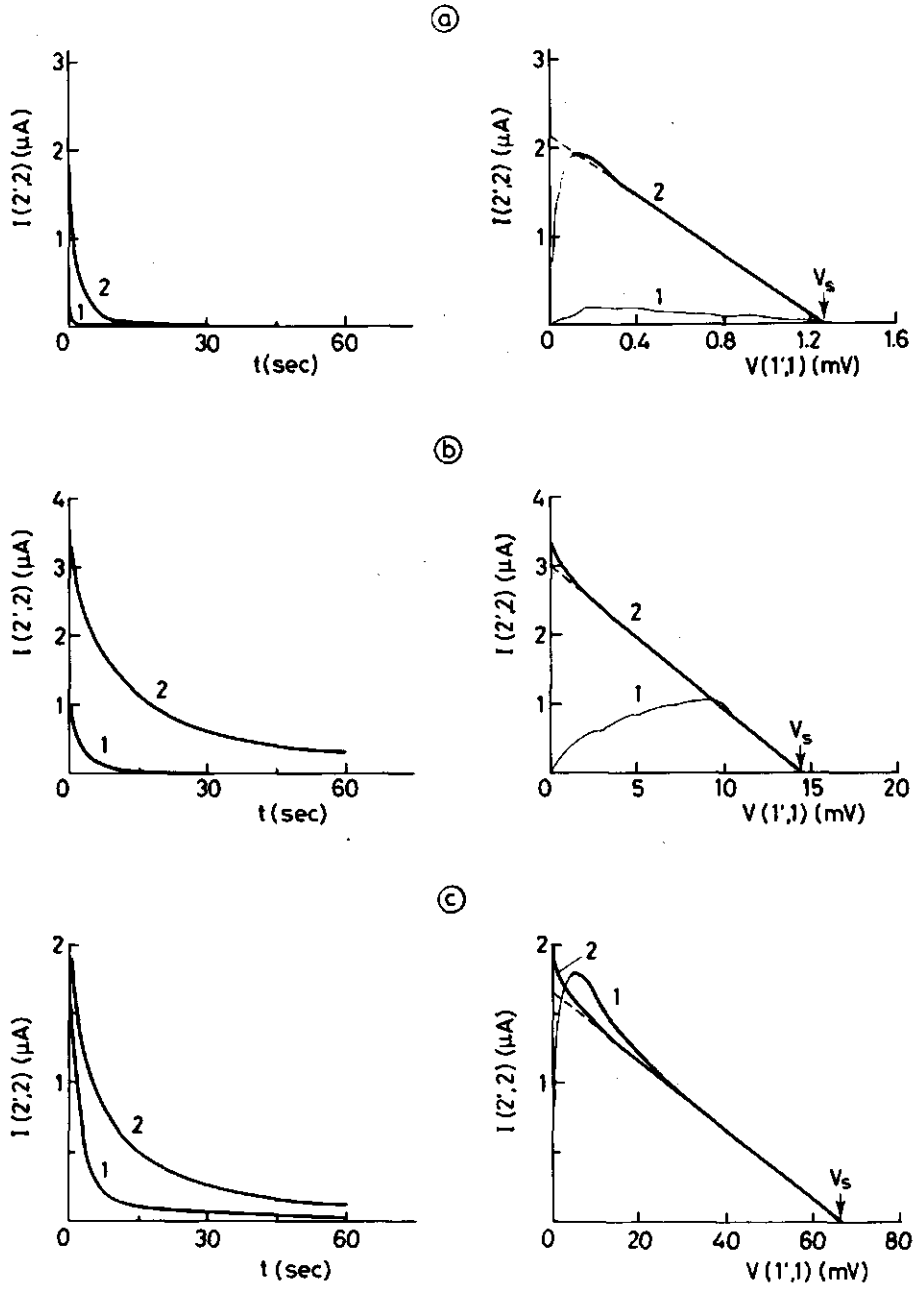

Fig. 3.13 - Current retardation and corresponding I-V plots as obtained with bright Pt (1) and black Pt (2) plug electrodes (ΔP 0 → 30 cm Hg). a,b = plug I at 10^{-1} M and 5×10^{-3} M KCl, respectively; c = plug II at 7×10^{-4} M KCL. The independently determined streaming potentials are indicated as V_s.

when using Pt black electrodes. Consequently, the I-V plots obtained with Pt black electrodes have a more extended linear part, which highly improves the accuracy of the extrapolation method.

(iii) For all ionic strengths the potential obtained by extrapolating the I-V plot for Pt black electrodes to I = 0 equals the streaming potential, whereas in the case of Ag/AgCL electrodes at low salt content differences between these quantities exist.

As to the last observation it is reminded that we ascribed these deviations to the electrolysis processes taking place during streaming current measurements. Consequently, the absence of any discrepancy between the directly measured streaming potential and the potential obtained by extrapolating the I-V curve for Pt electrodes to I = 0, forces us to conclude that faradaic currents do hardly occur at the platinum-solution interface. This seems to be contradictory to the conclusion drawn from the electrode kinetic experiments, which revealed that in aqueous solutions oxidation-reduction reactions occur at Pt electrodes (section 3.5.1). It was also noted there, however, that the oxidation process becomes less reversible with increase of coverage and potential. In addition, Vetter and Schultze (32) report an exponentially decreasing current with increasing oxide layer thickness on the Pt electrode. Hence it seems reasonable to conclude that Pt electrodes behave irreversibly on the time scale of our streaming current measurements.

In the absence of faradaic processes, the streaming current must be completely "consumed" through the charging of the double layer at the platinum-solution interface. This charging process during current passage can be followed experimentally by monitoring the potential change (polarization) of a current-carrying plug electrode with respect to the reservoir electrode at the same side of the plug. By way of example in Fig. 3.14 the polarization of the plug electrodes is shown as it occurred during the streaming current experiment with plug II at 7×10^{-4} M KCL. The relative position of the polarization curves is related to the surface area of the plug electrodes. The polarization decreases with increasing electrode area. If it is assumed that faradaic processes are

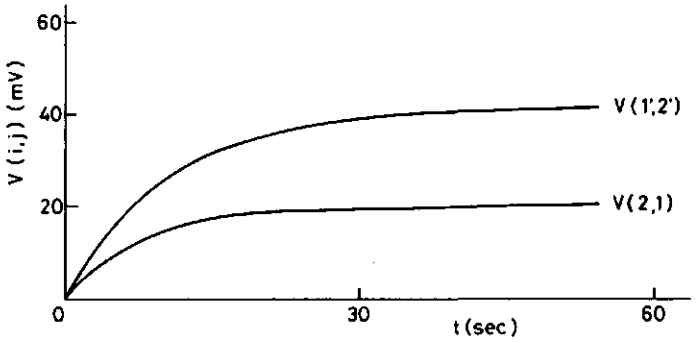

Fig. 3.14 - Polarization of Pt black electrodes during streaming current measurements (plug II, 7×10^{-4} M KCL, ΔP = 30 cm Hg).

absent, the ratio between the experimentally established electrode capacitance C_E and the calculated double layer capacitance C is a measure of the roughness factor RF of the Pt electrode. Comparison of these RF values with those usually reported for Pt black electrodes enables us to roughly verify the correctness of considering the Pt electrodes to be irreversible. C_E is obtained from the transferred amount of charge Q per unit area of the macroscopic electrode divided by the corresponding electrode polarization ΔV. In table 3.3 values of Q, ΔV and C_E at four values of the ionic strength are given, as obtained from the streaming current experiments to be presented in chapter 5 (Fig. 5.4). The results presented in Fig. 3.13 are not suitable for this analysis, because in these experiments the Pt black electrodes were not always the same.

The overall double layer capacitance C can be calculated from the capacitance of the Stern layer C_s and that of the diffuse double layer C_d according to

$$C^{-1} = C_s^{-1} + C_d^{-1} \qquad [3.6]$$

The value of C_s is found at high ionic strength, since then the diffuse contribution is negligible. For a solution of 1 M $HClO_4$ Formaro and Trasatti (33) measured a capacitance of 0.18 mF/m^2 (real surface area) at the open-circuit potential (about 0.9 V (E_H)). We adopt this value for C_s and assume it to be identical for every ionic strength. C_d can be computed from the Gouy-Chapman

equation for flat double layers (e.g. 34).

$$C_d = \varepsilon\kappa \cosh(zF\phi_d/2\ RT) \qquad [3.7]$$

where κ is the reciprocal thickness of the double layer and ϕ_d the potential at the boundary of the diffuse double layer. For the latter an arbitrary value of 50 mV was chosen for all salt concentrations. Table 3.3 presents the values of C thus obtained,

Table 3.3 - Estimation of the roughness factor RF of a Pt black electrode from the change in electrode potential ΔV as it results from the passage of an amount of charge Q in a streaming current experiment. Explanation given in the text.

KBr conc. (M)	3×10^{-4}	10^{-3}	10^{-2}	10^{-1}
Q (μC)	27.5	31.7	10.4	1.07
ΔV (mV)	16.8	17.8	5.45	0.51
C_E*(F/m^2)	16.4	17.9	19.1	21.0
C (mF/m^2)	43.6	66.3	117	154
RF	376	270	163	136

* Macroscopic electrode area 1 cm^2

together with the RF values subsequently computed from C_E and C. Since various simplifications have been made in the calculation of C, these RF values should only be considered as an indication of their order of magnitude. It can be remarked, however, that the choice of ϕ_d is not very critical. For all salt concentrations the RF value is of the order of a few hundreds, which is reasonable for Pt black electrodes (35). Consequently it is tempting to conclude that the Pt electrode current in the streaming current experiments can be ascribed to a pure charging mechanism.

3.5.2.3 COMPARISON BETWEEN THE STREAMING POTENTIAL METHOD AND THE STREAMING CURRENT METHOD

In table 3.4 results for the streaming current have been collected as they were obtained by the streaming current and (in-

Table 3.4 - Comparison between the results obtained with the streaming potential and the streaming current methods. The results are independent of the type of electrode. $K^{d.c.}$ taken from table 3.2, V_s taken from Fig. 3.7 (at ΔP = 30 cm Hg) and I_s taken from Fig. 3.9.

Plug	KCl conc. (M)	Streaming potential method $K^{d.c.} \times V_s$ (μA)	Streaming current method I_s (μA)
I	10^{-1}	2.18	2.17
I	5×10^{-3}	3.07	3.03
II	7×10^{-4}	1.64	1.66

directly) the streaming potential method, employing the four electrode technique. The latter were calculated from the product of the d.c. conductance (taken from table 3.2) and the streaming potential at ΔP = 30 cm Hg (from Fig. 3.7). In all cases we observe close agreement between the two methods. Thus the results are in accordance with the theoretical requirements (section 3.1), demonstrating again the usefulness of the discussed measuring technique.

3.6 CONCLUDING REMARKS

Various types of polarization may interfere with the signals in streaming current and electrical conductance measurements. Employing a four electrode cell enables to correct for the effect of these polarizations. When Pt black electrodes are used the four electrode method is most accurate and generally applicable. Moreover, the electrolysis taking place at the current-carrying elec-

trodes is negligible then, so that the system under investigation is not disturbed.

An I-V plot measured with Pt black electrodes, contains considerable "colloid chemical" information, such as:

(i) the current value obtained by extrapolating the linear part in the I-V curve to V = 0 informs us about the hydrodynamically mobile part of the double layer.

(ii) since the potential obtained by extrapolating the I-V curve to I = 0 coincides with the streaming potential, the slope of this curve represents the d.c. conductance of the plug. Besides the bulk and the hydrodynamically mobile part of the double layer, the fixed layer behind the shear plane may also contribute to this conductance, as will become apparent in chapters 5, 6 and 7. Since the first contribution is known and the second can be calculated from the streaming current, the fixed layer contribution can be assesed. Thus, in fact the slope of the I-V plot informs us about the stagnant part of the double layer.

(iii) as a consequence of the extended linear part in the I-V plot, it is easy to discriminate between the effects of electrode polarization and intrinsic polarization. In chapter 5 we will show that the latter gives access to the surface structure of polystyrene particles.

3.7 REFERENCES

1. Overbeek, J.Th.G. in "Colloid Science (H.R. Kruyt, Ed.), Vol. 1, Elsevier. Amsterdam, 1952.
2. Dukhin, S.S. and Derjaguin, B.V. in "Surface and Colloid Science" (E. Matijević, Ed.), Vol. 7, Wiley, New York, 1974.
3. Katchalsky, A. and Curran, P.F., "Nonequilibrium Thermodynamics in Biophysics", Harvard University Press, Cambridge, 1975.
4. Watillon, A. and de Backer, R., J. Electroanal. Chem. 25, 181 (1970).
5. Ardizzone, S. and Formaro, L., Chim. Ind. 60, 801 (1978).
6. Van der Put, A.G., Thesis, Agricultural University, Wageningen (1980).
7. Schausberger, A. and Schurz, J., Angew. Makromol. Chem. 80, 1

(1979).
8. Goring, D.A.I. and Mason, S.G., Can. J. Res. B 28, 323 (1950).
9. Van der Put, A.G. and Bijsterbosch, B.H., Acta Polym. 32, 311 (1981).
10. Aichele, W., Schollmeyer, E. and Herlinger, H., Makromol. Chem. 178, 2025 (1977).
11. Jednacak, J., Pravdić, V. and Haller, W., J. Colloid Interface Sci. 49, 16 (1974).
12. Somasundaran, P. and Kulkarni, R.D., J. Colloid Interface Sci. 45, 591 (1973).
13. Sidorova, M.P., Tasev, D.K. and Fazylova, M., Kolloidn. Zh. 38, 723 (1976).
14. Goring, D.A.I., Biefer, G.J. and Mason, S.G., Can. J. Res. B. 28, 339 (1950).
15. Subrahmanyan, V. and Lakshminarayanaiah, N., J. Phys. Chem. 72, 4314 (1968).
16. Holmes, H.F., Shoup, C.S. and Secoy, C.M., J. Phys. Chem. 69, 3148 (1965).
17. Eversole, W.G. and Boardman, W.W., J. Phys. Chem. 46, 914 (1942).
18. Wijga, P.W.O., Thesis, State University, Utrecht (1946).
19. Zorin, Z.M., Lashnev, V.I., Sidorova, M.P., Sobolev, V.D. and Churaev, N.V., Kolloidn. Zh. 39, 1012 (1977).
20. Schwan, H.P., Biophysik 3, 181 (1966).
21. Pravdić, V. and Bonacci, N. in "Colloid and Interface Science" (M. Kerker, Ed.), Vol. 4, Academic Press. New York, 1976.
22. Gur, Y., J. Colloid Interface Sci. 72, 222 (1979).
23. Brown, A.S., J. Am. Chem. Soc. 56, 646 (1934).
24. De Keizer, A., Thesis, Agricultural University, Wageningen (1981).
25. Ives, D.J.G. and Janz, G.J., "Reference Electrodes", p. 106. Academic Press, New York, 1961.
26. Angerstein-Kozlowska, H., Conway, B.E. and Sharp, W.B.A., J. Electroanal. Chem. 43, 9 (1973).
27. Delahay, P., "Double Layer and Electrode Kinetics", p. 258, Interscience, New York, 1965.
28. Korpi, G.K. and de Bruyn, P.L., J. Colloid Interface Sci. 40,

263 (1972).
29. Hunter, R.J. and Alexander, A.E., J. Colloid Sci. 17, 781 (1962).
30. Horn, J.M. and Onoda, G.Y., J. Colloid Interface Sci. 61, 272 (1977).
31. Lakshminarayanaiah, N., "Transport Phenomena in Membranes", p. 230. Academic Press, New York, 1969.
32. Vetter, K.J. and Schultze, J.W., J. Electroanal. Chem. 34, 131 (1972).
33. Formaro, L. and Trasatti, S., Electrochim. Acta 12, 1457 (1967).
34. Bijsterbosch, B.H. and Lyklema, J., Adv. Colloid Interface Sci. 9, 147 (1978).
35. Formaro, L., personal communication.

CHAPTER 4

INFERENCE OF DOUBLE LAYER CHARACTERISTICS FROM ELECTROKINETIC AND ELECTRICAL CONDUCTANCE DATA

4.1 INTRODUCTION

Electrokinetic and electrical conductance data obtained on dispersions can yield valuable information on the electrical double layer. The relations employed in this evaluation have to meet a number of requirements. Firstly, the expressions should be based upon a geometric model that is appropriate to the actual internal structure of the system under investigation. Secondly, the influence of surface conductance and double layer interaction must have been taken into account. When dealing with systems in which the applied electrical and/or hydrodynamic field lines in the double layer do not run parallel to the wall, the formulae should include the effect of the ensuing change in the volume charge distribution (double layer polarization).

Theories on electrokinetic phenomena as well as electrical conductivities are available for various geometric structures, e.g. slits, capillaries and arrays of identical spherical particles (cell models). From a geometric point of view the latter are the most suitable ones for our polystyrene plugs. Another attractive feature of cell model theories is that, at least partially, the polarization concept has been incorporated. Unfortunately, however, cell model calculations on electrokinetic phenomena are still rather incomplete. The most elaborate ones have been formulated by Levine et al. They presented results for the electrophoretic and electroosmotic velocity (1) and the sedimentation potential (2). The latter can easily be transformed into an expression for the streaming potential (3). All formulae, however, have been derived for the limiting case of small zeta potentials (< 25 mV). Consequently, valid application to most of the electrokinetic data obtained in this work is precluded. In addition, the usefulness of the cell model predictions is restricted because the hydrodynamically induced double layer polarization has not been incorporated in the equations for the convection current. Therefore, in the

analysis of electrokinetic data obtained on polystyrene plugs we will restrict ourselves to the more elaborate capillary models.

For the analysis of the data obtained with the silver iodide plugs, the capillary model appears to be the most suitable one. Cell model theories can not be applied, since silver iodide suspensions are neither monodisperse nor composed of spherical particles.

In the following sections the theories will be discussed, that have been applied in obtaining zeta potentials and surface conductivities from electrokinetic phenomena and electrical conductivities, respectively. Thereafter the theoretical connection between the zeta potential and surface conductivity will be considered.

4.2 EVALUATION OF THE ZETA POTENTIAL FROM ELECTROKINETIC PHENOMENA BY MEANS OF CAPILLARY MODELS

Electrokinetic flow through capillaries of cylindrical cross-section has been the subject of various theoretical studies, in which conditions of constant surface potential (e.g. 4,5,6) as well as constant surface charge (7,8) have been treated. The constant charge models are the most appropriate ones for polystyrene systems, but these have not been applied, because even the most elaborate one (that of Anderson and Koh (8)) does not completely cover the range of charge densities and electrokinetic radii (= ratio of the capillary radius a to the double layer shielding length κ^{-1}) encountered in our experiments. Anderson and Koh considered κa values below 10, whereas for the pore sizes of our polystyrene plugs (a = about 100 nm) their numerical calculations refer only to charge densities below about 20 mC/m^2.

Most of the capillary theories referring to constant surface potential include formulae relating both the streaming current I_s and streaming potential V_s (or electroosmosis) to ζ, a and κ^{-1}. Unfortunately, all expressions for V_s appear to be incorrect in varying degrees, because they do not take proper account of the conduction current flowing under streaming potential conditions. Firstly, the contribution of surface conductance is either not (4) or only partly (6) (i.e. as far as occurring outside the shear plane) incorporated in the expressions for the capillary conductance. As will become apparent in the following chapters, the con-

ductance in the immobile as well as the hydrodynamically mobile part of the double layer may contribute substantially to the overall conductance of a porous medium. Consequently, the omission of this contribution in the theoretical description of the conductance and the streaming potential seriously reduces the applicability of these theories. Another, though less serious, simplification in the derivation of the equations for V_s concerns the assumption that the cations and anions have identical mobilities. Obviously these problems can be overcome by simply using the measured value of the conductance in the streaming potential equations. As a matter of fact, the theoretical analysis is then confined to a description of the streaming current.

The Helmholtz-Smoluchowski (H-S) formula (eq. 3.1) may be considered the most simple capillary model prediction for the streaming current. Apart from adopting laminar flow and constant values of the permittivity ε and the viscosity η of the solution throughout the capillary, a crucial assumption underlying this formula is that the double layer is thin compared to the capillary radius ($\kappa a >> 1$). This assumption allows considerable simplification of the mathematics. Firstly, the liquid velocity profile in the region of the double layer, being strictly parabolic, can be considered as linear (see e.g. ref. 9). Secondly, the Poisson equation can be used in the one-dimensional form. It is noted that the assumption $\kappa a >> 1$ implies the double layer to be developed completely, so that no overlap takes places.

The H-S equation can be extended to arbitrary κa values by combining the complete Navier-Stokes and Poisson equations. The following general expression results (6):

$$\frac{I_s}{\Delta P} = \frac{\varepsilon \zeta}{\eta C_p} \left[1 - G(\kappa a, \tilde{\zeta})\right] \qquad [4.1]$$

$$\text{with } G(\kappa a, \tilde{\zeta}) = \frac{2}{(\kappa a)^2 \tilde{\zeta}} \int_0^{\kappa a} \tilde{r}\, \tilde{\psi}(\tilde{r}) d\tilde{r} \qquad [4.2]$$

where ΔP denotes the applied pressure drop across the matrix and C_p its cell constant. $\tilde{r}$, $\tilde{\psi}(\tilde{r})$ and $\tilde{\zeta}$ represent, in dimensionless form, the radial distance from the axis ($r = \kappa r$), the double layer potential at r ($\tilde{\psi}(\tilde{r}) = e\psi(r)/kT$) and the electrokinetic potential

($\tilde{\zeta} = e\zeta/kT$), respectively. $G(\kappa a, \tilde{\zeta})$ is the ratio of the mean potential over the capillary cross-section to the ζ-potential. This term becomes zero for high values of the electrokinetic radius κa. In fact (1-G) represents the correction factor to the Helmholtz-Smoluchowski result when dealing with systems with small electrokinetic radii.

To enable the evaluation of G, the potential profile $\tilde{\psi}(\tilde{r})$ has to be known. Unfortunately, there is no analytical expression for ψ that satisfies the Poisson-Boltzmann equation for cylindrical geometry. For potentials sufficiently low to permit the Debye-Hückel approximation, however, an exact expression for $\tilde{\psi}(\tilde{r})$ is available. Rice and Whitehead (4) have shown that under these conditions

$$1-G(\kappa a) = 1 - \frac{2\, I_1(\kappa a)}{\kappa a\, I_0(\kappa a)} \qquad [4.3]$$

in which I_0 and I_1 are zero- and first-order modified Bessel functions of the first kind, respectively. Starting from different approximate descriptions of the potential distribution in the capillary, Oldham et al. (5) and Levine et al. (6) have derived analytical formulae for G for arbitrary values of the zeta potential. The results predicted by both approximate treatments differ only within a few percent. Despite the analytical expressions both theories can not conveniently be applied because the expressions are mathematically very difficult to handle. In order to bridge the gap between these theories and practical electrokinetic investigations, Olivares et al. (10) recently extended the Rice and Whitehead theory to higher potentials, while preserving its algebraic simplicity. In their treatment they appproximate the actual solution of the Poisson-Boltzmann equation by a trial function of the simple form

$$\tilde{\psi}(\tilde{r}) = \tilde{\zeta}\, \frac{I_0(q\tilde{r})}{I_0(q\kappa a)} \qquad [4.4]$$

q represents a parameter which for $1 \leq \kappa a \leq 1000$ and $\tilde{\zeta} \leq 6$ within a few percent can be given by

$$q = [\exp(0.0412\ \tilde{\zeta}^2) + 0.0698\ (\tilde{\zeta}/\kappa a)^2]^{\frac{1}{2}} \qquad [4.5]^*$$

Although Olivares et al. don't explicitly state it, it is possible (11) to derive an analytical expression for (1-G) by substituting eq. 4.4 and 4.5 into eq. 4.2. The resulting expression has a form that is analogous to the Rice and Whitehead formula 4.3 and reads

$$1-G(\kappa a,\tilde{\zeta}) = 1 - \frac{2}{q\kappa a}\ \frac{I_1(q\kappa a)}{I_0(q\kappa a)} \qquad [4.6]$$

Note that for low ζ-potentials eq. 4.6 reduces to eq. 4.3 indeed. In Fig. 4.1 graphs of (1-G) versus log(κa) have been given as

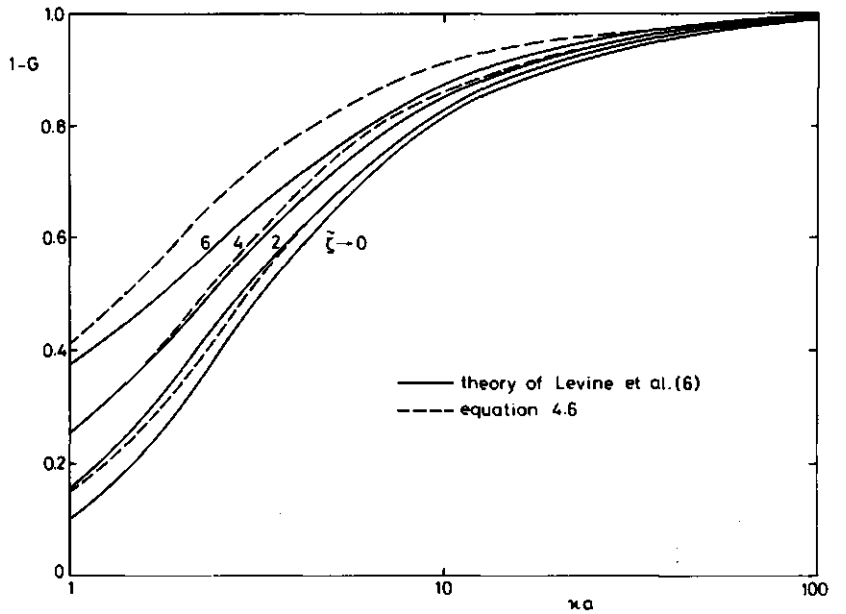

Fig. 4.1 - The quantity (1-G) as a function of log(κa) for various values of $\tilde{\zeta}$ as obtained from the theory of Levine et al. (ref. 6, Fig. 4) and as computed from eq. 4.6.

* In the original paper the proportionality constant for the second term is given as 0.698. Correspondence with the authors pointed out that eq. 4.5 is the correct form.

computed from eq. 4.6 for $\tilde{\zeta}$ = 0, 2, 4 and 6. The results are in complete agreement with those obtained by numerical calculations of Olivares et al. Comparison with curves referring to the Levine theory, which coincide within a few percent with the Oldham predictions, shows satisfactory agreement for $\tilde{\zeta} < 4$.

Since the κa and $\tilde{\zeta}$ values of the polystyrene plugs are in the region where eq. 4.6 completely fits the Levine and Oldham theories, the evaluation of zeta potentials from streaming current data (or for that matter the product of streaming potential and d.c. plug conductance) obtained on these plugs has been performed with eq. 4.1 using expression 4.6 for (1-G). This evaluation involves the following steps:

1. computation of κa from

$$\kappa = \left(\sum_i \frac{c_i z_i^2 F^2}{\epsilon RT}\right)^{\frac{1}{2}} \qquad [4.7]$$

and

$$a = \frac{1-p}{3p} d \qquad [4.8]$$

in which c_i and z_i are the bulk concentration and valency of ion i, respectively. p denotes the volume fraction and d the diameter of the particles composing the plug. Formula 4.8 is the expression for the hydraulic radius (12), when the plug is assumed to be equivalent to a bundle of parallel capillaries of equal size.

2. Calculation of ζ from I_s by means of the H-S equation 3.1. The required value of C_p is obtained as the ratio of the bulk conductivity to the plug conductance at high salt content (10^{-1} M), where the contribution of surface conductance can be neglected.
3. Calculation of the correction factor (1-G) according to eq. 4.6. Then, a first corrected zeta potential ζ_1 is determined from

$$\zeta_1 = \frac{\zeta}{1-G(\kappa a, \tilde{\zeta})} \qquad [4.9]$$

4. Repetition of the correction procedure described in step 3 until the difference between two subsequently corrected zeta potentials is negligible.

All experiments on silver iodide plugs refer to conditions of large electrokinetic radii ($\kappa a > 70$), so that, according to Fig. 4.1 $(1-G) \approx 1$. Hence, the simple H-S equation can be applied.

Conversion of the zeta potential into the electrokinetically displaceable charge σ_{ek} and subsequent comparison with the surface charge density σ_o gives information on the charge distribution in the electrical double layer. For high values of the electrokinetic radius this conversion can be achieved with the Gouy-Chapman theory for flat double layers

$$\sigma_{ek} = (8\ \varepsilon RTc)^{\frac{1}{2}} \sinh(\tilde{\zeta}/2) \qquad [4.10]$$

This expression is applicable to all results obtained with silver iodide plugs, because of the high κa values. For the low κa values encountered in the measurements on polystyrene plugs, the influence of the (spherical) particle shape on the diffuse double layer structure has to be taken into account. Unfortunately, no exact analytical charge-potential relation exists for this geometry. Applying the available numerical data (13) to the lowest experimental κa value (about 5) and a typical ζ-potential of 50 mV, it appears that eq. 4.10 underestimates σ_{ek} by about 10 percent. Thus it can be stated that eq. 4.10 is also useful for the electrokinetic data obtained on the polystyrene plugs, especially so since, as will become apparent, at low salt content σ_{ek} constitutes only a small part of the total double layer charge.

4.3 EVALUATION OF THE SURFACE CONDUCTIVITY FROM CONDUCTANCE DATA BY MEANS OF CAPILLARY AND CELL MODELS

The ion excess in the electrical double layer near a charged interface provides an additional contribution to the conductance of a system. This contribution is called surface conductivity and may be considered an important source of information about the properties of the electrical double layer. Most commonly the surface conductivity κ^σ in a diaphragm is calculated according to the Street equation (14), which may be written as

$$\kappa^\sigma = (KC_p - K_o)\ \frac{V}{S}\ (1-p) \qquad [4.11]$$

where K is the conductance of the plug, C_p its conductometric cell constant, K_o the conductivity of the solution, V the overall plug volume, S the overall surface area and p the volume fraction of the dispersed phase. For plugs consisting of monodisperse spherical particles of diameter d eq. 4.11 becomes

$$\kappa^\sigma = (KC_p - K_o) \frac{(1-p)}{6p} d \qquad [4.12]$$

whereas for an arrangement of parallel capillaries of radius a one may write

$$\kappa^\sigma = (KC_p - K_o) \frac{a}{2} \qquad [4.13]$$

The Street theory depicts the plug as a bundle of parallel capillaries. Consequently, the effect of double layer polarization is inherently ignored. In general, however, the double layer around charged particles in a colloidal dispersion will be deformed under the influence of an external electrical field. As a result, a polarization field is generated counteracting the externally applied one. Contrary to hydrodynamically induced double layer polarization, theoretical expressions have been derived for the polarization field induced by an electrical field. Booth (15) and Henry (16) calculated the distribution of the polarization potential around a conducting spherical particle, surrounded by a shell with different conductivity. From their expressions the induced dipole moment μ of a single non-conducting spherical particle with surface conductivity κ^σ can be obtained as

$$\mu = - \frac{d^3}{16} E \left(1 - \frac{6\ \kappa^\sigma/K_o d}{1 + 2\ \kappa^\sigma/K_o d}\right) \qquad [4.14]$$

where E denotes the externally applied electrical field strength.

In the Henry and Booth theory it is assumed that the ionic transfer processes between double layer and bulk region are fast enough to maintain the tangential surface currents occurring when an external electrical field is applied. It has been shown (17), however, that in polarizing the double layer the ion concentrations not only change within the double layer, but also in the bulk re-

gion beyond it, in such a way that concentration differences along the external boundary of the double layer arise. Taking account of this so-called double layer concentration polarization, Dukhin and Semenikhin (18) have derived an analytical expression for the potential distribution in a deformed double layer around a spherical particle. The ensuing potential distribution corresponds to the following dipole moment (19)

$$\mu = \frac{d^3}{16} E \left(1 - \frac{6\ \kappa^{\sigma}/K_o d}{1 + 4\ \kappa^{\sigma}/K_o d}\right) \qquad [4.15]$$

This expression holds for relatively high κa and low ζ values. Comparing eqs. 4.15 and 4.14 it appears that incorporation of the concentration polarization concept leads to an increase of the calculated induced dipole moment, reflecting the retarding effect of concentration polarization on surface conductance.

Based on the above expressions for the induced dipole moment and thus accounting for the effect of double layer polarization, Van der Put and Bijsterbosch (20) recently presented formulae relating the surface conductivity in concentrated dispersions to K_o, K and p. Following a procedure previously employed by Bruggeman (21), they obtained their expressions by integrating the Wagner equation for dilute dispersions. In differential form this equation reads

$$d\bar{K}(p) = \frac{4\pi\mu(\bar{K}, \kappa^{\sigma})}{vE} \bar{K}(p) \frac{dp}{1-p} \qquad [4.16]$$

in which $\bar{K}$ is the conductivity of the whole dispersion (= $K.C_r$, where C_r represents the cell constant of the plug holder) and v the volume of one particle. As noted by Dukhin and Derjaguin (22) and experimentally confirmed by Van der Put and Bijsterbosch (20), μ is determined by $\bar{K}$ rather than by K_o.

Integrating eq. 4.16 either substituting expression 4.14 or 4.15 one arrives at the following expressions for κ^{σ}, respectively:

$$\kappa^{\sigma} = \frac{K_o\, d\, [(1-p)(\bar{K}/K_o)^{1/3} - \bar{K}/K_o]}{4(1-p)(\bar{K}/K_o)^{1/3} - 4} \qquad [4.17]$$

$$\kappa^{\sigma} = \frac{K_o\, d\, [(1-p)^{\frac{1}{2}}(\bar{K}/K_o)^{2/3} - \bar{K}/K_o]}{2(1-p)^{\frac{1}{2}}(\bar{K}/K_o)^{2/3} - 2} \qquad [4.18]$$

Formula 4.17 is identical to the Bruggeman equation concerning suspensions of conducting particles (21), when $2\kappa^{\sigma}/a$ is taken to represent the particle conductance.

The evaluation of surface conductances from conductance data obtained on polystyrene plugs will be performed with eq. 4.12, 4.17 and 4.18. The data obtained on silver iodide plugs will be analyzed using eq. 4.13.

It can yet be remarked that other conversion models have been published as well (see, e.g. ref. 20), but these are not considered, since they are either less sophisticated or empirical, i.e. missing a physical background.

4.4 SURFACE CONDUCTIVITY AS CONTRIBUTED BY THE MOBILE AND THE STAGNANT PART OF THE DOUBLE LAYER

The contribution to the surface conductivity of the diffuse double layer ions residing outside the shear plane can be computed from the zeta potential. Among the various theories concerning this relationship, that of Bikerman (23) is the most rigorous. In this theory the contribution of migration as well as electroosmotic displacement of the excess charge density due to counterions σ_t and the charge density deficit due to co-ions σ_c is accounted for. For a symmetrical monovalent electrolyte the Bikerman equation reads:

$$\kappa^{\sigma} = F^{-1}\,[\sigma_t\lambda_t - \sigma_c\lambda_c + \sigma_t(2\,\varepsilon RT/\eta) - \sigma_c(2\,\varepsilon RT/\eta)] \qquad [4.19]$$

where F denotes the Faraday constant and λ_t and λ_c the equivalent conductivities of the counter- and co-ions, respectively.
The first two terms in eq. 4.19 represent the migration, the last two the electroosmosis. By relating σ_t and σ_c to the zeta potential via the theory for flat double layers, eq. 4.19 can be transformed into

$$\kappa^{\sigma} = (2\,\varepsilon RTc/F^2)^{\frac{1}{2}}\,[(\exp(\tilde{\zeta}/2) - 1)(\lambda_t + 2\,\varepsilon RT/\eta) +$$

$$+ (\exp(-\tilde{\zeta}/2) - 1)(\lambda_c + 2\,\varepsilon RT/\eta)] \qquad [4.20]$$

As to the validity of this equation at small κa values we refer to section 4.2.

For mixtures of 1-1 electrolytes, as used in this work, eq. 4.20 can be extended to

$$\kappa^{\sigma} = (2\ \varepsilon RTc_t/F^2)^{\frac{1}{2}} \sum_i (c_i/c_t)[(\exp(\tilde{\zeta}/2) - 1)(\lambda_t^i + 2\ \varepsilon RT/\eta) +$$

$$+ (\exp(-\tilde{\zeta}/2) - 1)(\lambda_c^i + 2\ \varepsilon RT/\eta)] \qquad [4.21]$$

where $c_t = \sum_i c_i$

More often than not, the fixed layer between the slipping plane and the solid surface also contributes to the conductance. This contribution can be incorporated in eq. 4.19 as follows (24)

$$\kappa^{\sigma} = F^{-1}[\sigma_t^{\Delta}\lambda_t^{\Delta} - \sigma_c^{\Delta}\lambda_c^{\Delta} + \sigma_t\lambda_t - \sigma_c\lambda_c + \sigma_t(2\ \varepsilon RT/\eta) -$$

$$- \sigma_c(2\ \varepsilon RT/\eta)] \qquad [4.22]$$

where σ_t^{Δ} is the excess charge density in the fixed layer due to the counterions, σ_c^{Δ} the charge density in that layer due to the deficit of co-ions and λ_t^{Δ} and λ_c^{Δ} are the equivalent conductivities of the counter- and co-ions in the boundary layer, respectively. Note that σ_t and σ_c in eq. 4.22 refer only to the double layer region outside the plane of shear. We will refer to this expression as the modified Bikerman equation.

Assuming also a Gouy-Chapman distribution of ions in the fixed layer, for flat double layers in mixtures of 1-1 electrolytes eq. 4.22 can be written as

$$\kappa^{\sigma} = (2\ \varepsilon RTc_t/F^2)^{\frac{1}{2}} \sum_i (c_i/c_t)[(\exp(\tilde{\psi}_d/d) - \exp(\tilde{\zeta}/2))\lambda_t^{i,\Delta} +$$

$$+ (\exp(-\tilde{\psi}_d/2) - \exp(-\tilde{\zeta}/2))\lambda_c^{i,\Delta} + (\exp(\tilde{\zeta}/2) - 1)(\lambda_t^i + 2\ \varepsilon RT/\eta) +$$

$$+ (\exp(-\tilde{\zeta}/2) - 1)(\lambda_c^i + 2\ \varepsilon RT/\eta)] \qquad [4.23]$$

in which $\tilde{\psi}_d$ represents the dimensionless diffuse double layer potential.

4.5 REFERENCES

1. Levine, S. and Neale, G.H., J. Colloid Interface Sci. 47, 520 (1974).
2. Levine, S., Neale, G. and Epstein, N., J. Colloid Interface Sci. 57, 424 (1976).
3. Van der Put, A.G. and Bijsterbosch, B.H., J. Colloid Interface Sci. 92, 499 (1983).
4. Rice, C.L. and Whitehead, R., J. Phys. Chem. 69, 4017 (1965).
5. Oldham, I.B., Young, F.J. and Osterle, J.F., J. Colloid Sci. 18, 328 (1963).
6. Levine, S., Marriott, J.R., Neale, G. and Epstein, N., J. Colloid Interface Sci. 52, 136 (1975).
7. Sørensen, T.S. and Koefoed, J., J. Chem. Soc. Faraday Trans. II 70, 665 (1974).
8. Anderson, J.L. and Koh, W., J. Colloid Interface Sci. 59, 149 (1977).
9. Dukhin, S.S. and Derjaguin, B.V., in "Surface and Colloid Science" (E. Matijević, Ed.), Vol. 7, p. 69, Wiley, New York, 1974.
10. Olivares, W., Croxton, T.L. and McQuarrie, D.A., J. Phys. Chem. 84, 867 (1980).
11. Bowman, F., "Introduction to Bessel Functions", Dover Publ. Inc., New York (1958).
12. Bird, R.B., Stewart, W.E. and Lightfoot, E.N., "Transport phenomena", p. 197, Wiley, New York (1960).
13. Loeb, A.L., Wiersema, P.H. and Overbeek, J.Th.G., "The electrical double layer around a spherical colloid particle", MIT Press, Cambridge (1960).
14. Street, N., Aust. J. Chem. 9, 333 (1956).
15. Booth, F., Trans. Faraday Soc. 44, 955 (1948).
16. Henry, D.C., Trans. Faraday Soc. 44, 1021 (1948).
17. Derjaguin, B.V. and Dukhin, S.S. in "Surface and Colloid Science" (E. Matijevic, Ed.), Vol. 7, p. 297, Wiley, New York, 1974.
18. Dukhin, S.S. and Semenikhin, N.M., Kolloidn.Zh. 32, 360 (1970).
19. Pilgrimm, H., Sonntag, H. and Dukhin, S.S., Colloid & Polymer Sci. 253, 750 (1975).

20. Van der Put, A.G. and Bijsterbosch, B.H., J. Colloid Interface Sci . 75, 512 (1980).
21. Reference 9, p. 228.
22. Reference 9, p. 227.
23. Bikerman, J.J. Kolloid. Z. 72, 100 (1935).
24. Watillon, A. and De Backer, R., J. Electroanal. Chem. 25, 181, (1970).

CHAPTER 5

ELECTROKINETIC PROPERTIES AND CONDUCTANCE RELAXATION OF POLYSTYRENE PLUGS

5.1 INTRODUCTION

Polymer latices are widely used as model systems in colloid chemistry, mainly because of their geometric ideality (monodispersity, spherical particles). To serve as a model colloid, however, other requirements should also be fulfilled. In particular, the surface of the polymer particles has to be smooth and rigid, i.e. the polymer chains in the outer region of the particles should be firmly bound to the core. However, a number of recent investigations (1,2) indicate this not to be the case.

In the present chapter the structure of the polystyrene-solution interface is investigated by analyzing data obtained with the electrokinetic techniques described in chapter 3. In addition, frequency-spectra of the a.c. conductance of polystyrene plugs have been measured in order to obtain further insight into the relaxation phenomena taking place during streaming current measurements (chapter 3). In combination with the electrokinetic data these spectra provide additional information on the properties of the surface layer on polystyrene particles.

Experiments have been conducted for various salt concentrations, using polystyrene latices prepared and handled according to the procedures described in chapter 2.

5.2 EXPERIMENTAL

5.2.1 MATERIALS

Monodisperse polystyrene latex was prepared by emulsifier-free dispersion polymerization, according to the method of Furusawa et al. (3). The initiator and buffer ($KHCO_3$) concentration were 1.85×10^{-3} M and 10^{-2} M, respectively.

After preparation the electrolyte content of the latex sample was adjusted to 10^{-1} M. This treatment was prompted by the obser-

vation that the surface charge density of untreated latex irreversibly increases upon the first contact with a solution of high ionic strength (see chapter 2). A second treatment has no further influence. When omitting the salt treatment before preparing the plug, the charging process may occur during the various measurements, thereby prohibiting a reliable analysis of the experimental data.

Subsequently, the sample was purified by ion exchange and steam stripping, and stored at pH = 7 (chapter 2).

The number average particle diameter as determined from electron micrographs amounted to 638 ± 3 nm. The surface charge density as obtained by conductometric titration was 83 ± 1 mC/m^2. Only strong acidic groups were observed.

KBr, KCl and KI (A.R. quality) were used as electrolytes. The water used was distilled once.

5.2.2 PLUG PREPARATION

Several plugs were prepared by centrifuging the latex at about 2000 g. With this centrifugal acceleration the critical coagulation pressure (4) was exceeded by an order of magnitude. Using untreated latex, completely coagulated, mechanically very stable plugs were obtained irrespective of the ionic strength (up to 10^{-1} M). In preparing plugs from treated samples, however, the ionic strength proved to be critical. Stable plugs were only obtained when the latex contained about $3x10^{-2}$ M electrolyte. Plugs prepared at other salt levels were swampy. When positioned in the electrokinetic equipment some immediately disintegrated upon pressure application, others continuously produced clouds of latex during liquid permeation, indicating incomplete coagulation. Increasing the coagulation pressure by a factor of ten had no effect. It is difficult to explain this phenomenon, but some mechanisms that may be involved can be indicated. The salt treatment may have promoted the association of particles in the latex sample. It is conceivable that the presence of aggregates lowers the homogeneity and consequently the mechanical stability of the plug. Another possibility is that the salt treatment has affected the surface and electrical double layer properties of the polystyrene particles, through which the stab-

ility of the latex sample has changed.

The porosity of the plugs was calculated from the overall plug volume and the density (1.05×10^3 kg/m^3) and the weight of the total assembly of plug particles. The latter was determined by drying the plug at 80 °C until no changes in the weight were observed any longer. For all stable plugs the porosity was close to 0.4, which is considerably higher than corresponds to a hexagonal close-packing of the particles (0.26). Apparently, to some extent a disordered array of particles has been formed. The same conclusion follows from an examination of scanning electron micrographs of cross-sections of polystyrene plugs. An example is shown in Fig. 5.1. The scanning electron microscopy was carried out on a Jeol JSM-35. Prior to scanning the (wet) plug was freeze-dried, treated with osmium vapour and sputter-coated with a layer of gold.

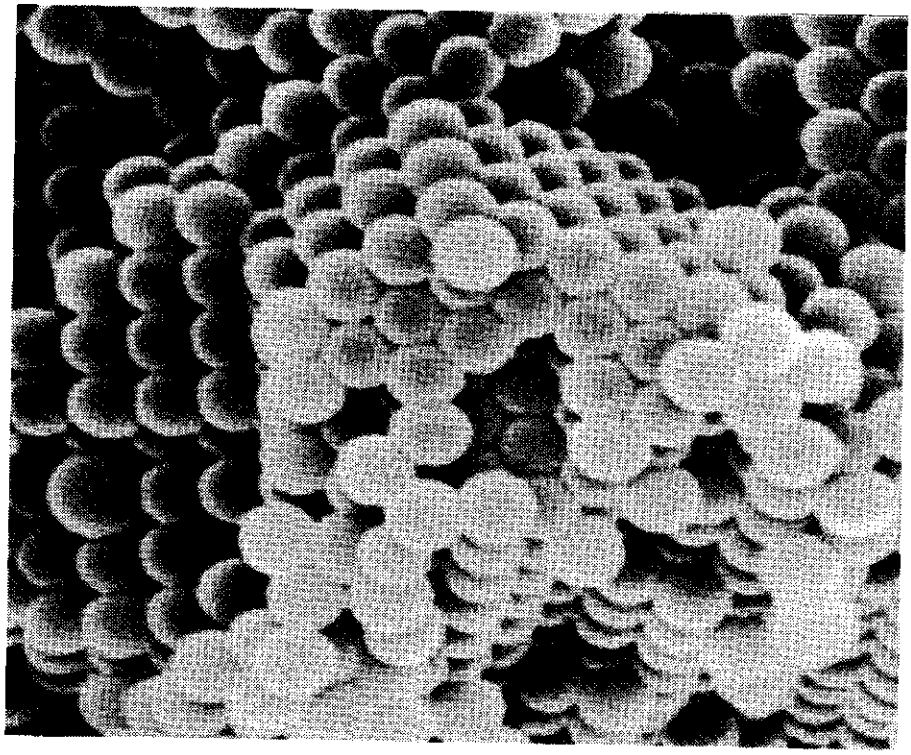

Fig. 5.1 - Scanning electron micrograph of part of a polystyrene plug.

Of the various plugs studied only one representative example will be discussed (porosity = 0.400, conductometric cell constant = 729 m^{-1}).

5.2.3 METHODS

Electrokinetic data were obtained using the four electrode (Pt black) technique described in chapter 3. The equipment employed in these experiments has also been described there.

The liquid permeability of the plug was determined from the rate of displacement of the liquid meniscus in a capillary connected to the electrokinetic cell (see Fig. 3.4) and the radius of this capillary. The latter was obtained by weighing the capillary twice, once empty and once filled with mercury.

A.c. conductances (admittances) of the plug in the frequency range from 0.01 to 1000 Hz were determined by the four electrode technique. In this way any interference by electrode polarization was excluded. In Fig. 5.2 the electrical circuit of the experimental set-up is presented. An alternating (sinusoidal) current of frequency f was passed through the medium under investigation by means of an a.c. generator (Feedback FG 600) connected to the

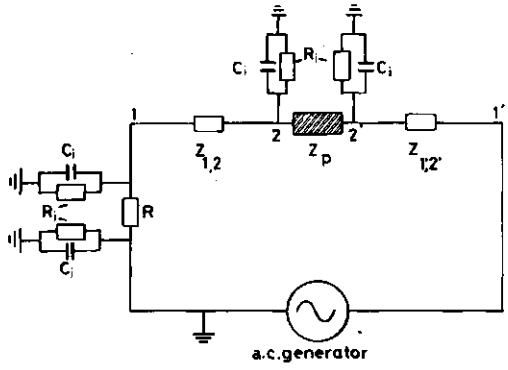

Fig. 5.2 - Electrical circuit of the experimental set-up for measuring a.c. conductances (admittances). The symbols are defined in the text.

reservoir electrodes 1 and 1'. The magnitude of this current (varying from a few μA at $3x10^{-4}$ M to about 100 μA at 10^{-1} M) was determined from the potential drop V_R across a known precision resistor R, which was chosen in the same order of magnitude as the plug impedance Z_p. The latter was calculated from the ensuing change in potential difference between the electrodes 2 and 2' making direct contact with the plug, V(2',2), according to

$$Z_p = \frac{V(2',2)}{V_R} R \qquad [5.1]$$

An oscilloscope (Tektronix 5103 N with differential input) was used as potential measuring device. At frequencies below about 0.1 Hz use was also made of a digital electrometer (Keithley 616).

An essential requirement in applying this method is that the currents through the resistor and through the plug are identical, implying leakage currents to earth to be absent in the circuit encompassing Z_p, $Z_{1,2}$ and R. $Z_{1,2}$ represents the impedance of the solution between the reservoir electrode 1 and the plug electrode 2. From Fig. 5.2 it is readily seen that the said condition is met when R, Z_p and $Z_{1,2}$ are small as compared to the input impedance Z_i of the oscilloscope, which is given by

$$Z_i = R_i \, (1+ 4\pi^2 f^2 C_i^2 R_i^2)^{-\frac{1}{2}} \qquad [5.2]$$

where R_i and C_i denote the input resistance (10^6 Ω) and capacitance (47 pF) of the oscilloscope, respectively.
In this connection the value of $Z_{1',2'}$, representing the impedance of the solution between the electrode 1' and 2' is less important. In all the experiments to be described in this thesis, Z_p and R did not amount to more than a few percent of the oscilloscope impedance. $Z_{1,2}$ however, exceeded Z_i when measurements were performed at low electrolyte concentration and high frequencies. Thus to enable a correct determination of the plug impedance, $Z_{1,2}$ had to be reduced, which was achieved by replacing the three-way cock between electrodes 1 and 2 in the electrokinetic equipment (see Fig. 3.4) by a wide-bore tube. The input impedance of the electrometer ($R_i = 10^{14}$ Ω, C_i = a few pF) was sufficiently large in all cases.

A.c. conductance-frequency characteristics of plugs as well as of cells only containing electrolyte (reference cells) have been measured. Reference cells were incorporated in the experiments in order to test the technique of measuring a.c. conductances. Two reference cells were investigated, one being the plug holder (geometrical cell constant = 192 m^{-1}), the other a cylindrical rod of perspex with the same overall dimensions as the polystyrene plug, perforated with 37 0.1 mm diameter parallel capillaries. The latter has a geometrical cell constant of 523 m^{-1}, i.e. of the order of the conductometric cell constant of the polystyrene plug.

Conductances of solutions in the electrokinetic equipment were determined by means of a Philips conductance cell with platinized electrodes (PW 9501) positioned in reservoir 1 or 2, and a Wayne Kerr Universal Bridge B224 (internal frequency 1592 Hz). The cell was calibrated with accurately prepared KCL solutions over a wide concentration range (10^{-4} - 10^{-1} M, reference data taken from Parsons (5)). The values for the cell constant thus obtained depend on the cell conductance, as illustrated in Fig. 5.3. This dependence indicates that for the given experimental conditions (frequency, cell dimensions), the electrode polarization impedance can-

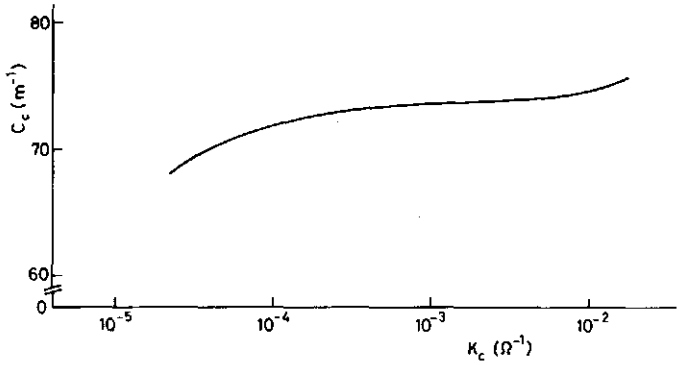

Fig. 5.3 - The apparent cell constant C_c as a function of the conductance of the measuring solution K_c; frequency 1592 Hz.

not be ignored. Furthermore, at low conductances, impurities (e.g. CO_2) may have contributed to the cell conductance. In any event, it

follows from Fig. 5.3 that the traditional procedure of adopting one value for the cell constant for all ionic strengths may introduce errors.

The solution conductivity was calculated from the cell conductance and the cell constant pertaining to this conductance. In this procedure it is assumed that the electrode polarization impedance depends only on the bulk conductance. Ion-specific effects are thought to be absent.

5.3 RESULTS AND DISCUSSION

5.3.1 DATA ON ELECTROKINETICS, ELECTROCONDUCTIVITY AND PERMEABILITY

5.3.1.1 ELECTROKINETICS

Electrokinetic measurements have been performed for an extensive range of concentrations of KCL, KBr and KI. No differences were observed between these salts, either in the electrokinetic or in the a.c. conductance experiments. Therefore only the results obtained with one salt, i.e. KBr, will be discussed.

In Fig. 5.4 a survey is given of the current retardation and I-V curves as obtained for various ionic strengths at a pressure drop ΔP = 30 cm Hg. From the I-V plots streaming currents have been determined by extrapolating the linear part to zero potential, thereby eliminating the influence of electrode as well as intrinsic polarization phenomena (chapter 3). The resulting data is presented in table 5.1.

As noted in chapter 3, during a short period following pressure application (usually less than 10 seconds) intrinsic rearrangement processes may also contribute to the measured current. From Fig. 5.4 it is seen that such intrinsic processes are the more significant the lower the ionic strength. At 3×10^{-4} M the initial current even exceeds the streaming current I_s by a factor of about two. It can also be inferred that the intrinsic processes become slower with decreasing electrolyte content. Below about 10^{-4} M these processes become even slower than the electrode polarization process. Since the I-V curve then obtained has no linear part, the

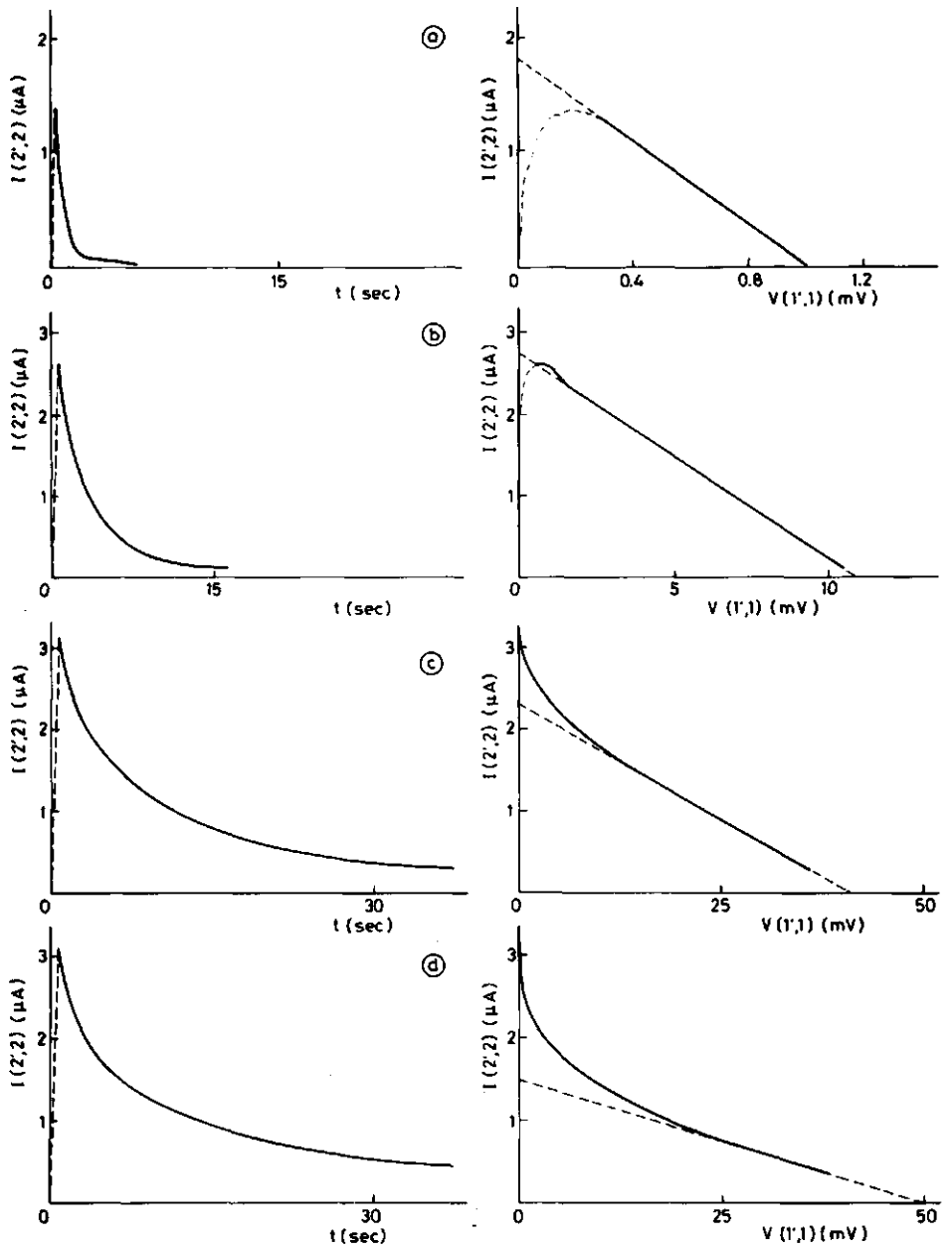

Fig. 5.4 - Current retardation and corresponding I-V plots for KBr concentrations of 10^{-1} M (a), 10^{-2} M (b), 10^{-3} M (c) and $3x10^{-4}$ M (d) (ΔP 0 → 30 cm Hg).

Table 5.1 - Electrokinetic data for various KBr concentrations as obtained from I-V plots and streaming potential measurements. ΔP = 30 cm Hg. Bulk conductivities are also included.

	I-V plot		Streaming potential method			Bulk conductivity
c(M)	I_s(μA)	$K^{d.c.}$(Ω^{-1})	V_s(mV)	$K^{d.c.}$(Ω^{-1})	$V_s x K^{d.c.}$(μA)	K_o(Ω^{-1} m^{-1})
$3x10^{-4}$	1.55	$3.15x10^{-5}$	50.4	$3.15x10^{-5}$	1.59	$4.50x10^{-3}$
10^{-3}	2.33	$5.88x10^{-5}$	39.4	$6.02x10^{-5}$	2.37	$1.50x10^{-2}$
$5x10^{-3}$	2.80	$1.56x10^{-4}$	18.1	$1.55x10^{-4}$	2.81	$7.28x10^{-2}$
10^{-2}	2.80	$2.52x10^{-4}$	11.2	$2.56x10^{-4}$	2.87	$1.39x10^{-1}$
10^{-1}	1.80	$1.80x10^{-3}$	1.02	1.79^3x10^{-3}	1.83	1.30^8

extrapolation method cannot be applied. Consequently, for very low ionic strengths streaming currents cannot be obtained in this way. A detailed discussion of the physical nature of the intrinsic processes is postponed until the results of other electrokinetic and electrical measurements have been presented (section 5.3.3). Suffice it to note at this stage, that the intrinsic currents do not reflect changes in the plug structure occurring upon pressure application. This can be concluded from the facts that

(i) the conductance of the plug (d.c. and a.c.) does not change upon an instantaneous pressure change

(ii) plots of the streaming current, streaming potential and volume flow rate against pressure are perfectly linear.

In order to illustrate the linear dependence of I_s on the applied pressure, in Fig. 5.5 I-V curves are displayed as obtained for various values of ΔP at $3x10^{-4}$ M. This graph also shows the slope of the linear part of the I-V curves, representing the d.c. plug conductance $K^{d.c.}$, to be independent of ΔP. Values of $K^{d.c.}$ computed from the I-V plots are presented in column 3 of table 5.1.

Table 5.1 also comprises the results of the streaming potential V_s (column 4) and direct $K^{d.c.}$ (column 5) measurements. The values

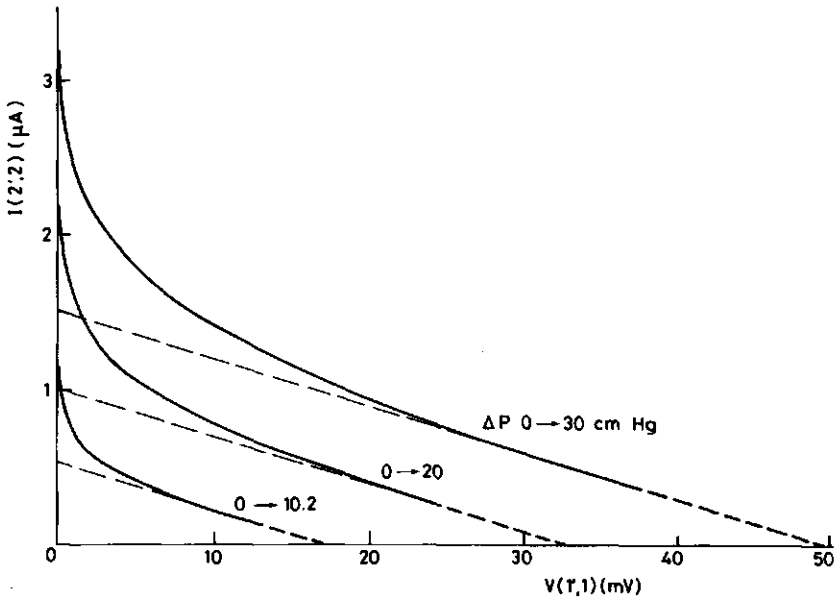

Fig. 5.5 - I-V plots as obtained for $3x10^{-4}$ M KBr at various pressure differences.

of V_s resulted from least-squares regression of the data for ΔP = 5, 10, 15, 20, 25 and 30 cm Hg. The data on $K^{d.c.}$ have been determined by the four electrode method. They showed no dependence on the applied current up to at least 50 μA. Close agreement is observed with the $K^{d.c.}$ data inferred from the I-V plots. Combining the independently obtained data on streaming potentials and d.c. conductances to provide streaming currents ($I_s = V_s x K^{d.c.}$) it is clear, as noted previously (chapter 3), that there is close agreement with the streaming current values directly determined from I-V plots.

Irreversibility of electrokinetic parameters with respect to the electrolyte concentration, as found for plugs prepared from latices without advance salt treatment, was not observed. Apparently, the salt treatment before preparing the plug has been effective in preventing charging processes during the electrokinetic experiments.

5.3.1.2 CONDUCTANCE-FREQUENCY CHARACTERISTICS OF REFERENCE CELLS

Conductance-frequency curves obtained for the reference cells are presented in Fig. 5.6 (geometric cell constant C_r = 192 m^{-1}) and Fig. 5.7 (C_r = 523 m^{-1}) for various concentrations of KBr.

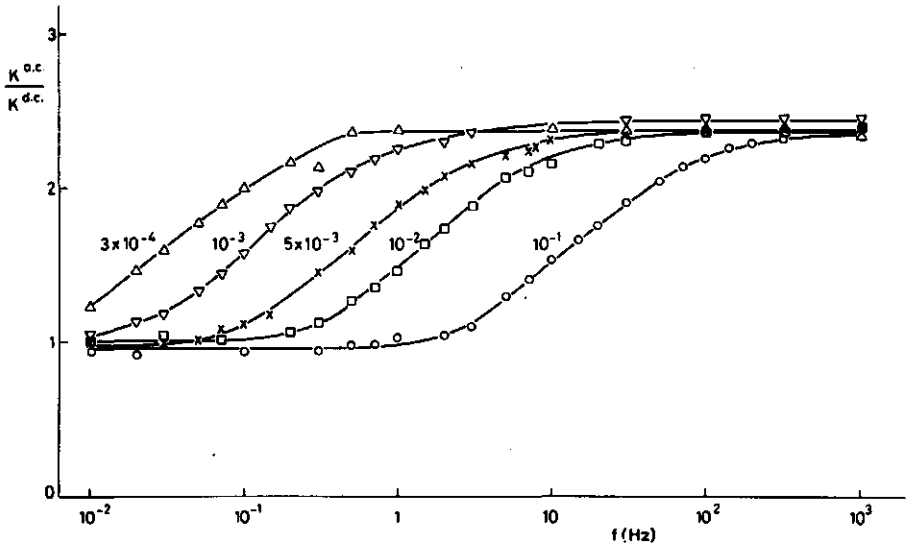

Fig. 5.6 - Dependence of the reduced conductance upon frequency for a cell only containing electrolyte at different KBr concentrations (M). Geometric cell constant 192 m^{-1}; Pt black electrodes.

In order to facilitate a comparison between results obtained at different ionic strengths, the reduced cell conductance has been plotted, i.e. the a.c. conductance $K^{a.c.}$ (admittance) divided by the conductance at d.c. conditions, $K^{d.c.}$. In all cases the reference cell conductance exhibits a low frequency dispersion. These dispersions display the following trends:

(i) The dispersion frequency f_d, defined as the frequency where the $K^{a.c.}/K^{d.c.}$-f curve has its maximum slope, increases approximately linearly with increasing electrolyte concentration. f_d does not depend on the cell dimensions.

(ii) The relative conductance increment is independent of ionic strength. It is smaller, the larger the value of C_r.

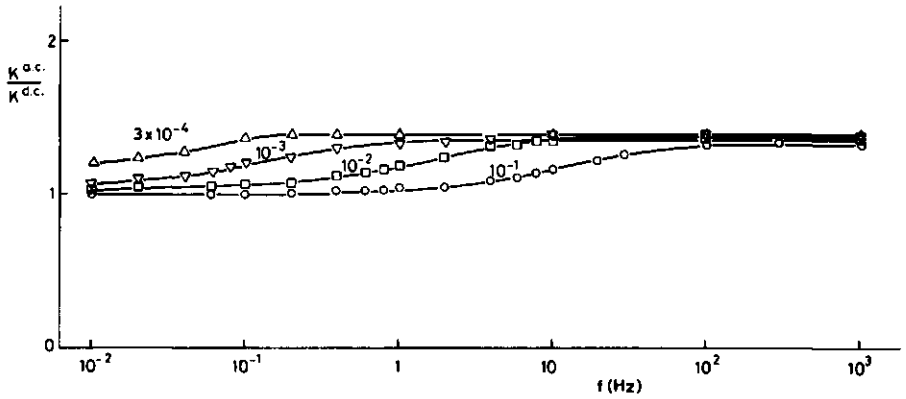

Fig. 5.7 - As Fig. 5.6. Geometric cell constant 523 m^{-1}.

(iii) The dispersion curves are not ion-specific. Solutions of different ion types (KNO_3, TBABr) but with the same conductivity yield identical dispersion curves.

(iv) Both the dispersion frequency and the increment increase upon decreasing surface area of the electrodes making contact with the reference cell. In this respect it is worth while remarking that the results in Figs. 5.6 and 5.7 have been obtained using the same Pt black electrodes.

No satisfactory explanation for these phenomena can be presented. Referring to (i) and (iv) it is tempting to think in terms of some process taking place at the cell electrodes. Double layer relaxation effects cannot be responsible, since these occur at much higher frequencies (6).

5.3.1.3 CONDUCTANCE-FREQUENCY CHARACTERISTICS OF POLYSTYRENE PLUGS

Frequency-spectra of the conductance of the polystyrene plug for various KBr concentrations are presented in Fig. 5.8. As before, reduced conductances have been plotted. Values of the reduced plug conductance at 1592 Hz as obtained with an R-C bridge connec-

ted to the plug electrodes are also given in Fig. 5.8. These values are in close agreement with those obtained with the four electrode technique at 1000 Hz, indicating that the contribution of electrode polarization to the overall impedance can be ignored under these experimental conditions.

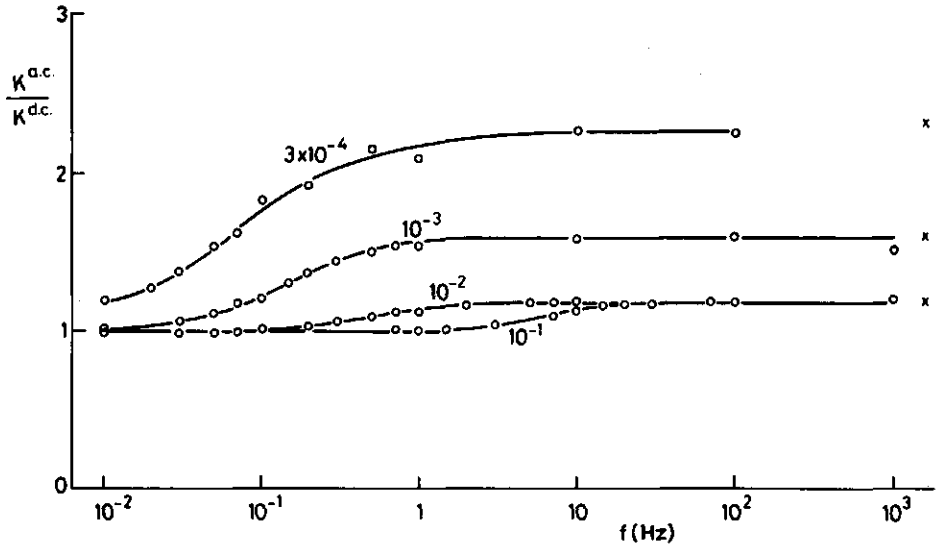

Fig. 5.8 - Dependence of the reduced plug conductance upon frequency for different KBr concentrations (M); o, obtained with the four electrode method; x, obtained with an R-C bridge connected to the plug electrodes.

For all ionic strengths the plug conductance varies markedly with frequency. These dispersions have to be carefully considered in relation to the relaxation phenomena observed in the reference cell. For electrolyte concentrations above about 10^{-2} M the increment of the plug conductance is independent of ionic strength. The dispersions found for the reference cells are independent of ionic strength over the whole range. Furthermore, the reduced conductance of the plug above 10^{-2} M (= 1.20) is close to the value obtained for the reference cell with similar cell constant (Fig. 5.7, $K^{a.c.}/K^{d.c.}$ = 1.35-1.40). Consequently, in all probability the dispersions for the plug as found above 10^{-2} M reflect processes

taking place at the plug electrodes. Below 10^{-2} M, however, the dispersion curves as obtained for the plug and the reference cells differ strongly. Whilst the conductance increment for the reference cells is independent of ionic strength, the plug conductance increment increases drastically with decreasing electrolyte concentration, indicating the occurrence of polarization phenomena related to the polystyrene plug itself. This conclusion finds support in the observation that for ionic strengths below 10^{-2} M the plug conductance increment strongly reduces when tetraalkylammonium ions are adsorbed in the plug (chapter 6). As noted in the previous section (point (iii)) these ions do not change the dispersion curves of reference cells. From Fig. 5.8 it can be inferred, that at low ionic strengths the contribution of the relaxation phenomena in the plug to the increment greatly exceeds that of the electrode processes. At $3x10^{-4}$ M the contribution of the latter is negligible.

Formally the frequency dependence of the plug conductance at low salt concentrations could have been predicted from the observed time-dependence of the streaming current (section 5.3.1.1). Since the corresponding streaming potential is constant over the period during which this time dependence occurs, the conduction current balancing the convection current must necessarily be time dependent, and thus must vary in the corresponding frequency domain. Comparing Figs. 5.4 and 5.8 it is possible to qualitatively indicate the relationship between the streaming current retardation and the frequency dispersion of the plug conductance. Both figures demonstrate the relaxation processes to

(i) contribute increasingly the lower the ionic strength

(ii) become slower when the salt concentration decreases. At $3x10^{-4}$ M the dispersion frequency is about 0.07 Hz, which value agrees quite well with the time constant that is estimated from the I-V and current retardation curves in Fig. 5.4d.

A more rigorous analysis of the time-dependent streaming current, employing the Laplace transform procedure, confirms the mentioned relationship quantitatively (see Appendix).

Effects of relaxation phenomena occurring within the time of

pressure adjustment (about 0.2 seconds) do not emerge in the I-V plot. Since the technique of measuring a.c. conductances covers a wider time range, it is more appropriate for studying intrinsic polarizations than are the I-V plots.

As far as it is known, electrical relaxation phenomena in porous media at low frequencies have not been investigated before. Springer (7) recently studied relaxation phenomena in dilute polystyrene suspensions in the kiloherz region, by measuring the frequency dependence of the permittivity. In his analysis, the various mechanisms that could possibly account for the observed dielectric dispersions are all based upon the relaxation of the dipole moment that results from the deformation of the ionic atmosphere by the external field. None of these theories predicts relaxation times higher than 100 μs. Therefore, double layer polarization cannot account for the conductance dispersions as found for the plug. Nevertheless, one might argue that double layers around neighbouring plug particles may overlap, thereby extending the region in which the rearrangement of double layer ions occurs. As a result, the relaxation time τ pertaining to this rearrangement would be larger for concentrated than for dilute dispersions ($\tau \sim d^2$). It seems very unlikely, however, that double layer overlap causes the dispersion region to shift from the kiloherz to the Herz region. In addition, it is interesting to note that Springer's dispersion curves (reference 7, chapter 4, Figs. 10, 11, 18-21) clearly show the onset of a second dispersion mechanism covering the frequency region studied in this work. This second dispersion arises at higher frequency the lower the ionic strength. The same trend emerges from the dispersion curves in Fig. 5.8.

As to the observed conductance dispersions, two alternative mechanisms have yet to be considered. Firstly, the electroosmotic contribution to the surface conductance may be frequency dependent. However, this concept predicts a decrease of the conductance with increasing frequency and must therefore be rejected. Secondly, owing to the ion excluding properties of the plug, passage of a current through the plug at low ionic strength may lead to concentration polarization at the plug boundaries, thereby lowering the conductance of the porous medium (8). This salt sieving process becomes the more significant the lower the frequency. In sec-

tion 3.5.2.1 it was shown, however, that for small current amplitudes (a few μA, as applied in the conductance experiments at low ionic strength) and short pulse durations (less than a few minutes, corresponding to frequencies above 10^{-2} Hz) concentration polarization does not lead to observable changes in the experimental signals. Hence, no contribution of this polarization process to the observed conductance dispersions is to be expected.

An explanation for the conductance dispersions is presented in section 5.3.3.

5.3.1.4 PERMEABILITY

Permeabilities of the plugs were determined from plots of the volume flow rate J_v versus applied pressure difference ΔP. Generally these plots were linear. The Reynolds number, for porous media defined by

$$R_e = \frac{d\ J_v\ \rho}{2\ \eta\ A\ p} \qquad [5.3]$$

never exceeded 10^{-5}, indicating laminar flow (9). In eq. 5.3 ρ denotes the liquid density, p the volume fraction of the particles composing the plug and A the cross-sectional area of the plug.

The permeability of most plugs increased (reversibly) with increasing electrolyte concentration. The magnitude of this concentration effect, however, varied strongly from one specimen to another and tended to be irreproducible. Moreover, a few plugs showed just the opposite trend. Unfortunately, it had to be concluded that the permeability data is not a reliable source of information on the structure of the boundary layer.

It is recalled that the electrokinetic data did show a high degree of reproducibility.

Recently, Van der Put (10) presented an analysis of the boundary layer structure of polystyrene, based among other things on permeability data on plugs. He used the same flow measuring device, but assembled it on top of the completely filled electrolyte reservoir at the low pressure side. The same arrangement was used here in some preliminary experiments, but it turned out that, due to the large volume of solution between plug and measuring

capillary, even temperature fluctuations of a few hundredth °C induced liquid displacements in the capillary of the same order as those caused by the applied pressure difference. In order to eliminate these temperature effects and thus enhance the accuracy of the measurements, the entrance to the capillary was positioned between the plug and the electrolyte reservoir (see Fig. 3.4). It is therefore surprising that the permeability data obtained with our equipment scatters more than that presented by Van der Put.

Values of the equivalent pore radius as obtained from permeability data using the Kozeny-Carman equation (eq. 7.2) and as inferred from the particle diameter using eq. 4.8 differed by less than 20 percent, indicating cracks to be absent. Furthermore, it demonstrates the correctness of the κa values adopted in calculating the correction factors to be applied to the Helmholtz-Smoluchowski zeta potentials (section 4.2).

5.3.2 DOUBLE LAYER CHARACTERISTICS

5.3.2.1 ZETA POTENTIAL AND ELECTROKINETIC CHARGE DENSITY

From the mean value of the streaming current as obtained from the I-V plot and as calculated from the streaming potential and d.c. conductance (see table 5.1), zeta potentials have been calculated according to the procedure described in section 4.2. The correction factor (1-G) to the H-S equation varied from 1 at 10^{-1} M to 0.77 at 3×10^{-4} M KBr. Results are given in Fig. 5.9 (drawn line), where the ζ-log c curve is seen to display a maximum. This result is completely at variance with the course of the potential at the boundary of the diffuse double layer, ψ_d (dotted line). ψ_d was calculated from the surface charge density, using the Gouy-Chapman diffuse double layer theory (11).

Maxima in ζ as a function of electrolyte concentration have also been found in electrophoresis measurements (4, 12, 13). De Backer and Watillon (14), investigating the electrokinetic properties of polystyrene films deposited on glass plates, did not observe a maximum. However, they prepared polystyrene by thermal polymerization of the monomer, so that the surface properties of their samples are quite different and cannot be compared with those

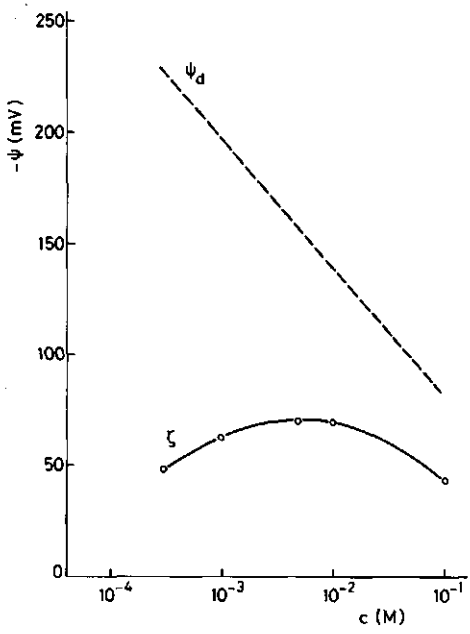

Fig. 5.9 - Zeta potential and diffuse double layer potential as a function of ionic strength.

of our latices.

The anomalous behaviour of polystyrene emerges even more dramatically when the electrokinetic charge density σ_{ek} (as computed from ζ using eq. 4.10) is plotted as a function of the electrolyte concentration (see Fig. 5.10). A continuous decrease of σ_{ek} with decreasing ionic strength is observed, whilst constancy or an increase would have been expected.

Several mechanisms can be considered to explain the anomalous course of the ζ-log c and σ_{ek}-log c curves. Firstly, it could be that anions are preferentially bound to the latex surface. In that case, differences in the electrokinetic data obtained for chloride, bromide and iodide ions would have to be expected. As noted previously, nowhere in the studied concentration range were such differences observed. Secondly, a gradually increasing (apparent) depression of ζ with decreasing ionic strength owing to surface conductance effects has to be considered, as discussed by Overbeek and Wijga (15). In their analysis, these authors pictured the plug as a

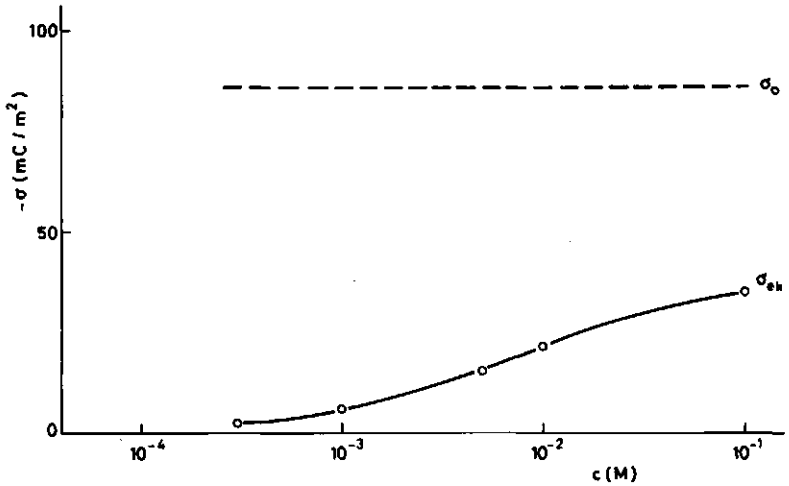

Fig. 5.10 - Electrokinetic and surface charge density as a function of ionic strength.

system of capillaries of different radii, arranged parallel and in series. However, incorporating a more realistic gradual change in pore cross-sections, Fridrikhsberg (16) established the influence of surface conductance to be insignificant. It is therefore unlikely, that effects of this kind are responsible for the decrease of ζ in the low concentration range. In addition, if there was to be an effect of surface conductance, the streaming current might be expected to be dependent on the mobility of the counterion, but experiments with Na^+, K^+ and H^+ dit not reveal such an ion-specificity. These findings also indicate that the streaming current is not significantly opposed by polarization fields induced as a result of the curvature of the pore wall (double layer polarization). Thirdly, influences of the double layer field on viscosity and permittivity and consequently ζ may play a role (17). Although not to be excluded, these influences cannot account for the maxima, since in constant charge systems the double layer field in the relevant region close to the surface does not depend on ionic strength. Moreover, comparison with theoretical predictions (reference 17, Fig. 2) shows that effects of the double layer field can

only partly explain the observed difference between ψ_d and ζ at low ionic strength. A fourth possibility is that the effective plane of shear shifts outwardly upon decreasing ionic strength.
Because there is evidence against the first three explanations, the latter is the most likely one. We will revert to this issue in section 5.3.3.

5.3.2.2 SURFACE CONDUCTIVITY

From the parameters on electroconduction presented in table 5.1, surface conductivities were calculated according to the Street (eq. 4.12), Bruggeman and Dukhin-Semenikhin models discussed in chapter 4. Results are presented in Fig. 5.11 (dotted lines). In order to assess the validity of these models, we included the theoretically predicted values for the surface conductivity in the

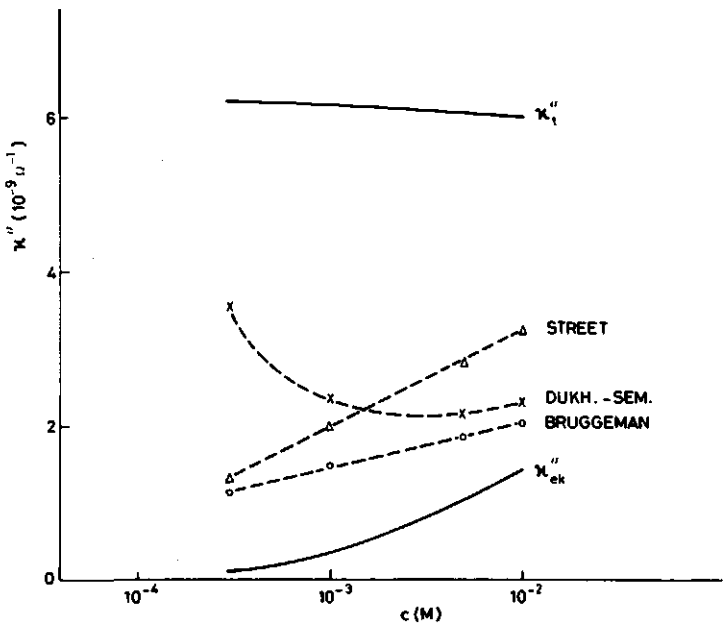

Fig. 5.11 - Theoretical (eqs. 4.20 and 4.22, lower and upper drawn line, respectively) and experimental (dotted lines) values of the surface conductivity as a function of KBr concentration.

mobile part of the double layer, κ^{σ}_{ek}, and in the double layer as a whole, κ^{σ}_{t} (drawn lines). Thus, κ^{σ}_{t} includes the contribution from the stagnant layer to the surface conductance κ^{σ}_{Δ}. Values for κ^{σ}_{ek} were computed from the Bikerman expression (eq. 4.20), those for κ^{σ}_{t} from the modified Bikerman expression (eq. 4.22). The required values of σ^{Δ}_{t} and σ^{Δ}_{c} were calculated from ψ_d and ζ by using the L.O.W. conversion tables (11) and thus also assuming a Gouy-Chapman distribution of ions in the fixed layer. The calculations were carried out assuming all equivalent conductivities to have bulk values (5). It is clear from Fig. 5.11 that in the studied concentration range all $\bar{K}$-κ^{σ} conversion models give values exceeding κ^{σ}_{ek} but being (far) below κ^{σ}_{t}. Apparently, conductance occurs in the stagnant layer behind the slipping plane, but ionic transfer in this layer is less effective than in the bulk solution. Stated otherwise, only part of the charge carriers in the stagnant layer is electrically mobile and/or the mobility of the ions in this layer is reduced compared to that of the bulk ions. Assuming ionic transfer in the stagnant layer to be effective only for about 17 percent, eq. 4.22 appears to fit the Bruggeman line within experimental error. Such a fit is not possible for the curves obtained with the other conversion models. Therefore, the Bruggeman model seems to be the most suitable one for our polystyrene plugs. Recently, Van der Put and Bijsterbosch (18) arrived at the same conclusion, but their analysis is open to criticism. As reference for the predictions of the various $\bar{K}$-κ^{σ} conversion models they used surface conductance data calculated from ψ_d, using Bikerman's theory. The experimentally obtained zeta potentials were not considered. Hence their analysis completely ignores any effects of the ionic strength on the location of the shear plane.

The Street curve in Fig. 5.11 follows the Bruggeman line reasonably well, indicating that under the given experimental circumstances double layer polarization effects are not significant. The shape of the Dukhin-Semenikhin line, on the contrary, strongly deviates at low electrolyte concentration. Apparently, concentration polarization does not play an important role in the plugs. An explanation for this observation, which fits in with the findings of Van der Put and Bijsterbosch (18), is that the ion atmospheres around the plug particles contacting each other, overlap, thereby eliminating the local concentration gradients beyond the double

layer limits.

Comparison with the data obtained by Van der Put (10) shows that the surface conductivity of our latices is somewhat smaller. This may arise from differences in the structure of the stagnant layer, caused by the removal of monomers and oligomers from the surface of our latices in the steam stripping process.

5.3.3 THE HAIRY LAYER MODEL

The electrokinetic data as well as the conductance dispersions can be accounted for by assuming the polystyrene particles to be covered with a layer of flexible polyelectrolyte chains (hairs). This suggestion has recently also been made by Van der Put and Bijsterbosch (1).

In the concept of hairiness (part of) the sulfate surface groups are thought to be end groups of polystyrene chains that partially protrude into the solution. Presumably, a broad distribution of surface charges perpendicular to the surface exists, a feature also encountered in biological systems (19). The extent of protrusion of the polymers results from the competition between the hydrophobic interaction between the dissolved polymers and the particle surface on one hand, and the electrostatic repulsion between the charged end groups on the other. Consequently, the thickness of the hairy layer is controlled by the electrolyte concentration. More specifically, upon decreasing the ionic strength the surface layer expands, due to the reduced shielding of the surface groups. The expansion causes an outward shift of the slipping plane and a reduction of the electrokinetically displaceable charge. Thus the hairy layer model explains the shape of the ζ-log c and σ_{ek}-log c curves very well.

The data on surface conductivity also support the concept of hairiness. In the first place, merely because they show that conductance takes place behind the shear plane. Secondly, because they indicate the conductance in the stagnant layer (= difference between the Bruggeman and κ^{σ}_{ek} curves in Fig. 5.11) to increase with decreasing electrolyte concentration, a phenomenon fitting in with the postulated expansion of the hairy layer.

The most direct proof of the polyelectrolyte character of the

polystyrene surface is constituted by the occurrence of plug conductance dispersions and streaming current relaxations. It is conceivable that the protruding polystyrene chains are prone to limited displacement in a tangential electrical or hydrodynamical field. When measuring a.c. conductances (admittances) the following frequency dependence has then to be expected. At high frequency (part of) the surface groups may oscillate and thus contribute to the conductance current. When lowering the frequency the a.c. conductance remains constant until some intermediate (dispersion) region is reached, where the characteristic time of displacement of the hairs is of the order of the oscillation time of the external field. Below this frequency, the displacement occurs within the oscillation time. Consequently, the lower the frequency, the larger the part of a cycle during which the surface groups behave as fixed charges. As a result the contribution of these groups to the overall conductance decreases. Eventually, under d.c. conditions, there is no contribution at all. This frequency dependence is exemplified by the a.c. conductance curves in Fig. 5.8. These curves also show the characteristic time of displacement to increase with decreasing ionic strength, a trend to be expected because of the expansion of the hairy layer. As compared to free sulfate groups, the characteristic time of displacement of the surface sulfate groups is small. This may be due to low flexibility of the protruding polymer chain and to structural water around the hair (hydrophobic effect).

In a streaming current experiment, the shear forces will deform the outer part of the hairy layer, thereby initially displacing the excess counter charge residing in this part of the diffuse layer. As a result an intrinsic current is generated that positively contributes to the streaming current. This contribution gradually decreases, and ultimately becomes zero when the hairs have reached their maximum displacement. The characteristic time of hair displacement and streaming current relaxation will increase as the hairy layer expands, i.e. upon decreasing ionic strength. Thus the hairy layer model also accounts for the relaxation of the streaming current (Fig. 5.4).

The a.c. conductance curves, as well as the ζ-log c curve,

indicate the expansion of the hairy layer to commence at about 10^{-2} M, suggesting effective electrostatic repulsion between the sulfate groups starts at this ionic strength. This is in accordance with the fact that the double layer shielding length at 10^{-2} M (3 nm) exceeds the distance between the surface groups, even when these groups are assumed to be homogeneously distributed over the entire particle surface (the distance is then 1.4 nm).

It is worth while mentioning that other investigations tend to support the concept of a hairy layer on polystyrene particles:

(i) characterizing the surface of carboxylated polymer latices by photon correlation spectroscopy, Goossens and Zembrod (20) observed the hydrodynamic particle radius to increase with increasing pH.

(ii) In an ultrasonic study of polystyrene latices Barrett-Gültepe et al. (21) found excess absorptions not accountable for by classical concepts of ultrasonic absorption in dispersions. As one of the alternative mechanisms they considered the relaxation of "dangling" chains at the polystyrene solution interface.

(iii) Studying the configuration of adsorbed poly(ethylene oxide) at the polystyrene-solution interface by n.m.r., Barnett et al. (22) obtained very low values (sometimes "experimentally indistinguishable from zero") for the bound fraction. This quantity was estimated from the concentration ratio of immobile and mobile segments, identifying the former as part of trains (i.e. in contact with the surface) and the latter as part of loops and tails. Obviously this approach is only justified when the surface is rigid. In the case of a hairy polystyrene surface, the trains may retain a certain mobility, through which the n.m.r. data underestimates the bound fraction.

5.4 CONCLUDING REMARKS

In this work the electrokinetic techniques described in chapter 3 prove to be useful tools to gain insight into the structure of the polystyrene-solution interface. In combination with a.c.

conductance measurements these techniques demonstrate the surface layer of polystyrene particles to consist of protruding, partly mobile polymer chains. This surface layer shrinks upon increasing the ionic strength.

APPENDIX RELATIONSHIP BETWEEN THE STREAMING CURRENT RELAXATION AND THE LOW FREQUENCY CONDUCTANCE DISPERSION IN PLUGS

The relationship between the time dependence of the streaming current and the dispersion of the conductance can be evaluated by transforming the former transient into the frequency domain, using the Laplace transform procedure (23). Prior to this transformation the current retardation curve has to be corrected for electrode polarization effects, which can be achieved by means of the corresponding I-V plot (see Fig. 5.12). The electrode polarization contribution to the current decay at any time t_1, $\Delta I_e(t_1)$, is found by considering that potential in the I-V plot that corresponds with $I(t_1)$. At this potential $\Delta I_e(t_1)$ is found as the difference between I_s and the extrapolated linear I-V curve. The corrected retardation curve is subsequently obtained by adding $I(2',2)$ and ΔI_e for all values of t.

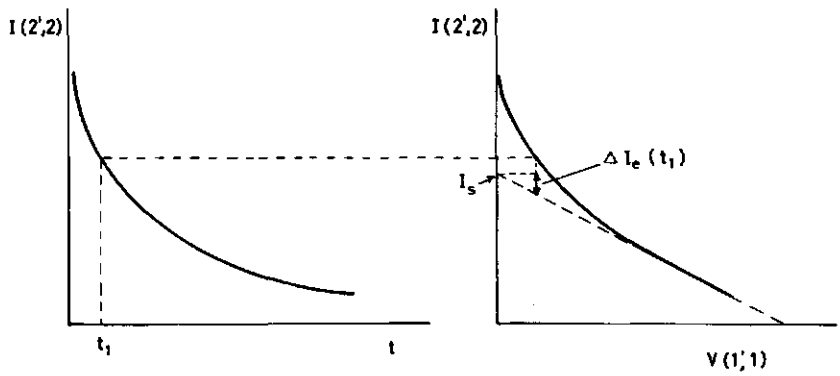

Fig. 5.12 - Determination of the electrode polarization contribution to the current retardation during streaming current measurements.

The current retardation curve thus obtained for $3x10^{-4}$ M at ΔP = 30 cm Hg from Fig. 5.4 was transposed into the frequency domain with a computer program developed for the analysis of coulostatic transients (24). From the resulting real and imaginary components of the impedance spectrum, the a.c. conductances presented in Fig. 5.13 were obtained. Transformation of current-time curves

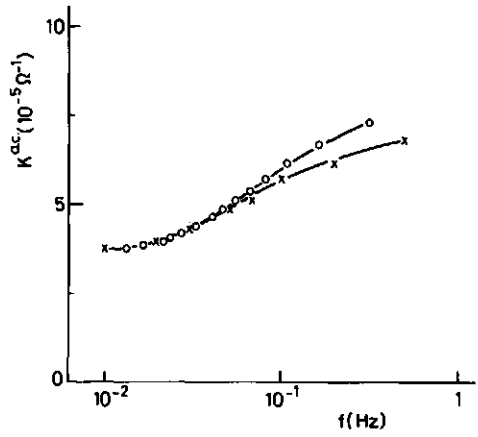

Fig. 5.13 - Comparison between the low frequency dispersion of the plug conductance as measured directly (x) and as obtained from the streaming current relaxation by the Laplace transform procedure (o). KBr concentration = $3x10^{-4}$ M.

obtained at other pressure drops yielded identical spectra. The directly measured a.c. conductances are also included in Fig. 5.13. The agreement between the two sets of data is quite satisfactory. The divergence of the curves at the high frequency side must be attributed to the inaccuracy of the determination of I(2',2) shortly after pressure application. It can be concluded that the intrinsic polarizations observed in the hydrodynamical and electrical measurements have a common origin.

5.5 REFERENCES

1. Van der Put, A.G. and Bijsterbosch, B.H., J. Colloid Interface Sci. 92, 499 (1983).
2. Bensley, C.N. and Hunter, R.J., J. Colloid Interface Sci. 92,

448 (1983).
3. Furusawa, K., Norde, W. and Lyklema, J., Kolloid Z.Z. Polymere, 250, 908 (1972).
4. Meijer, A.E.J., Van Megen, W.J. and Lyklema, J., J. Colloid Interface Sci. 66, 99 (1978).
5. Parsons, R., "Handbook of Electrochemical Constants", Butterworths, London, 1959.
6. Buck, R.P., J. Electroanal. Chem. 23, 219 (1969).
7. Springer, M.M., Thesis, Agricultural University, Wageningen (1979).
8. Läuger, P., Richter, J. and Lesslauer, W., Berichte der Bunsengesellschaft 71, 906 (1967).
9. Bird, R.B., Stewart, W.E. and Lightfood, E.N., "Transport Phenomena", p. 198, Wiley, New York (1960).
10. Van der Put, A.G., Thesis , Agricultural University, Wageningen (1980).
11. Loeb, A.L., Wiersema, P.H. and Overbeek, J.Th.G., "The electrical double layer around a spherical colloid particle", MIT Press, Cambridge (1960).
12. Baran, A.A., Dudkina, L.M., Soboleva, N.M. and Chechik, O.S., Kolloidn. Zh. 43, 211 (1981).
13. Ottewill, R.H. and Shaw, J.N., J. Electroanal. Chem. 37, 133 (1972).
14. De Backer, R. and Watillon, A., VI Intern. Kongress Grenzflächenaktive Stoffe, Zürich (1972); Berichte, Band II, 651.
15. Overbeek, J.Th.G. and Wijga, P.W.O., Rec. Trav. Chim. 65, 556 (1946).
16. Dukhin, S.S. and Derjaguin, B.V. in "Surface and Colloid Science" (E. Matijević, Ed.), Vol. 7, p. 150, Wiley, New York, 1974.
17. Lyklema, J. and Overbeek, J.Th.G., J. Colloid Sci. 16, 501 (1961).
18. Van der Put, A.G. and Bijsterbosch, B.H., J. Colloid Interface Sci. 75, 512 (1980).
19. Donath, E. and Pastushenko, V., J. Electroanal. Chem. 104, 543 (1979).
20. Goossens, J.W.S. and Zembrod, A., Colloid & Polymer Sci. 257, 437 (1979).

21. Barrett-Gültepe, M.A., Everett, D.H. and Gültepe, M.E. in "Polymer Colloids II" (R.M. Fitch Ed.), p. 313, Plenum Press, New York, 1980.
22. Barnett, K.G., Cosgrove, T., Vincent, B., Burgess, A.N. Crowley, T.L., King, T., Turner, J.D. and Tadros, Th.F., Polymer 22, 283 (1981).
23. Levart, E. and Poirier d'Ange d'Orsay, E., J. Electroanal. Chem. 12, 277 (1966).
24. Peverelli, K.J. and Van Leeuwen, H.P., J. Electroanal. Chem. 110, 119 (1980).

CHAPTER 6

THE INFLUENCE OF ADSORBED TETRAALKYLAMMONIUM IONS ON THE STRUCTURE OF THE POLYSTYRENE-SOLUTION INTERFACE

6.1 INTRODUCTION

Adsorption is an interfacial phenomenon of frequent occurrence, that plays an important role in nature, in technical sciences and in many applications. Consequently, the literature on such disciplines as biology, environmental sciences and colloid chemistry contains an immense amount of reports on this issue. By far the larger part of them refers to such quantities as surface occupancy, energy of adsorption and structure of the adsorbed layer. Little or no attention has been paid to changes in the structure of the adsorbent surface itself, as possibly created by adsorption. When using non-rigid adsorbents like polymer colloids, however, such changes cannot be entirely excluded. The results presented in the foregoing chapter, e.g., indicate polystyrene particles to be covered with a layer of polyelectrolyte chains. The structure of this layer is controlled by electrostatic repulsive forces and will therefore be sensitive to the presence of charged species.

In this chapter we present a study on the effect adsorbed tetraalkylammonium (TAA^+) ions exert on the surface properties of polystyrene particles and on those of the double layer. Quaternary ammonium salts have previously been used in adsorption studies on mercury (1,2) and silver iodide (3), mainly because of their spherical molecular shape and essentially complete dissociation in solution. Another attractive feature of these salts is that, in contrast with uncharged low molecular weight adsorbates like alcohols (4), they already adsorb at low concentrations, so in a concentration region where the bulk properties remain practically unchanged. This considerably facilitates the interpretation of electrokinetic and electroconduction data. Three TAA^+ compounds have been used, the tetrapropylammonium ($TPrA^+$), tetrabutylammonium ($TBuA^+$) and tetraamylammonium ($TAmA^+$) ion.

The study has been carried out by measuring electrokinetic parameters and conductance-frequency characteristics of polystyrene

plugs as a function of the adsorbed amount of TAA^+, using the techniques described in chapters 3 and 5. In addition, the adsorption of the three types of TAA^+ ions on polystyrene has been measured. The experiments have been conducted for varying concentration of TAA^+ and fixed ionic strength ($5x10^{-3}$ M) as well as for varying ionic strength and fixed TAA^+ concentration ($3x10^{-4}$ M $TBuA^+$). In this way the influence of TAA^+ adsorption and salt concentration could be independently established.

6.2 EXPERIMENTAL

6.2.1 MATERIALS

All quaternary ammonium compounds used were Fluka products. $TPrA^+$ and $TBuA^+$ were used in the bromide as well as the iodide form, $TAmA^+$ in the bromide form only. The purity of these compounds as determined by potentiometric titration with $AgNO_3$, was higher than 99.4 %.

Bromothymol blue (Merck) was of indicator quality.

All other chemicals were of A.R. quality and distilled water was used throughout.

Polystyrene plugs were prepared by centrifuging the latex sample described in chapter 5 (σ_0 = 83 ± 1 mC/m^2, d = 638 ± 3 nm).

6.2.2 METHODS

6.2.2.1 ADSORPTION MEASUREMENTS

Adsorption isotherms were determined by the depletion method. In small glass tubes (ca. 15 ml) known volumes of polystyrene latex and tetraalkylammonium and KBr (KI) standard solutions were mixed. The amount of latex was chosen such that the overall area represented by the polystyrene particles varied from about 1 m^2 at low surface occupancies to about 3.5 m^2 in the plateau region. KBr (KI) solutions were added to adjust the mixture to the desired overall salt concentration. The TAA^+ contribution to the ionic strength at equilibrium was estimated from preliminary adsorption data. In this way, all along the isotherms the ionic strength could be kept con-

stant within 2 %. The samples were equilibrated by end-over-end rotation for at least 16 hours. Then the latex was removed by filtering the samples through a 0.025 μm Millipore filter (overpressure 100 kPa). The first few drops of the filtrate were discarded. The latex could not be separated by centrifugation, since the samples flotated owing to the rotation.

For determination of the TAA^+ concentration an anionic dye (bromothymol blue) was added to the filtrate, whereafter the formed TAA^+-dye complex was extracted with chloroform. The concentration in this solution was obtained spectrophotometrically. We followed essentially the method described by de Keizer (5). The main modification to his procedure was the use of a buffer solution of pH = 11.0 (Merck, Puffer Titrisol) instead of pH = 9.5 (borax) for the extraction of tetraamylammonium ions. This adaptation improved the extractability, as can be inferred from Fig. 6.1, where the calibration curves at both pH values are depicted. This improvement

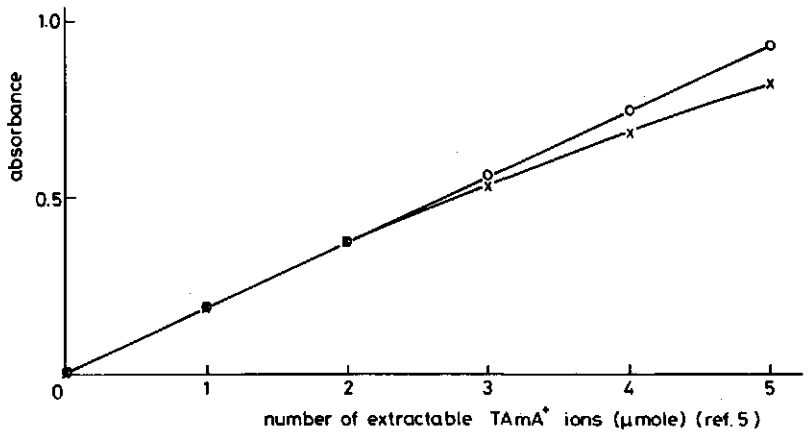

Fig. 6.1 - Calibration curves for determination of $TAmA^+$ concentrations at pH = 9.5 (x) and 11.0 (o).

results from the enhanced dissociation of the dye at pH = 11, through which the complex formation has been promoted. The borax buffer was sufficiently effective for the extraction of the other quaternary ammonium compounds. For the adsorption experiments at varying ionic strength the salt content of the buffer was enhanced up to 10^{-1} M in order to avoid any effect of a varying ionic

strength on the extractability of the TAA^+ compounds.

The adsorbed amount Γ of tetraalkylammonium ions, expressed as moles per m^2, was calculated from the concentration difference in solution before and after adsorption, the volume of the aqueous phase, the overall weight of the latex particles and their specific surface area S. S was obtained from the diameter d and density ρ of the particles according to $S = 6/\rho d$.

Preliminary experiments stressed the importance of steam stripping the latex (chapter 2). Without this purification step, the extraction liquid of blank samples sometimes showed intense absorption at the employed wavelength. Apparently, the latex then contains impurities which also complexate with the bromothymol blue dye.

6.2.2.2 ELECTROKINETIC AND A.C. CONDUCTANCE MEASUREMENTS

Electrokinetic and a.c. conductance measurements were performed by first permeating polystyrene plugs with the proper TAA^+ solution, until no changes in the I-V plot and the plug conductance at 1592 Hz were observed any longer. Then electrokinetic data and the frequency-spectrum of the plug conductance were determined using the techniques presented in chapters 3 and 5, respectively. Owing to the large surface to volume ratio of the pores in the plug, rather long permeation times were needed. At 10^{-4} M $TBuA^+$, for instance, equilibrium was only attained after more than three days (at ΔP = 30 cm Hg).

For each of the five TAA^+ compounds studied, a plug of (bare) polystyrene was prepared. The relevant geometric data of these plugs are listed in table 6.1. The porosity and the conductometric cell constant were determined according to the methods described in sections 5.2.2 and 4.2, respectively.

Bulk conductivities were determined according to the method described in section 5.2.3.

All measurements were performed at 25 °C.

Table 6.1 - Porosities (1-p) and conductometric cell constants (C_p) of the various plugs, with cell constants of the pertaining plug holder (C_r).

Plug code	Adsorbate	1-p	C_p (m^{-1})	C_r (m^{-1})
V	TPrABr	0.403	709	193
IV	TBuABr	0.400	729	192
VI	TAmABr	0.412	666	186
VII	TPrAI	0.420	697	198
VIII	TBuAI	0.410	684	191

6.3 RESULTS AND DISCUSSION

6.3.1 MEASUREMENTS AT CONSTANT IONIC STRENGTH ($5x10^{-3}$ M) BUT VARYING TAA^+ CONCENTRATION

6.3.1.1 ADSORPTION ISOTHERMS

In Fig. 6.2 isotherms are shown for the adsorption of tetrapropyl-, tetrabutyl- and tetraamylammonium ions on polystyrene, at an ionic strength of $5x10^{-3}$ M. To indicate the accuracy of the measurements, the experimental error in the $TAmA^+$ results has been included. The curves in Fig. 6.2 refer to the bromides, but when using iodide as the anion, within experimental error identical results were obtained.

All isotherms tend to a maximum adsorbed amount of about 0.8 μmole/m^2, corresponding to an area per adsorbed TAA^+ ion of approximately 200 $Å^2$. This value considerably exceeds the molecular cross-sectional area of $TPrA^+$, $TBuA^+$ and $TAmA^+$. These areas can be estimated from the crystal radii given in reference 6. (The value for $TAmA^+$ was estimated by extrapolation.) Assuming TAA^+ ions to be perfect spheres the values obtained are 64, 77 and 92 $Å^2$, respectively. It can be concluded that, when the adsorption sites are homogeneously distributed over the surface, in the plateau region the tetraalkylammonium ions are located at relatively large distan-

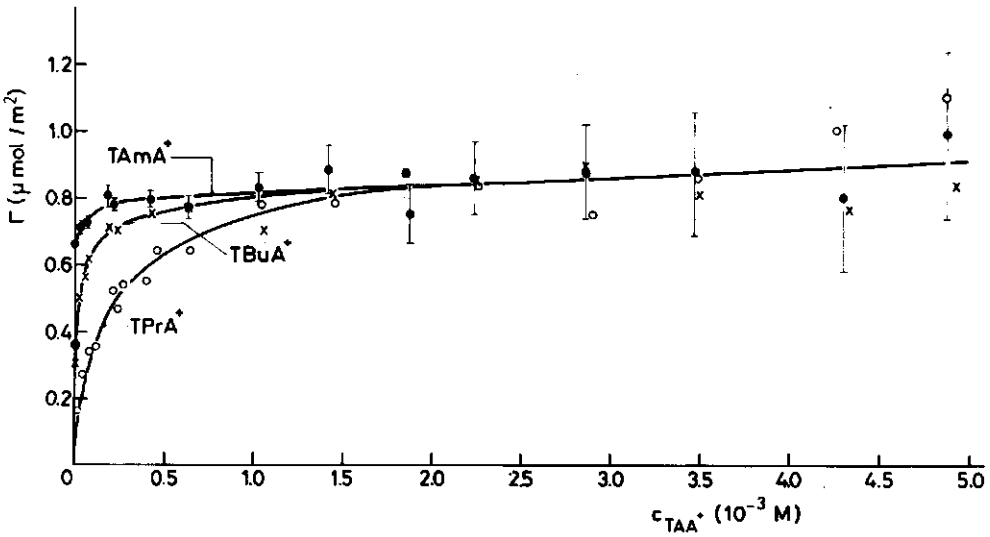

Fig. 6.2 - Adsorption isotherms of $TPrA^+$, $TBuA^+$ and $TAmA^+$ on polystyrene. Ionic strength 5×10^{-3} M.

ces. When, on the other hand, a patchwise distribution of sites exists, locally compact monolayers may still be present.

At the mercury-solution interface, where localized adsorption is very unlikely, TAA^+ ions tend to form a saturated monolayer (1,2). In a recent study on the adsorption of TAA^+ ions on silver iodide, de Keizer (3) could not come to decisive conclusions as to the surface coverage, because of the uncertainties existing about the specific surface area of this colloid.

The plateau value of 0.8 μmole/m^2 corresponds to a charge density of 80 mC/m^2, reflecting quite closely the surface charge density of the latex sample (σ_0 = 83 mC/m^2). In combination with the incomplete monolayer coverage, this indicates that the adsorption mechanism of TAA^+ ions on polystyrene involves mainly coulombic interaction between the TAA^+ ions and the negatively charged surface groups.

In the plateau region the isotherms exhibit a slight rise. This possibly results from the onset of adsorption onto hydrophobic sites between the charged surface groups.

Fig. 6.2 also illustrates that the concentration at which the isotherms attain their plateau, decreases with increasing length of the hydrocarbon chains in the TAA^+ ions. This trend is generally observed for the adsorption of organic compounds from aqueous solutions. More specifically, it has been shown (Traube's rule (7)), that the concentration required to achieve a certain surface occupancy within a homologous series reduces by a factor of about 3 when adding one - CH_2 group to the hydrocarbon chain, other things being equal. Inferring these reduction factors from the TAA^+ adsorption isotherms at $\Gamma = 0.7$ μmole/m^2, where such an analysis is most accurate, we obtain 3.9 and 5.6 for the $TPrA^+ \rightarrow TBuA^+$ and $TBuA^+ \rightarrow TAmA^+$ transition, respectively. Interpreting these data with Traube's rule, would lead us to conclude that only 1-2 of the four additional - CH_2 groups are involved in the adsorption process and thus are in contact with the surface. However, this conclusion is premature, because Traube's rule supposes the electrical contribution to the adsorption free energy to be fixed within a homologous series and this condition is certainly not met by TAA^+ compounds. With increasing length of the hydrocarbon chains the distance between the charged group and the surface increases, so that the electrical interaction reduces.

6.3.1.2 ELECTROKINETICS

Electrokinetic data of plugs V (TPrABr), IV (TBuABr) and VI (TAmABr) for varying concentrations of tetraalkylammonium ions, obtained from the I-V plots as well as the streaming potential and d.c. conductance measurements, is compiled in tables 6.2 till 6.4. The sign of I_s and V_s corresponds to that of the surface charge. Bulk conductivities are also included. The salt concentration of all solutions was adjusted to 5×10^{-3} M with KBr. Since no significant differences in double layer properties were observed when using iodide as the anion, the data of plugs VII (TPrAI) and VIII (TBuAI) have been omitted.

The I-V plots revealed the relative contribution of the intrinsic processes to the measured current (see section 5.3.1.1) to decrease upon increasing TAA^+ concentration. This effect emerges more clearly in the I-V plots at lower ionic strength and will

Table 6.2 - Electrokinetic data of plug V for various TPrABr concentrations, obtained from both I-V plots and streaming potential and d.c. conductance measurements (ΔP = 30 cm Hg). Ionic strength 5×10^{-3} M. Bulk conductivities are also included.

	I-V plot		Streaming potential method		Bulk conductivity
c_{TPrABr}(M)	I_s(μA)	$K^{d.c.}$(Ω^{-1})	V_s(mV)	$K^{d.c.}$(Ω^{-1})	K_o($\Omega^{-1}m^{-1}$)
0	-2.74	1.51×10^{-4}	-18.0	1.52×10^{-4}	7.22×10^{-2}
10^{-4}	-2.60	1.33×10^{-4}	-19.6	1.34×10^{-4}	7.15×10^{-2}
3×10^{-4}	-2.29	1.21×10^{-4}	-19.3	1.19×10^{-4}	7.05×10^{-2}
10^{-3}	-1.82	1.03×10^{-4}	-18.0	1.03×10^{-4}	6.68×10^{-2}
2.5×10^{-3}	-1.37	8.46×10^{-5}	-16.3	8.46×10^{-5}	5.89×10^{-2}
5×10^{-3}	-0.98	6.45×10^{-5}	-15.4	6.33×10^{-5}	4.63×10^{-2}

Table 6.3 - Electrokinetic data of plug IV for various TBuABr concentrations, obtained from both I-V plots and streaming potential and d.c. conductance measurements (ΔP = 30 cm Hg). Ionic strength 5×10^{-3} M. Bulk conductivities are also included.

	I-V plot		Streaming potential method		Bulk conductivity
c_{TBuABr}(M)	I_s(μA)	$K^{d.c.}$(Ω^{-1})	V_s(mV)	$K^{d.c.}$(Ω^{-1})	K_o($\Omega^{-1}m^{-1}$)
0	-2.80	1.56×10^{-4}	-18.1	1.55×10^{-4}	7.28×10^{-2}
10^{-4}	-1.89	1.11×10^{-4}	-17.1	1.12×10^{-4}	7.13×10^{-2}
3×10^{-4}	-1.45	1.00×10^{-4}	-14.2	1.02×10^{-4}	6.95×10^{-2}
10^{-3}	-0.71	8.75×10^{-5}	- 8.07	8.83×10^{-5}	6.61×10^{-2}
2.5×10^{-3}	not measurable		- 2.30	7.84×10^{-5}	5.78×10^{-2}
5×10^{-3}	+0.26	-	+ 3.87	6.27×10^{-5}	4.38×10^{-2}

Table 6.4 - Electrokinetic data of plug VI for various TAmABr concentrations, obtained from both I-V plots and streaming potential and d.c. conductance measurements (ΔP = 30 cm Hg). Ionic strength 5×10^{-3} M. Bulk conductivities are also included.

	I-V plot		Streaming potential method		Bulk conductivity
c_{TAmABr}(M)	I_s(μA)	$K^{d.c.}$(Ω^{-1})	V_s(mV)	$K^{d.c.}$(Ω^{-1})	K_o($\Omega^{-1}m^{-1}$)
0	-2.99	1.65×10^{-4}	-18.1	1.69×10^{-4}	7.20×10^{-2}
2×10^{-4}	+0.022	1.08×10^{-4}	+ 0.19	1.05×10^{-4}	7.15×10^{-2}
3×10^{-4}	+0.268	1.02×10^{-4}	+ 2.65	1.02×10^{-4}	7.07×10^{-2}
10^{-3}	+1.05	1.01×10^{-4}	+10.4	1.01×10^{-4}	6.68×10^{-2}
2.5×10^{-3}	+1.54	9.87×10^{-5}	+15.6	9.83×10^{-5}	5.67×10^{-2}
5×10^{-3}	+1.80	8.61×10^{-5}	+20.8	8.53×10^{-5}	4.42×10^{-2}

therefore be illustrated in section 6.3.2, where the measurements at varying salt concentration are discussed.

From the mean value of the streaming current data as obtained from the I-V plot and as calculated from the streaming potential and d.c. conductance, zeta potentials have been calculated according to the procedure described in section 4.2. Results are displayed in Fig. 6.3. A decrease in ζ upon increasing TAA^+ concentration is observed. Charge reversal occurs for $TBuA^+$ and $TAmA^+$ at 3.5×10^{-3} M and 2×10^{-4} M, respectively. In the studied concentration range no isoelectric point (i.e.p) is found for $TPrA^+$. The initial slopes of the ζ-c_{TAA^+} curves follow the affinity trend that is inferred from the adsorption isotherms. In other respects, however, the adsorption isotherms and ζ-c_{TAA^+} curves seem to be contradictory. E.g., the latter continue to decrease in a region where the former reach a plateau. This apparent discrepancy stems from differences in the sensitivity of ζ and the experimentally determined Γ to changes in the actual adsorbed amount. According to the Gouy-Chapman theory for flat double layers (eq. 4.10) a change in ζ from 0 to 50 mV at 5×10^{-3} M corresponds to a change in the electrokin-

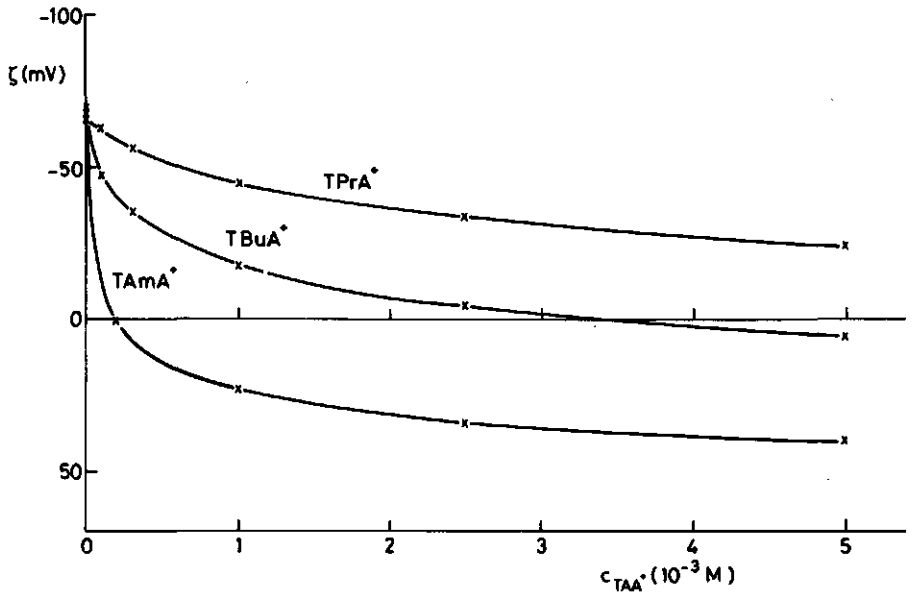

Fig. 6.3 - Zeta potential of polystyrene as a function of the equilibrium concentration of TPrABr, TBuABr and TAmABr. Ionic strength 5×10^{-3} M.

etic charge density of 9.4 mC/m^2. Assuming TAA^+ ions to adsorb as free ions, the latter would correspond to a change in the adsorbed amount of only 0.094 μmole TAA^+ per m^2. This value is of the order of the experimental error in the low concentration part of the plateau region. As a matter of fact, our results demonstrate that, for not too low surface coverages, alterations in the adsorbed amount can be much more sensitively pursued by electrokinetic techniques than by depletion methods.

In principle the combination of adsorption isotherms and electrokinetic data enables information to be obtained on the charge distribution in the electrical double layer as a function of the adsorbed amount of tetraalkylammonium ions. Such an analysis, however, requires knowledge about the adsorption process, i.e. it has to be known whether only free TAA^+ ions adsorb or that also coadsorption of anions occurs. This can be inferred by comparing the surface charge density σ_0 with the adsorbed TAA^+ charge σ_{TAA^+} at

the i.e.p. where

$$\sigma_0 + \sigma_{TAA^+} + \sigma_{Br^-} = 0 \qquad [6.1]$$

Here σ_{Br^-} denotes the charge density contributed by bromide ions coadsorbed in the hydrodynamically immobile part of the double layer. From Figs. 6.2 and 6.3 it can be inferred that at the i.e.p. $\sigma_{TAmA^+} = + 79 \pm 3$ mC/m^2 and $\sigma_{TBuA^+} = 90 \pm 18$ mC/m^2. Since $\sigma_0 = - 83 \pm 1$ mC/m^2 it follows that, within experimental error, σ_{Br^-} equals zero. Unfortunately such an analysis is not possible for $TPrA^+$ because no i.e.p. is attained, but in all probability for $TPrA^+$ the coadsorption of anions is also negligible. This can be inferred from the absence of any difference between the results obtained with tetrapropylammonium bromide and - iodide (see above). If ion pairs had formed at the polystyrene surface, a dependence on the nature of the halide anion would have been implied (2). Thus it can be concluded that the TAA^+ ions adsorb as free ions onto the polystyrene surface.

At the mercury-solution interface considerable TAA^+-halide ion pairing occurs. Hamdi et al. (2) found at a charge density comparable to that of our latex sample equal amounts of paired ($TBuA^+$-CL^-) and non-paired ions at the surface. At silver iodide, on the contrary, TAA^+ ions adsorb mainly as free ions. Using nitrate as the anion, de Keizer (3) estimated the number of coadsorbed anions to be less than 20 %. The difference in the extent of ion pairing at the mercury, silver iodide and polystyrene surface seems to be related to the differing tendency of these systems to specifically adsorb anions. Halides adsorb strongly onto negatively charged mercury (8), whereas no specific adsorption of these ions at polystyrene occurs (chapter 5). One might imagine the specifically adsorbed anions to promote the adsorption of tetraalkylammonium ions. This concurs with the suggestion of Devanathan and Fernando (9) that bridge formation of specifically adsorbed anions between the mercury surface and TAA^+ ions takes place.

Having established the absence of coadsorption of bromide ions, it is possible to compute the "effective surface charge density" $\sigma_0 + \sigma_{TAA^+}$ from the adsorption isotherms. Results are given in Fig. 6.4. The data for TAA^+ concentration above 10^{-3} M has been

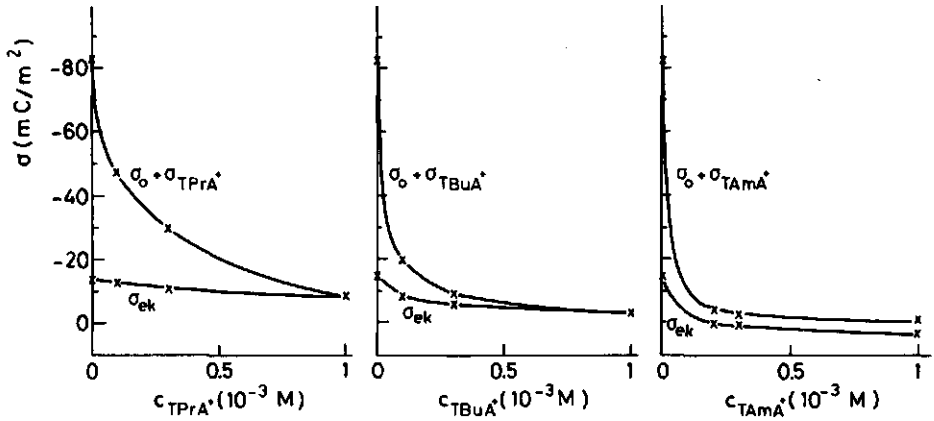

Fig. 6.4 - Electrokinetic (σ_{ek}) and effective surface charge density ($\sigma_0 + \sigma_{TAA^+}$) as a function of the solution concentration of TPrABr, TBuABr and TAmABr. Ionic strength 5×10^{-3} M.

omitted because of their limited accuracy. Electrokinetic charge densities, computed from the corresponding zeta potentials using eq. 4.10, have also been displayed. Actually, Fig. 6.4 provides information on the charge distribution over the hydrodynamically mobile (σ_{ek}) and immobile ($\sigma_\Delta = \sigma_0 + \sigma_{TAA^+} - \sigma_{ek}$) part of the electrical double layer as a function of the equilibrium TAA^+ concentration. At bare polystyrene more than 80 percent of the double layer charge resides behind the slipping plane. Upon increasing the TAA^+ concentration the amount of immobilized charge appears to be reduced drastically and ultimately to become zero. The change in σ_{ek} is comparatively small. These observations suggest that tetraalkylammonium ions affect the structure of the surface layer on the polystyrene particles. We will return to this issue in section 6.3.3.

Additional information on the effect of TAA^+ adsorption on the properties of the surface layer is provided by the surface conductivity data depicted in Fig. 6.5. The dashed lines represent the experimental values of the surface conductivity κ_B^σ. These values have been calculated from the data on electroconduction given in tables 6.2 till 6.4 by means of Bruggeman's equation 4.17. The

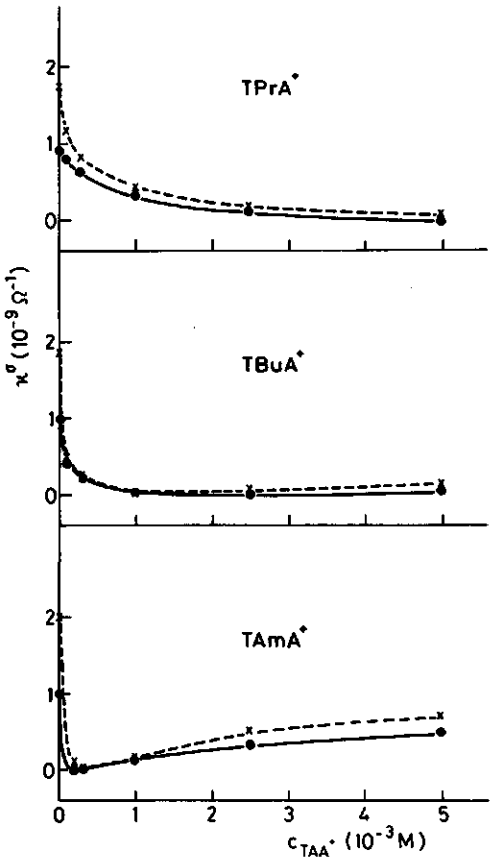

Fig. 6.5 - Theoretical (Bikerman (eq. 4.21), drawn lines) and experimental (Bruggeman (eq. 4.17), dashed lines) values for the surface conductivity as a function of the solution concentration of TPrABr, TBuABr and TAmABr. Ionic strength 5×10^{-3} M.

drawn lines, representing the theoretically predicted values for the surface conductivity in the layer outside the slipping plane, κ^{σ}_{ek}, have been obtained by inserting ζ into the extended Bikerman equation 4.21 and assuming the equivalent conductivity of all ions to be identical to their bulk value (10). Fig. 6.5 shows that the adsorption of tetraalkylammonium ions goes along with a drastic reduction of the overall surface conductance. For one part this

reduction is caused by the decrease in the amount of electrokinetically displaceable charge (see Fig. 6.4), which effect is quantitatively expressed in the Bikerman curves. For another part, the decrease in κ_B^σ stems from the strong reduction of the conductance in the stagnant layer (= difference between Bruggeman and Bikerman curves). This so-called anomalous conductance contributes to the surface conductance of bare polystyrene by about 50 percent, but (within experimental error) equals zero for $10^{-3} < c_{TPrA^+} < 5x10^{-3}$, $10^{-4} < c_{TBuA^+} < 2.5x10^{-3}$ and $3x10^{-4} < c_{TAmA^+} < 10^{-3}$. Then the experimental and theoretical (Bikerman) values of surface conductivity are identical, which is extremely unusual. Obviously, the disappearance of the anomalous conduction is related to the reduction in the number of charge carriers inside the fixed layer (see Fig. 6.4) and with the lower equivalent conductivity of TAA^+ ions as compared with K^+ ions.

For $TBuA^+$ as well as $TAmA^+$, the κ^σ-c_{TAA^+} curves pass through a minimum coinciding approximately with the i.e.p. Here no surface conductance occurs, indicating the adsorbed TAA^+ ions to be immobile in the applied electrical field. Beyond the minimum, both κ_{ek}^σ and the anomalous surface conductance slightly increase, suggesting the creation of an electrical double layer in which the ions are distributed over a hydrodynamically mobile and immobile part. Presumably this double layer originates from the adsorption of TAA^+ ions onto hydrophobic sites.

6.3.1.3 CONDUCTANCE-FREQUENCY CHARACTERISTICS

Frequency-spectra of the conductance for various concentrations of tetrapropyl-, tetrabutyl- and tetraamylammonium ions are shown in Fig. 6.6. Data at 1592 Hz obtained with an R-C bridge connected to the plug electrodes is also included. These results agree satisfactorily with those obtained by the four electrode technique at 1000 Hz. The conductance increment appears to reduce strongly upon increasing TAA^+ concentration, suggesting the underlying intrinsic relaxation phenomena are suppressed when TAA^+ ions get adsorbed inside the plug. We will return to this matter in section 6.3.2.3.

The ultimate increment amounts to about 15 percent and presumably stems from processes taking place at the plug electrodes

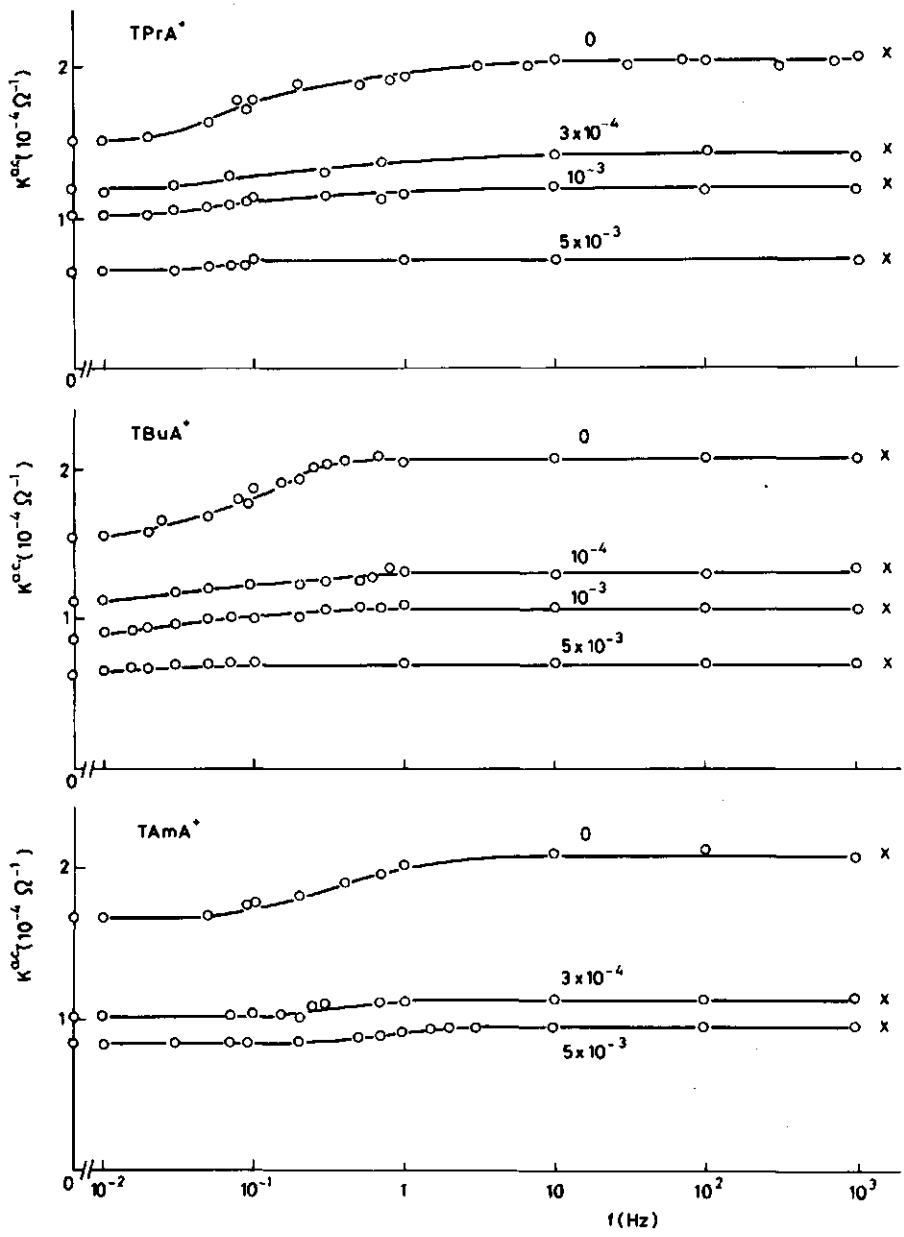

Fig. 6.6 - Dependence of the plug conductance upon frequency, for various TPrABr, TBuABr and TAmABr concentrations (M): o, obtained with the four electrode method; x, obtained with an R-C bridge connected to the plug electrodes.

(section 5.3.1.3).

Unfortunately, the data in Fig. 6.6 scatter too much to unequivocally establish the effect of TAA^+ adsorption on the dispersion frequency.

6.3.1.4 DESORPTION

At the end of the electrokinetic and a.c. conductance measurements, the polystyrene plugs have been permeated with $5x10^{-3}$ M KBr with the purpose of desorbing all tetraalkylammonium ions. After a 150-fold displacement of the pore liquid, $TPrA^+$ and $TBuA^+$ had desorbed completely as could be inferred from the zeta potential, the surface conductivity and a.c. conductance data. For the plug contacted with $TAmA^+$, however, a discrepancy with the data corresponding to the bare surface was still observed. For instance, ζ and κ_B^σ amounted to 61 mV and $1.3x10^{-9}$ Ω^{-1}, respectively, whereas for the bare surface 68.2 mV and $2x10^{-9}$ Ω^{-1} was obtained, respectively. These differences did not diminish upon another 60-fold volume displacement, indicating that $TAmA^+$ ions do not desorb completely from polystyrene upon dilution.

6.3.2 MEASUREMENTS AT CONSTANT $TBuA^+$ CONCENTRATION BUT VARYING IONIC STRENGTH

6.3.2.1 ADSORPTION MEASUREMENTS

Fig. 6.7 shows the amount of adsorbed $TBuA^+$, Γ_{TBuA^+}, as a function of ionic strength. The equilibrium $TBuA^+$ concentration actually varied from $3.5x10^{-4}$ M to $3.9x10^{-4}$ M. A decrease in Γ_{TBuA^+} upon increasing salt concentration is observed. This has to be attributed to a reduction of the electrical component of the interaction between the $TBuA^+$ ions and the polystyrene surface due to an enhanced shielding of the charged groups.

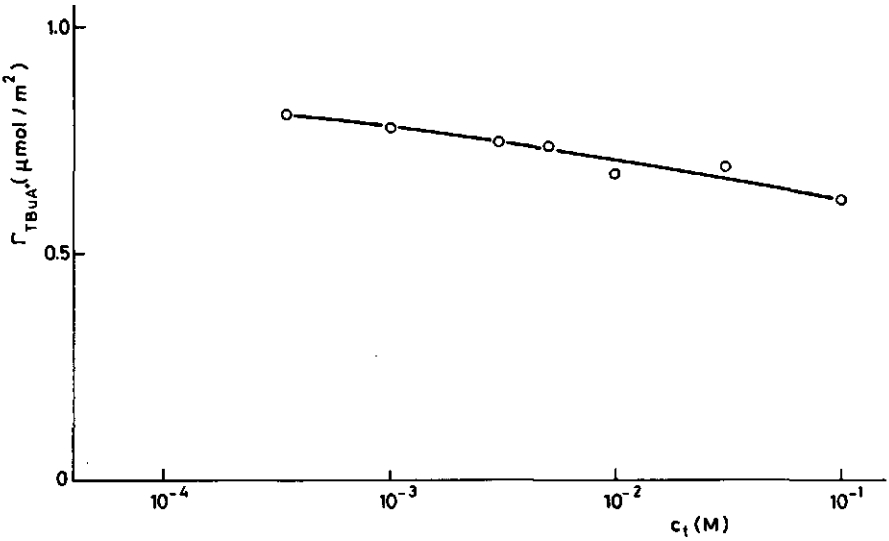

Fig. 6.7 - The adsorption of $TBuA^+$ on polystyrene as a function of ionic strength. $c_{TBuA^+} = 3.5\text{-}3.9 \times 10^{-4}$ M.

6.3.2.2 ELECTROKINETICS

In Fig. 6.8 current retardation and I-V plots are presented as obtained for ionic strengths of 3×10^{-4} M and 10^{-3} M at ΔP = 30 cm Hg. Comparing these I-V curves with those obtained with bare polystyrene particles for corresponding salt concentrations (chapter 5, Figs. 5.4c and d.), it turns out that the contribution of the intrinsic processes to the measured current is drastically reduced. Once more this proves the origin of the upward curvature in the I-V plots to be mainly located at the polystyrene - aqueous solution interface. Furthermore, these results may be considered as an unequivocal proof of the correctness of the extrapolation method in determining streaming currents.

The I-V plots obtained at ionic strengths above 10^{-2} M (and $c_{TBuA^+} = 3 \times 10^{-4}$ M) showed the same shape as those obtained with plugs of bare polystyrene particles.

Table 6.5 comprises the electrokinetic data of plug IV for varying ionic strength, as obtained from I-V plots, and streaming potential and d.c. conductance measurements. Bulk conductivities

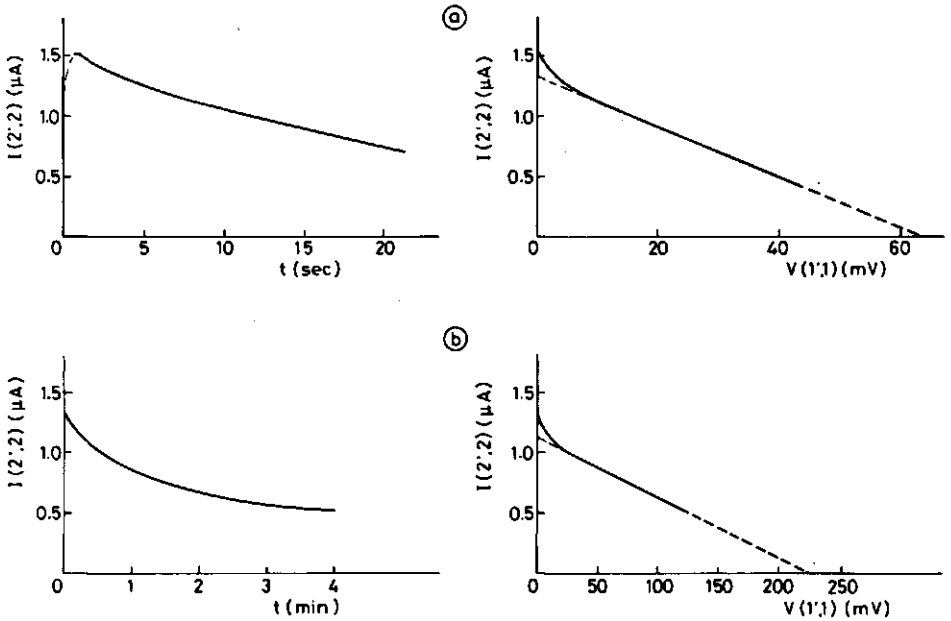

Fig. 6.8 - Current retardation and corresponding I-V plots at $c_{TBuA^+} = 3x10^{-4}$ M, $c_{KBr} = 7x10^{-4}$ M (a) and at $c_{TBuA^+} = 3x10^{-4}$ M (b) (ΔP 0 → 30 cm Hg).

Table 6.5 - Electrokinetic data of plug IV for various ionic strengths (KBr) and constant TBuABr ($3x10^{-4}$ M) concentration, obtained from both I-V plots and streaming potential and d.c. conductance measurements (ΔP = 30 cm Hg). Bulk conductivities are also included.

	I-V plot		Streaming potential method		Bulk conductivity
c_t (M)	I_s (μA)	$K^{d.c.}$ (Ω^{-1})	V_s (mV)	$K^{d.c.}$ (Ω^{-1})	K_o ($\Omega^{-1}m^{-1}$)
$3x10^{-4}$	-1.15	$5.07x10^{-6}$	- 224	$5.09x10^{-6}$	$2.72x10^{-3}$
10^{-3}	-1.35	$2.13x10^{-5}$	-63.6	$2.11x10^{-5}$	$1.36x10^{-2}$
$5x10^{-3}$	-1.45	$1.00x10^{-4}$	-14.2	$1.02x10^{-4}$	$6.95x10^{-2}$
10^{-2}	-1.38	$1.97x10^{-4}$	- 6.90	$1.99x10^{-4}$	$1.43x10^{-1}$
10^{-1}	-1.00	$1.72x10^{-3}$	- 0.582	1.76^7x10^{-3}	1.28^9

are also presented. Following the procedures described in section 6.3.1.2, the adsorption, electrokinetic and electroconduction data have been converted into ζ-potentials (Fig. 6.9), effective

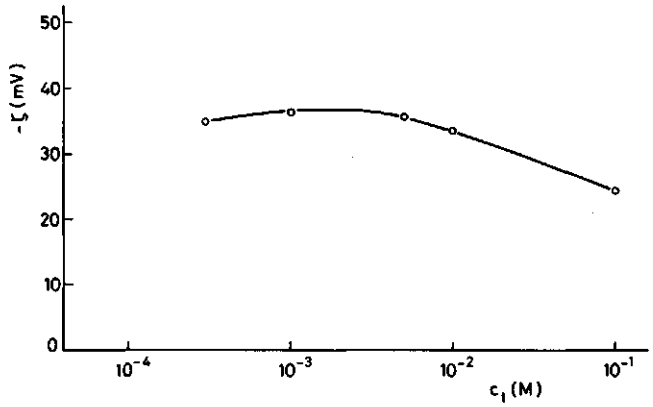

Fig. 6.9 - Zeta potential of polystyrene, covered with $TBuA^+$ ($c_{TBuA^+} = 3x10^{-4}$ M), as a function of ionic strength.

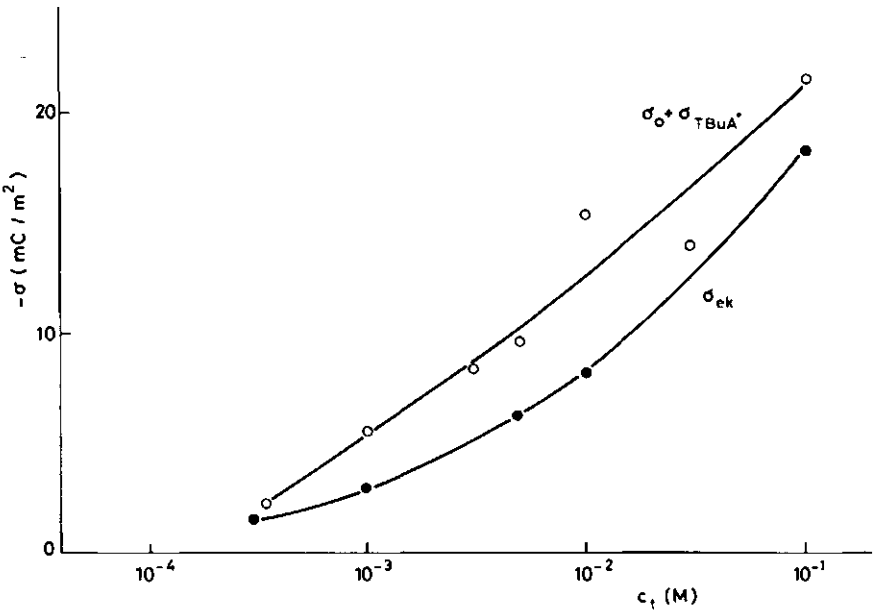

Fig. 6.10 - Electrokinetic (σ_{ek}) and effective surface charge density ($\sigma_0 + \sigma_{TBuA^+}$) at $c_{TBuA^+} = 3x10^{-4}$ M, as a function of ionic strength.

surface charge densities and electrokinetic charge densities (Fig. 6.10) and experimental and theoretical surface conductivities (Fig. 6.11). The error bars in Fig. 6.11 represent the uncertainty in the experimental surface conductivity κ_B^σ calculated from the experimental errors in $\bar{K}$, K_0, p and d, which were all assumed to be 1 percent. The uncertainties have been incorporated in order to illustrate the strongly increasing inaccuracy in κ_B^σ upon increasing the ionic strength.

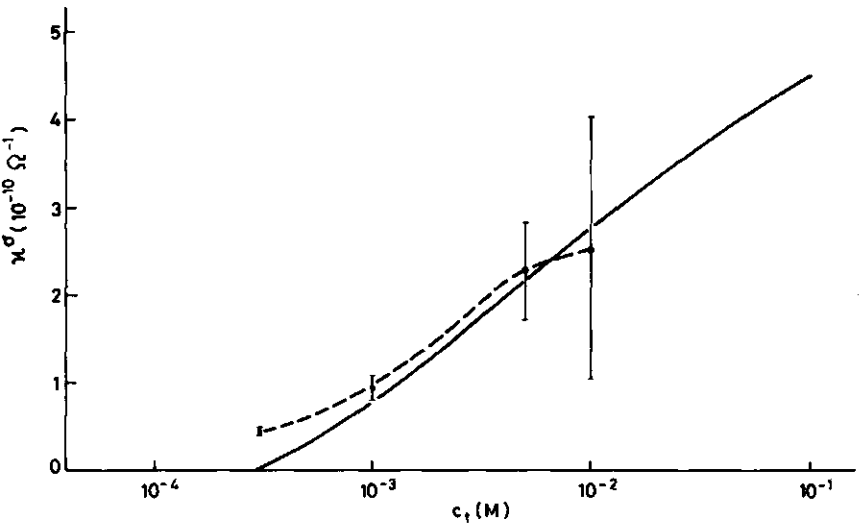

Fig. 6.11 - Theoretical (Bikerman (eq. 4.21), drawn line) and experimental (Bruggeman (eq. 4.17), dashed line) values for the surface conductivity at $c_{TBuA^+} = 3x10^{-4}$ M, as a function of ionic strength.

Comparing these results with those obtained for uncovered polystyrene (Figs. 5.9, 5.10 and 5.11), the strong influence of $TBuA^+$ adsorption on the electrokinetic and electroconduction properties of polystyrene latices becomes apparent. In the first place, the maximum in the ζ-log c curve fades away. Admittedly, below an ionic strength of 10^{-3} M the ζ-potentials of the $TBuA^+$ covered latex also decrease (slightly), but that decrease is connected with the reduction of the effective surface charge density (see Fig. 6.10, upper

line). Secondly, the fraction of the double layer charge that is electrokinetically displaceable greatly increases through $TBuA^+$ adsorption. In contrast with bare polystyrene, the electrokinetic and (effective) surface charge density of the $TBuA^+$-polystyrene system are of the same order of magnitude and display the same ionic strength dependence, indicating the location of the effective shear plane to be hardly or not dependent on ionic strength. Thirdly, the fixed layer contribution to the overall surface conductance reduces strongly when $TBuA^+$ ions adsorb onto the polystyrene surface. For ionic strengths above 10^{-3} M no significant differences between the experimental and theoretical surface conductivity values of the $TBuA^+$-polystyrene system exist, implying anomalous conductance does not occur at all.

6.3.2.3 CONDUCTANCE-FREQUENCY CHARACTERISTICS

Frequency-spectra of the plug conductance for various ionic strengths are presented in Fig. 6.12. As before, the reduced cell

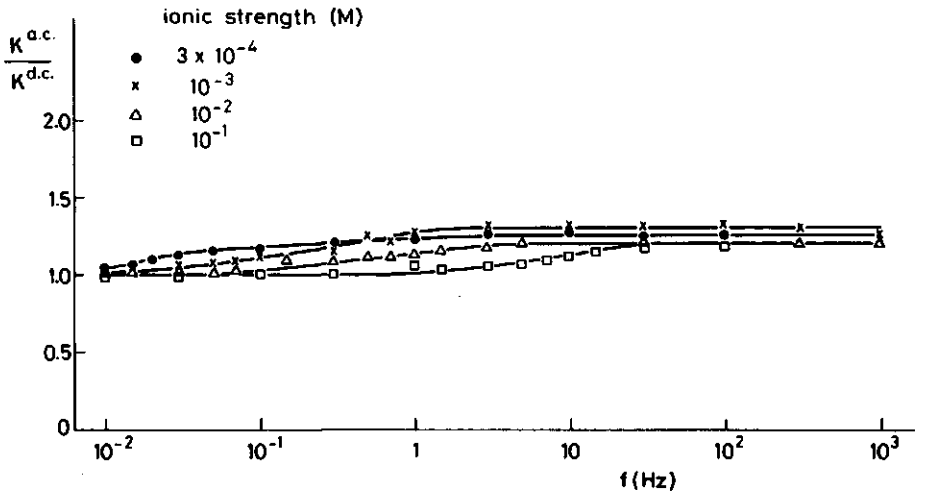

Fig. 6.12 - Dependence of the reduced plug conductance upon frequency at $c_{TBuA^+} = 3x10^{-4}$ M, for different ionic strengths.

conductance has been plotted, i.e. the ratio of the a.c. conductance $K^{a.c.}$ and the d.c. conductance $K^{d.c.}$. The ralative conductance increment is seen to be independent of ionic strength over the whole range, a feature also observed for cells only containing electrolyte (section 5.3.1.2) In addition, the ultimate reduced conductance of the plug (= 1.2-1.3) is of the order of the value obtained for a reference cell with similar cell constant (Fig. 5.7, $K^{a.c.}/K^{d.c.}$ = 1.35-1.40). Therefore, it is likely that the dispersion of the conductance of the $TBuA^+$ covered polystyrene plug stems from the same polarization processes occurring in reference cells, i.e. processes taking place at the plug electrodes.

Comparison with the dispersion curves obtained for plugs of bare polystyrene particles (Fig. 5.8) shows that below an ionic strength of 10^{-2} M the conductance increment is drastically reduced. Apparently, the relaxation phenomena in a polystyrene plug are suppressed through $TBuA^+$ adsorption. A similar conclusion was obtained from the I-V plots.

Clear evidence of the influence of $TBuA^+$ adsorption on the dispersion frequency cannot be established.

6.3.3 IMPACT OF TAA^+ ADSORPTION ON THE SURFACE STRUCTURE OF POLYSTYRENE PARTICLES

In the preceeding chapter, the concept of a hairy surface layer on polystyrene particles was introduced in order to account for the anomalies in the electrokinetic (maximum in the ζ-log c curve, ionic transfer in the stagnant layer, relaxation of the streaming current) as well as the a.c. conductance data (low frequency conductance dispersions) obtained on plugs of this material. Such anomalies do either not appear at all or much less pronounced when the particles, constituting the plug, are covered with tetraalkylammonium ions (section 6.3.2). Apparently, these particles are not hairy. The results in section 6.3.1 show that the contribution of the immobilized layer to the surface conductance as well as to the overall diffuse charge reduces upon increasing the TAA^+ adsorption. Furthermore, the intrinsic polarization processes are increasingly suppressed. All evidence taken together, it must be concluded that the hairy layer on the surface of the polystyrene particles gra-

dually shrinks and ultimately disappears upon increasing adsorption of TAA^+ ions. The results in Figs. 6.2, 6.4 and 6.5 indicate the shrinkage of the hairy layer already starts at relatively small surface occupancies.

The collapse of the hairy layer might be visualized as due to the adsorption of TAA^+ ions between sulfate end groups of protruding polystyrene chains. As a result the electrostatic repulsion between these charged groups, and thus the expansion of the hairy layer, diminishes.

It is to be expected that the decrease in the extent of hairiness goes along with a decrease in the stability of the latex against coagulation, because the steric contribution to the repulsion between the particles is diminished. Unfortunately, this hypothesis cannot be experimentally verified, since TAA^+ adsorption also affects the electrostatic repulsion. Some indications on the relationship between "electrokinetic hairiness" and colloidal stability, however, could be obtained from some preliminary experiments with polyelectrolytes as the adsorbate. When adsorbing polylysine (molecular weight 4000) in a polystyrene plug, the anomalies in the electrokinetic as well as a.c. conductance data virtually disappeared, whereas the (absolute) value of ζ, characterizing the electrostatic repulsion, remained approximately constant. However, flocculation experiments showed the latex sample covered with polylysine to be less stable than the bare polystyrene sample.

6.4 CONCLUDING REMARKS

The combination of electrokinetic, a.c. conductance and adsorption measurements yields detailed information on the structure of the interface in the system under investigation. Insight is obtained with regard to the adsorption mechanism and the electrical double layer properties in addition to the surface structure of the adsorbent. The results show that adsorption of tetraalkylammonium ions largely eliminates the polyelectrolyte character of the polystyrene surface.

6.5 REFERENCES

1. Kůta, J. and Smoler, I., Collection Czechoslov. Chem. Commun. 40, 225 (1975).
2. Hamdi, M., Bennes, R., Schuhmann, D. and Vanel, P., J. Electroanal. Chem. 108, 255 (1980).
3. De Keizer, A. and Lyklema, J., J. Colloid Interface Sci. 75, 171 (1980).
4. Ottewil, R.H. and Vincent, B., J. Chem. Soc., Faraday Trans. I 68, 1533 (1972).
5. De Keizer, A., Thesis, Agricultural University, Wageningen (1981).
6. Wen, W-Y. in "Water and Aqueous Solutions" (R.A. Horne, Ed.), p. 622, Wiley, New York, 1972.
7. Traube, I., Ann. 265, 27 (1891).
8. Grahame, D.C. and Parsons, R., J. Am. Chem. Soc. 83, 1291 (1961).
9. Devanathan, M.A.V. and Fernando, M.I., Trans. Faraday Soc. 58, 368 (1962).
10. Parsons, R., "Handbook of Electrochemical Constants", Butterworths, London, 1959.

CHAPTER 7

ELECTROKINETIC PROPERTIES AND CONDUCTANCE RELAXATION OF SILVER IODIDE PLUGS

7.1 INTRODUCTION

Up to this stage the electrokinetic and electrical techniques presented in this thesis only referred to measurements on plugs made up of polystyrene latices. This approach resulted in revealing several anomalous phenomena connected with the model system itself. Amongst these is the occurrence of slow intrinsic relaxations, a phenomenon rarely referred to in existing literature.

The purpose of this chapter is to explore the applicability of the said techniques in a more general sense, by applying them to a rather different system. For this purpose, we chose plugs prepared from suspensions of silver iodide. This inorganic colloid has frequently been used in colloid chemical studies, including electrokinetic ones (1). For the major part, however, the latter concern measurements of electrophoretic mobilities, which were usually not converted into zeta potentials. Therefore, the amount of data on the zeta potential of silver iodide is very limited. In addition, simultaneous determination of zeta potential and surface conductivity as a function of a number of variables has not been carried out before. As shown in the preceeding chapters, in this way one may gain insight into possible differences between the electrokinetic potential and the potential at the Outer Helmholtz Plane (2).

Measurements have been performed for various salt concentrations and surface potentials. Furthermore, some preliminary experiments in the presence of tetrabutylammonium ions have been conducted to investigate the influence of adsorbing species. The latter measurements also provide information on the origin of the excess conductance in silver iodide plugs.

7.2 EXPERIMENTAL

7.2.1 MATERIALS

The silver iodide suspension used was kindly supplied by De Keizer. It was prepared by precipitation from $AgNO_3$ and KI solutions according to the recipe given in reference 3. The sample had been stored for three years in a stoppered flask in darkness. Scanning electron micrographs (Fig. 7.1) showed the presence of predominantly hexagonal crystals (long axis varying from 0.5 μm to 5 μm).

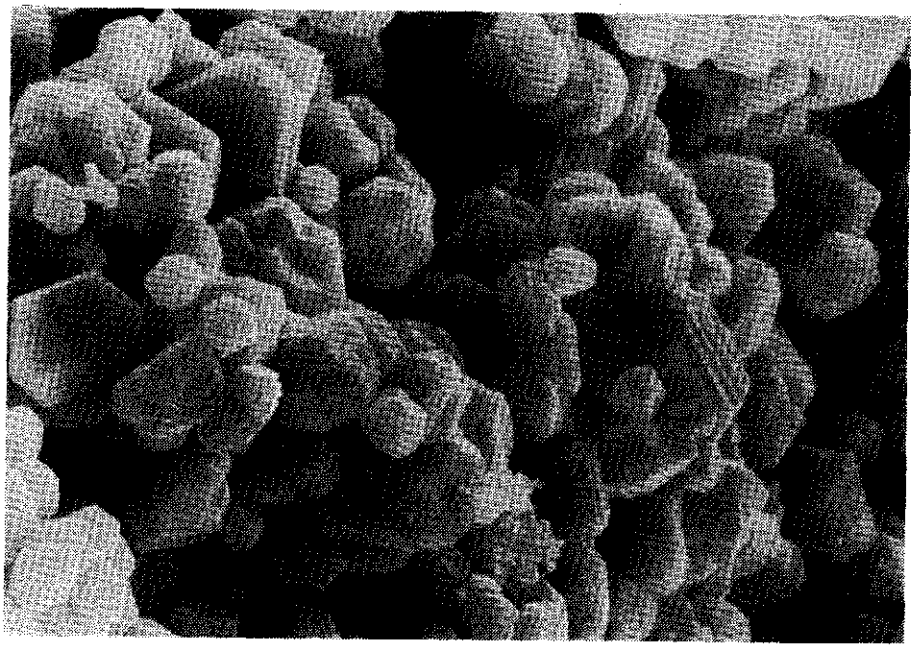

Fig. 7.1 - Scanning electron micrograph of the silver iodide particles (⊢⊣ = 1 μm).

A standard solution of tetrabutylammonium nitrate was prepared by potentiometric titration of a solution of the iodide salt (Fluka A.R.) with $AgNO_3$ up to the equivalence point. The precipitated silver iodide was removed by centrifugation.

All other chemicals were of A.R. quality. All water was dis-

tilled once and subsequently filtered through a column containing silver iodide in order to remove any component which otherwise may adsorb at the plug material.

7.2.2 PREPARATION AND CHARACTERIZATION OF THE PLUGS

Two plugs were made by compressing settled layers of silver iodide by centrifugation. The settled layers were prepared by introducing the silver iodide in small portions in order to obtain a homogeneous distribution of particle sizes along all the length of the plug. The extent of compression, and consequently the plug porosity, appeared to be dependent on the centrifugal pressure. One plug was obtained at a pressure of 10^6 N/m^2 (plug A), the other at $2x10^6$ N/m^2 (plug B). Both pressures considerably exceed the pressure differences applied in the electrokinetic and liquid permeability measurements (which extend up to $4x10^4$ N/m^2). Therefore the plugs may be expected to be mechanically stable during these experiments.

After completing the measurements, the porosity of both plugs was determined as described in section 5.2.2. For A and B porosities of 59.9 and 52.5 % were obtained, respectively. Van den Hul (4) obtained plugs with a comparable porosity by filtering silver iodide suspensions. By compressing dried suspensions, he could prepare plugs with a porosity down to about 25 %. However, we did not use this technique, since the wetting of the hydrophobic silver iodide after preparing the plug in the dry state may be incomplete, thereby trapping air bubbles in the plug.

Cross-sections of both plugs were studied by scanning electron microscopy according to the method described in section 5.2.2.

7.2.3 DETERMINATION AND ADJUSTMENT OF pAg

The concentration of potential determining ions in the solution making contact with the silver iodide plug was determined by measuring the EMF (E) of a cell consisting of the solution and an Ag/AgI and a saturated calomel electrode (Electrofact R111). According to Nernst's law, the relation between E and the negative logarithm of the Ag^+ (pAg) or I^- (pI) concentration in solution at

25 °C reads:

$$E = E' - 59.2\ pAg = E'' + 59.2\ pI \qquad [7.1]$$

where E' and E" are standard potentials depending on temperature and ionic strength. The values of E' and E" were determined by calibrating the cell-EMF with solutions of known pAg and pI and known concentration of inert electrolyte (10^{-3} M KNO_3).

For Ag^+ (I^-) concentrations above 10^{-5} M, the pAg (pI) of the solution in the pores of the plug could be adjusted by simply percolating a solution of the required pAg through the plug. At lower Ag^+ (I^-) concentrations, however, the ad-desorption of Ag^+ (I^-) ions at the silver iodide-solution interface in the plug usually led to measurable changes in the initial pAg of the solution. This effect becomes manifest because of the large surface to volume ratio of the plug pores. Therefore, in the region between 5 and 11, the pAg of the solution in the electrokinetic cell was adjusted by intermittently adding drops of a diluted KI or $AgNO_3$ solution, while permeating the plug, until constancy of the required pAg was attained. This procedure did not measurably increase the ionic strength, as could be inferred from conductivity data.

In passing it should be noted that ion-exclusion (Donnan effect) is not to be expected, because the effective pore radius of the plugs (section 7.3.1) largely exceeds the double layer thickness for all ionic strengths. Consequently, the pAg values of the solution within and outside the plug are identical.

7.2.4 METHODS

Electrokinetic and a.c. conductance measurements were performed using the techniques described in chapters 3 and 5, respectively. The electrodes making contact with the plug were of the Pt black type. Ag/AgI electrodes were used as reservoir electrodes. These were chosen instead of platinum because in solutions containing Ag^+ and I^- ions their potential is more stable. Moreover, the use of Ag/AgI electrodes enabled determination of the pAg of the solution in the electrokinetic cell.

Bulk conductivities were determined according to the method

described in section 5.2.3.

The hydrodynamic permeability of the plugs was determined by weighing the volume of liquid permeating in a given period for various pressure drops. The flow-measuring device described in section 3.4.1 could not be used, because of the rather high permeability of silver iodide plugs.

The effects of the following variables were investigated:
plug A: ionic strength at pI = 4; pAg at 10^{-3} M KNO_3
plug B: ionic strength at pI = 4; adsorption of tetrabutylammonium ions at pI = 4 and 10^{-3} M KNO_3.

After adjusting the solution in the cell, the plug was permeated until changes in the I-V plot and in the plug conductance at 1592 Hz could no longer be observed. Owing to the higher permeability of silver iodide plugs, equilibrium was attained much faster than for polystyrene plugs; usually a few hours of percolation were sufficient.

All measurements were performed at 25 °C.

7.3 RESULTS AND DISCUSSION

7.3.1 PERMEABILITY AND PORE DIMENSIONS

Permeabilities were obtained from plots of the volume flow rate J_v versus the applied pressure difference ΔP. At least up to ΔP values of 30 cm Hg these plots were linear, indicating laminar flow conditions.

During a series of electrokinetic experiments the permeability of both plugs was measured at regular intervals. The results are given in Fig. 7.2, showing that the permeability is not constant, but decreases continuously. For plug B the decay amounts to about 30 percent in 40 days. This phenomenon is not caused by compression of the diaphragm due to the applied pressure gradients. If compression occurred, the corresponding increase in the packing density would lead to a change in the plug conductance (except at the isoconductivity point). However, an instantaneous pressure change was never observed to have any effect on the plug conductance.

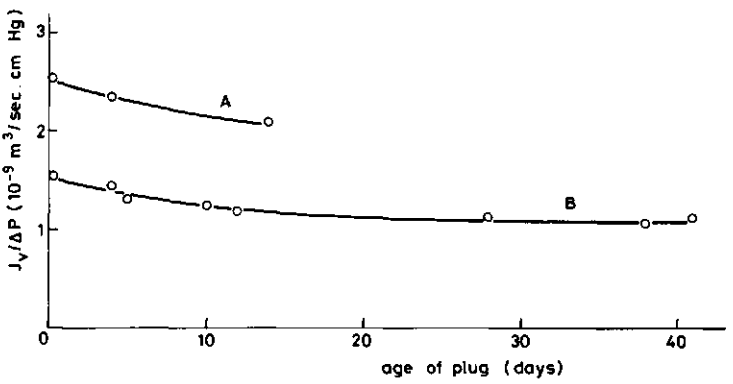

Fig. 7.2 - Permeability of plugs A and B as a function of their age

Another argument against compression is that the decay still proceeded when no liquid was permeated. Van den Hul (4), also investigating the permeability of silver iodide plugs, observed a similar decrease. He attributed this to the break-down of aggregates, leading to an increase in the number but a decrease in the radius of the capillaries. Since the volume flow is proportional to the first power of the number, but to the fourth power of the pore radius, the overall effect is a decrease of the permeability. The peptization possibly concerns flocs that were not present in the original precipitate, but that have been formed during the preparation of the plug. Another cause of the decrease in permeability might be that during liquid permeation small particles are displaced, through which capillaries are being (partially) blocked. After 40 days the permeability of plug B virtually becomes constant. Apparently, after this period the rearrangement of particles practically stops.

The fall in the permeability was accompanied with an increase of the conductometric cell constant C_p (defined as the ratio of bulk conductivity K_o and plug conductance K at 10^{-1} M), but these changes were comparatively small. C_p of plug B, e.g., increased from 599 m^{-1} immediately after preparation to 611 m^{-1} after 41 days, i.e. by only 2 percent. The increase in C_p may be explained by an increase in the effective path length of the electrical field

lines and a decrease in the overall cross-sectional area of the pores as a result of the break-down and rearrangement of particles.

From the permeability data the equivalent pore radius a was computed by using the Kozeny-Carman equation (5), which can be written as

$$a = \left(\frac{4\eta L}{(1-p)A} \frac{J_v}{\Delta P} K_c\right)^{\frac{1}{2}} \qquad [7.2]$$

where η is the viscosity of the solution. L represents the length (= 1.51×10^{-2} and 1.47×10^{-2} m for plug A and B, respectively), A the cross-sectional area (= 7.62×10^{-5} m^2 for both plugs) and p the volume fraction of the solid phase. K_c is a numerical constant which includes the tortuosity factor. Applying eq. 7.2 to the permeability data presented in Fig. 7.2 and the porosity data given in section 7.2.2, while taking K_c = 5 (5), the following pore radii were obtained: plug A, 3.36 μm and 3.04 μm after 0 and 14 days, respectively; plug B, 2.77 μm and 2.32 μm after 0 and 41 days, respectively.

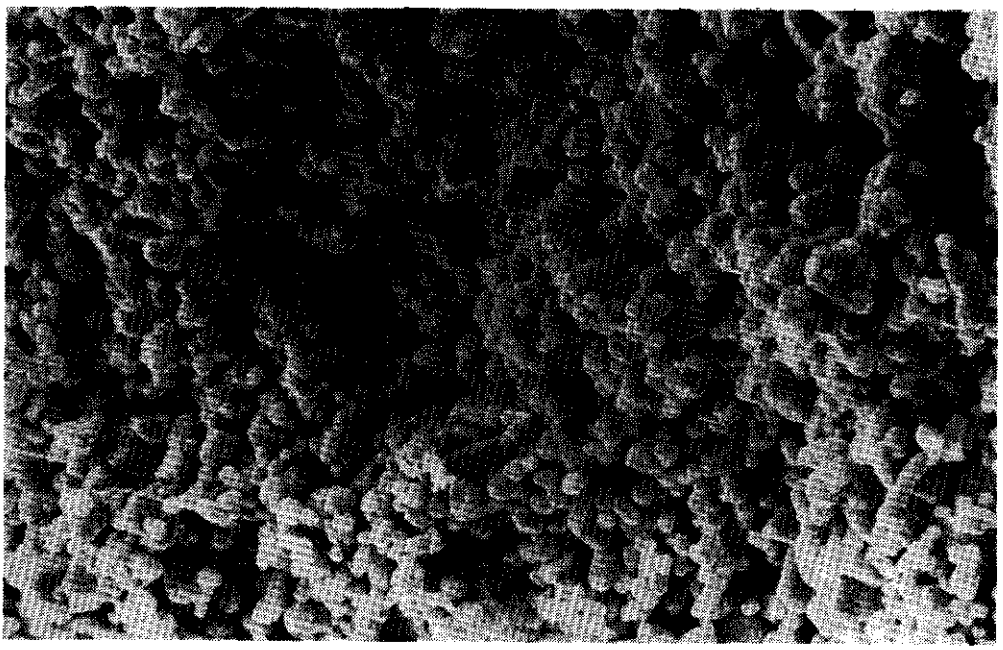

Fig. 7.3 - Scanning electron micrograph of a cross-section of plug B (⊢——⊣ = 10 μm).

Additional information about the pore sizes was obtained from electron micrographs of cross-sections of the plugs. A typical micrograph is shown in Fig. 7.3. A broad distribution of pore sizes is observed. The larger pores have dimensions in the same order of magnitude as inferred from the permeability data. This indicates that micro-cracks in the wet plug are not present, since these would cause a relatively large permeability.

7.3.2 ELECTROKINETICS

In general, the current retardation and I-V plots exhibited the same characteristic features as those obtained with polystyrene plugs (section 3.5.2.2 and 5.3.1.1). The only striking difference was, that also at low ionic strength hardly any contribution of intrinsic processes to the measured current was observed. To illustrate this feature, in Fig. 7.4 the I-V plot obtained for plug A at 10^{-4} M KI is shown. The initial current is seen to exceed the

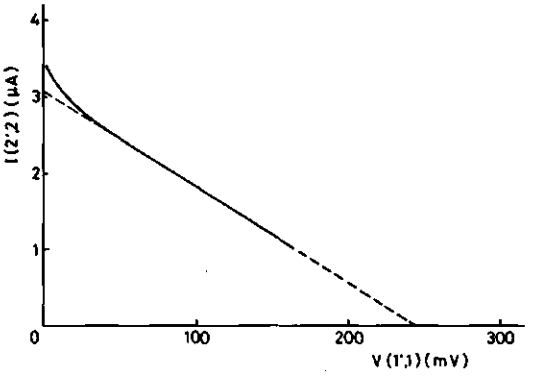

Fig. 7.4 - I-V plot as obtained with plug A for 10^{-4} M KI; ΔP = 20 cm Hg.

streaming current by only about 10 percent, whereas for polystyrene at low ionic strength differences of more than 100 percent were observed (Fig. 5.4). The upward curvature in the I-V plots was not affected, either by variations in the pAg or by adsorption of $TBuA^+$ ions. We return to this issue in section 7.3.3.

In the pressure range studied, the streaming potential and streaming current versus pressure curves were perfectly linear. Reversal of the flow direction yielded identical curves.

Electrokinetic data of plugs A and B obtained from I-V plots as well as from streaming potential and d.c. conductance measurements is collected in tables 7.1 till 7.3. The signs of I_s and V_s correspond to those of the surface charge. Bulk conductivities are also included.

In the following sections we will discuss the double layer characteristics that have been derived from the electrokinetic data at varying ionic strength, $TBuA^+$ concentration and pAg, respectively.

7.3.2.1 INFLUENCE OF THE IONIC STRENGTH

Table 7.1 contains the electrokinetic data of plugs A and B, as obtained for various ionic strengths (KNO_3) at pI = 4. From the mean value of the streaming current data as obtained from the I-V plot and as calculated from the combination of streaming potential and d.c. conductance, zeta potentials have been calculated. At 10^{-1} M the former data has not been considered, since, because of the fast and strong retardation, the I-V plot yielded less accurate results (section 3.5.2.2). Since for all ionic strengths the conditions of laminar flow and $\kappa a >> 1$ were met, ζ could be computed from the simple Helmholtz-Smoluchowski (H-S) formula 3.1. The conductometric cell constant of plug A amounted to 486 m^{-1}, that of plug B to 599 m^{-1}. The measurements with plug B at 1.1×10^{-3} M were performed in the series of experiments concerned with the effect of $TBuA^+$, where C_p amounted to 610 m^{-1}.

In Fig. 7.5 close agreement is observed between the ζ-potentials obtained for the two plugs. Thus, in the range studied the observed ζ-potential does not depend on porosity. Another striking aspect of Fig. 7.5 is that the ζ-log c curve passes through a maximum. The occurrence of such a maximum, which has also been found in electrophoresis measurements (6), is in complete contradiction to the Gouy-Chapman description of the diffuse double layer.

The anomalous behaviour of silver iodide is even more clearly illustrated in Fig. 7.6, where the charge density at the shear

Table 7.1 - Electrokinetic data of plugs A and B for various values of the ionic strength, obtained from both I-V plots and streaming potential and d.c. conductance measurements (ΔP = 20 cm Hg); pI = 4. Bulk conductivities are also included.

	I-V plot		Streaming potential method		Bulk conductivity
c_t(M)	I_s(μA)	$K^{d.c.}$(Ω^{-1})	V_s(mV)	$K^{d.c.}$(Ω^{-1})	K_o(Ω^{-1} m^{-1})
			A		
10^{-4}	-3.05	$1.25^5 \times 10^{-5}$	-244	*	1.54×10^{-3}
1.1×10^{-3}	-4.33	4.41×10^{-5}	- 98.0	4.39×10^{-5}	1.35×10^{-2}
5×10^{-3}	-5.43	1.74×10^{-4}	- 31.2	1.74×10^{-4}	7.01×10^{-2}
10^{-1}	-4.90	2.50×10^{-3}	- 1.93	2.48×10^{-3}	1.20^4
			B		
10^{-4}	-2.53	1.55×10^{-5}	-163	*	1.50×10^{-3}
1.1×10^{-3}	-3.49	4.92×10^{-5}	- 71.0	4.93×10^{-5}	1.57×10^{-2}
10^{-2}	-4.41	2.61×10^{-4}	- 16.7^5	2.61×10^{-4}	1.33×10^{-1}
10^{-1}	-3.62	1.91×10^{-3}	- 1.88	1.99×10^{-3}	1.19^2

* *Not measurable because of continuous drift of potential drop across the plug during current passage.*

plane σ_{ek} and that at the wall σ_o are given as a function of ionic strength. σ_{ek} was computed from ζ according to the $\sigma(\zeta)$ relation for flat double layers (eq. 4.10). The σ_o data, as obtained from potentiometric titrations of silver iodide suspensions at pAg = 11 (pI = 5), was taken from reference 1. No charge densities at pI = 4 have been published, but in all probability these will be close to those at pAg = 11, since σ_o is only weakly dependent on pI in this range. Two striking features are observed in Fig. 7.6:

(i) above an ionic strength of about 5×10^{-3} M, σ_{ek} exceeds σ_o. Physically this is only possible when specific adsorption of NO_3^- ions (at the negatively charged surface) would be excessive, but this is very unlikely, because the point of zero

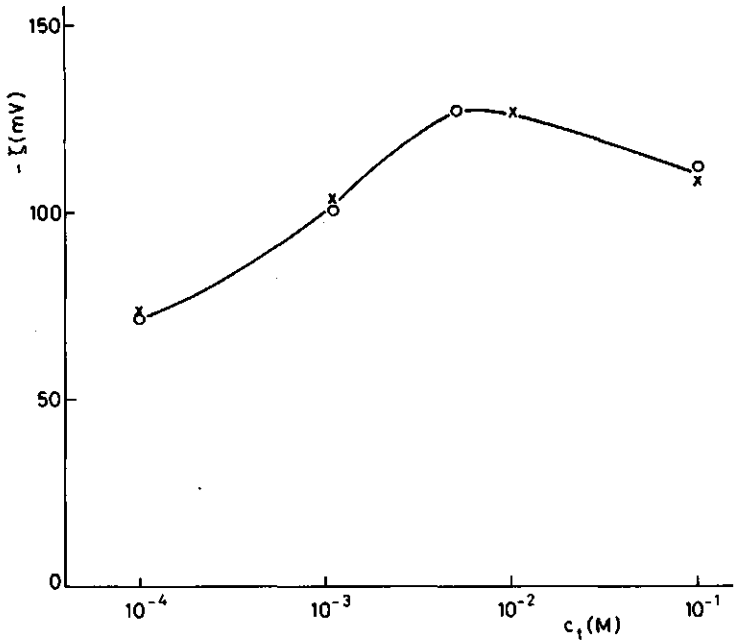

Fig. 7.5 - ζ-potentials of plug A (o) and B (x) as a function of ionic strength (KNO_3); pI = 4.

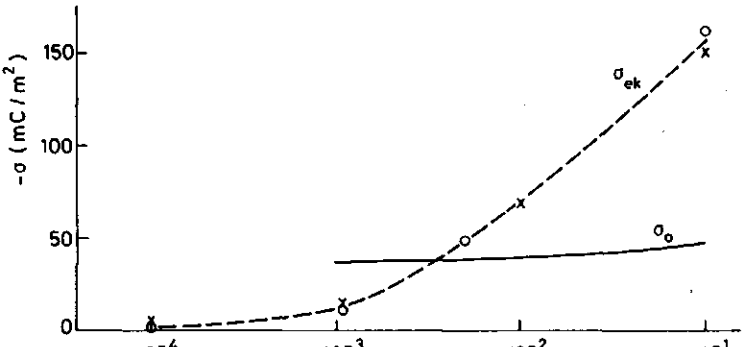

Fig. 7.6 - Electrokinetic (σ_{ek}, o = plug A, x = plug B) and surface charge density (σ_o, reference 1) as a function of ionic strength (KNO_3); pI = 4.

charge hardly depends on the KNO_3 concentration (1).

(ii) σ_{ek} decreases strongly with decreasing ionic strength, whereas σ_o remains comparatively constant.

These two features can be accounted for as follows.

ad (i). First of all it is emphasized that for these high salt concentrations the determination of ζ (and thus of σ_{ek}) is relatively straightforward. The applied experimental procedures guarantee a correct determination of the electrokinetic parameters. Furthermore, because of the high κa values (above 5×10^{-3} M $\kappa a > 650$), the conversion of these parameters into double layer characteristics is complicated neither by polarization and overlap of double layers nor by surface conduction. Doubt exists only about the use of bulk values for the permittivity ε and viscosity η in the Helmholtz-Smoluchowski equation. Particularly at high ionic strength the rather high ζ-potentials (Fig. 7.5, ζ = 110 mV at 10^{-1} M) are indicative of strong electrical fields in the diffuse double layer. These fields may orient the water molecules in the interfacial region, thereby decreasing ε (dielectric saturation) and increasing η (viscoelectric effect). The first attempt to account quantitatively for these phenomena was made by Lyklema and Overbeek (7). Their analysis shows that the H-S equation may require considerable corrections for the viscoelectric effect, whereas the influence of a variable ε is insignificant. The viscoelectric effect causes the effective shear plane to shift away from the surface, leading to a reduction of the observed ζ-potential (and electrokinetic charge density). Consequently, correcting the obtained zeta potentials for possible variations in η and ε within the electrical double layer would further enlarge the discrepancy between σ_{ek} and σ_o. Therefore the $\sigma_{ek} - \sigma_o$ inconsistency cannot be explained by effects of the double layer field on ε and η.

In passing it is noted, that for high surface potentials the Lyklema-Overbeek theory predicts ζ to become constant and independent of the diffuse double layer potential ψ_d. These limiting values amount to 76 mV at 10^{-2} M and 28 mV at 10^{-1} M. Comparison with the electrokinetic potentials of the silver iodide at corresponding concentrations and of polystyrene at 10^{-1} M (chapter 5) indicates that these authors overestimate the viscoelectric effect.

This is probably due to an improper choice of the viscoelectric constant.

It seems much more likely that the unrealistic σ_{ek}/σ_o ratio stems from uncertainties about the determination of the exact value of σ_o from potentiometric titrations. Whilst electrokinetic measurements render direct information on charge densities, from titrations only the amount of adsorbed potential determining ions per gram can be obtained. Conversion of this amount into a charge density requires the specific surface area of the silver iodide sample. Uncertainties exist as to this quantity, i.e. different methods of surface area determination give different results (4). More specifically, areas deduced from negative adsorption and capacitance measurements exceed those obtained by positive adsorption of several adsorbates or inferred from air permeability experiments by a factor of 3 to 3.5. No satisfactory physical explanation for this discrepancy has yet been offered. In calculating σ_o from titration data, the "capacitance area" is used. Adopting the "adsorption (permeability) area" would enlarge σ_o by a factor of 3 to 3.5. In that case σ_o would exceed σ_{ek} over the whole range of ionic strengths studied. Therefore it must be concluded that above 5×10^{-3} M electrokinetic and titration data are more compatible when the adsorption area is taken.

ad (ii). A decrease of ζ (and σ_{ek}) with decreasing electrolyte concentration has been found before, frequently because the effect of surface conductance had been ignored (e.g. 8). As noted in chapter 3, however, the contribution of surface conductance to the overall pore liquid conductance is accounted for in our experimental procedures. As another possibility the occurrence of double layer polarization under streaming current conditions has to be considered. When the hydrodynamic streamlines along the surface and the equipotential lines in the electrical double layer are not parallel, local polarization fields are induced, that counteract the convection current. The magnitude of this effect, for which no allowance is made in the H-S theory, can be assessed by means of the dimensionless parameter Rel (9).

$$Rel = [\exp(zF\psi_d/2RT) - 1]/\kappa a \qquad [7.3]$$

Identifying ψ_d with the ζ-potential, it appears that for all ionic strengths Rel << 1 (as a result of the large κa values). These small Rel values imply that the polarization effect on the streaming current can be neglected. Experimentally, this conclusion is supported by the coincidence of the ζ-log c curves of plugs A and B. If the polarization effect were significant, different ζ-potentials would have been obtained, since the two plugs have different pore sizes. Thus, all evidence taken together, the strong decrease of the electrokinetically displaceable charge density caused by decreasing the ionic strength seems to be well established. Since the surface charge density is much less dependent on ionic strength, it must be concluded that the effective shear plane shifts away from the silver iodide surface when the salt concentration decreases. This indicates the formation of immobilized layers close to the surface. Two possible mechanisms can be suggested to explain why this occurs, (i) retainment of water layers as a result of surface roughness and (ii) water structuring due to surface influences. However, in the former case one does not expect the ionic strength to control the location of the slipping plane. Moreover, K^+ as well as NO_3^- ions have a negative viscosity (Jones-Dole) coefficient (10), implying that both ions oppose structuring. This fits in with the break-down of the boundary layer upon increasing KNO_3 concentration. Therefore, water structuring seems to be most likely. In conclusion, the ionic strength dependence of the electrokinetic data reveals the presence of stagnant water layers at the surface of silver iodide particles. More experimental evidence in favour of this conclusion, which is contrary to current views (2), will be presented in section 7.3.2.3.

Fig. 7.7 shows surface conductivity data as obtained experimentally (κ_S^σ, dashed line) and as predicted theoretically for the layer beyond the slipping plane (κ_{ek}^σ, drawn line). The former results have been obtained from the electroconduction data presented in table 7.1 by means of the Street equation 4.13. The more sophisticated Bruggeman and Dukhin-Seminikhin conversion models are inapplicable, since silver iodide suspensions are neither homodisperse nor composed of spherical particles. The pore radius a in Street's equation has been calculated from permeability data (using

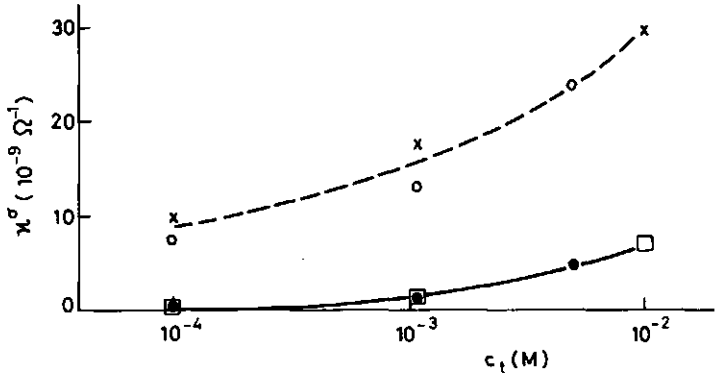

Fig. 7.7 - Experimental (Street, eq. 4.13; o = plug A, x = plug B) and theoretical (Bikerman, eq. 4.21; • = plug A, □ = plug B) values of the surface conductivity as a function of ionic strength (KNO_3); pI = 4.

eq. 7.2). For the experiments under consideration it amounted to 3.29 μm (plug A) and 2.54 μm (plug B). (During the experiment with plug B at $1.1x10^{-3}$ M, a was 2.44 μm). The κ^σ_{ek} data has been obtained from the extended Bikerman equation 4.21, substituting literature data (11) for the equivalent conductivities of the various counter- and coions. Fair agreement is observed between the experimentally obtained surface conductivities of the two plugs. These values are rather high in comparison with data obtained for other materials, such as glass (12), barium sulfate (13) and polystyrene (chapter 5). Moreover, the experimental values greatly exceed those calculated on the basis of Bikerman's theory. These discrepancies will be further analyzed in the discussion of the electrokinetic measurements at varying pAg (section 7.3.2.3).

7.3.2.2 INFLUENCE OF $TBuA^+$ ADSORPTION

The results of the $TBuA^+$ experiments enabled a more detailed analysis of the surface conductivity data obtained from the experiments at variable pAg and are therefore given priority.

Table 7.2 presents the electrokinetic data of plug B for

variable c_{TBuA^+} but fixed ionic strength (1.1×10^{-3} M) at pI = 4. This data has been converted into zeta potentials and surface conductivities according to the procedures described in the preceeding section. (For these experiments, C_p and a were 610 m^{-1} and 2.44 μm, respectively.) The results are shown in Figs. 7.8 and 7.9.

Table 7.2 - Electrokinetic data of plug B for various $TBuA^+$ concentrations, obtained from both I-V plots and streaming potential and d.c. conductance measurements (ΔP = 20 cm Hg); pI = 4, ionic strength = 1.1×10^{-3} M. Bulk conductivities are also included.

	I-V plot		Streaming potential method		Bulk conductivity
c_{TBuA^+}(M)	I_s(μA)	$K^{d.c.}$(Ω^{-1})	V_s(mV)	$K^{d.c.}$(Ω^{-1})	K_o(Ω^{-1} m^{-1})
0	-3.49	4.92×10^{-5}	-71.0	4.93×10^{-5}	1.57×10^{-2}
2.75×10^{-6}	-1.20	2.99×10^{-5}	-40.1	3.00×10^{-5}	1.58×10^{-2}
9.16×10^{-6}	-0.248	2.82×10^{-5}	- 8.80	2.76×10^{-5}	1.54×10^{-2}
1.40×10^{-5}	-	-	-	2.71×10^{-5}	1.54×10^{-2}
2.75×10^{-5}	+0.352	2.73×10^{-5}	+12.9	2.79×10^{-5}	1.55×10^{-2}
9.16×10^{-5}	+0.964	2.66×10^{-5}	+36.2	2.68×10^{-5}	1.52×10^{-2}
2.75×10^{-4}	+1.42	2.63×10^{-5}	+53.9	2.61×10^{-5}	1.40×10^{-2}
9.16×10^{-4}	+1.84	2.04×10^{-5}	+90.0	2.03×10^{-5}	9.71×10^{-3}

As to be expected, adsorption of $TBuA^+$ ions onto negatively charged silver iodide results in a decrease of ζ. At $pTBuA^+ = 4.85$, charge reversal occurs. From electrophoretic mobilities under comparable conditions, De Keizer (3) found the i.e.p. to be located at $pTBuA^+ = 5$. The electrophoresis measurements, however, are rather inaccurate, especially in the i.e.p. region, because of coagulation. Plug measurements, on the contrary, yield accurate data even at the i.e.p. as can be observed in Fig. 7.8. This is a definite advantage of the latter technique over electrophoresis.

The adsorption of $TBuA^+$ ions leads to a large reduction of the experimental surface conductance (Fig. 7.9). At the i.e.p. it is

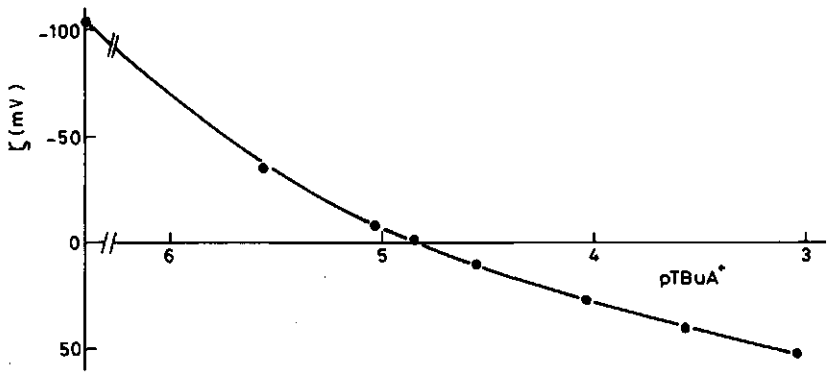

Fig. 7.8 - ζ-potential as a function of $TBuA^+$ concentration; pI = 4, ionic strength = 1.1×10^{-3} M.

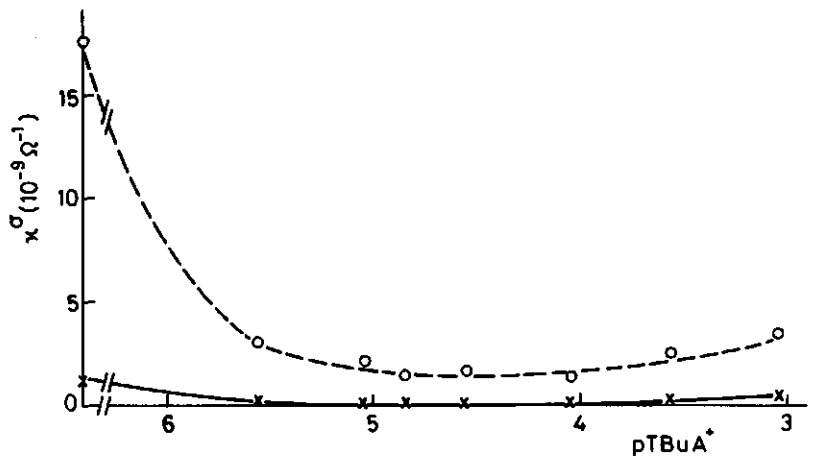

Fig. 7.9 - Experimental (o; Street, eq. 4.13) and theoretical (x; Bikerman, eq. 4.21) values of the surface conductivity as a function of $TBuA^+$ concentration; pI = 4, ionic strength = 1.1×10^{-3} M.

minimal but not zero. This feature can be attributed to either or both of two causes, conductance in the hydrodynamic immobile layer and conductance in the solid plug material. Obviously, in the latter case the term surface conductance would be incorrect. De-

cisive conclusions on this issue are obtained in the next section.

After performing the measurements at $pTBuA^+$ = 3.1, plug B was permeated with a 10^{-3} M KNO_3 solution (pI = 4) in order to desorb all $TBuA^+$ ions. Even after an almost 4000-fold displacement of the pore liquid, however, ζ and κ_S^σ still amounted to values (-73 mV and 12.4×10^{-9} Ω^{-1}, respectively) that deviate somewhat from those corresponding to the bare surface. These differences did not diminish upon another 300-fold volume displacement. Apparently, dilution can not cause $TBuA^+$ ions to desorb completely from silver iodide. In the $pTBuA^+$ range 3-5.6 no irreversibility of ζ and κ_S^σ with respect to the $TBuA^+$ concentration was observed.

7.3.2.3 INFLUENCE OF THE pAg

Electrokinetic data of plug A for various pAg values but constant KNO_3 concentration (10^{-3} M) is given in table 7.3. Converting these data into zeta potentials and surface conductivities, yields the results displayed in Figs. 7.10 and 7.11 (for these experiments C_p was 486 m^{-1} and a was 3.29 μm). The divergence of the results at pAg = 9.4 in both graphs is probably due to an erroneous assessment of the pAg of the pore liquid.

Table 7.3 - Electrokinetic data of plug A for various pAg values, obtained from both I-V plots and streaming potential and d.c. conductance measurements (ΔP = 20 cm Hg); KNO_3 concentration 10^{-3} M. Bulk conductivities are also included.

	I-V plot		Streaming potential method		Bulk conductivity
pAg	I_s (μA)	$K^{d.c.}$ (Ω^{-1})	V_s (mV)	$K^{d.c.}$ (Ω^{-1})	K_o (Ω^{-1} m^{-1})
4	+2.00	3.72×10^{-5}	+53.6	3.66×10^{-5}	1.54×10^{-2}
4.82	+0.598	3.29×10^{-5}	+18.9	3.30×10^{-5}	1.44×10^{-2}
5.92	-0.664	3.09×10^{-5}	-21.2	3.13×10^{-5}	1.43×10^{-2}
6.64	-1.73	3.12×10^{-5}	-55.0	3.17×10^{-5}	1.44×10^{-2}
9.40	-3.25	3.42×10^{-5}	-93.0	3.50×10^{-5}	1.43×10^{-2}
11.4	-4.33	4.41×10^{-5}	-98.0	4.39×10^{-5}	1.35×10^{-2}
12.3	-4.32	5.17×10^{-5}	-83.0	5.26×10^{-5}	1.56×10^{-2}

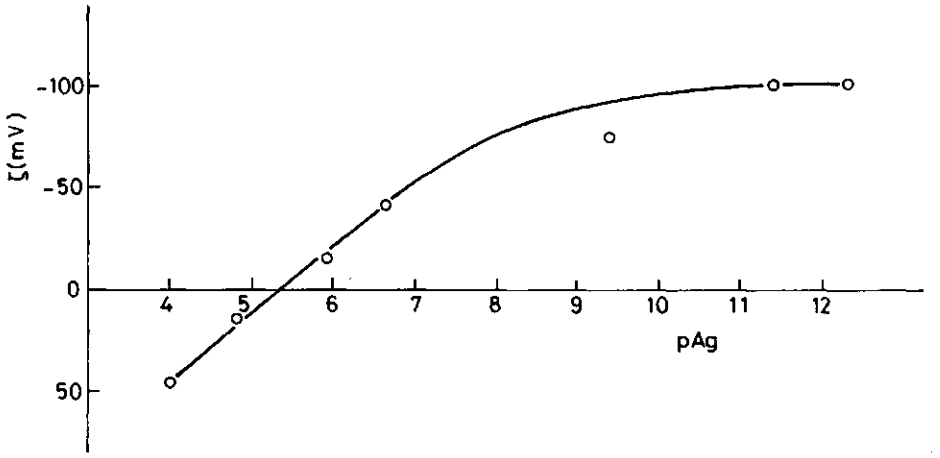

Fig. 7.10 - ζ-potential of plug A as a function of pAg; KNO_3 concentration = 10^{-3} M.

Fig. 7.10 shows that the i.e.p. is located at pAg = 5.35, in good agreement with the value of 5.34 that Bijsterbosch (14) obtained from streaming potential measurements. Using the electrophoresis technique, generally isoelectric points in the same pAg range are acquired (1). Around the i.e.p., the ζ-pAg curve is linear with a slope of 32 mV per pAg unit. Comparison with the streaming potential results of Bijsterbosch is not possible, since these have not been converted into zeta potentials. From electrophoresis, however, he obtained 104 mV/pAg for the slope at the i.e.p. (at 20 °C), which greatly exceeds the theoretical maximum value of 58.2 mV/pAg. The electrophoresis results of Troelstra (15) and, more recently, Billett et al. (16) show the same discrepancy. A satisfactory explanation for this observation has not yet been given and this feature has to be considered another drawback of electrophoresis compared with the streaming potential and streaming current methods.

In principle the slope of the ζ-pAg curve close to the i.e.p., $(d\zeta/dpAg)_{i.e.p.}$, provides information about the location of the

effective shear plane. According to Koopal and Lyklema (17) one can write

$$d\zeta/dpAg = (d\zeta/d\psi_d)(d\psi_d/d\sigma_d)(d\sigma_d/d\sigma_o)(d\sigma_o/dpAg) \qquad [7.4]$$

in which σ_d represents the charge density of the diffuse layer. The other symbols have their usual meaning. The first term at the right hand side can be obtained from the Poisson-Boltzmann equation for flat double layers ($\kappa a >> 1$). Close to the i.e.p. the Debye-Hückel approximation is allowed. Moreover, in that case specific adsorption can be neglected (1), so that $\sigma_d = -\sigma_o$ and consequently $(d\sigma_d/d\sigma_o) = -1$. By also remodelling the other terms (17), one arrives at

$$(d\zeta/dpAg)_{i.e.p.} = 59.1\ (C/C_d)\ \exp(-\kappa\Delta) \qquad [7.5]$$

where Δ denotes the distance between the outer Helmholtz ($\phi=\psi_d$) and the slipping plane ($\psi=\zeta$). C is the overall capacitance of the double layer, C_d the capacitance of the diffuse part. The latter can be computed from the Gouy-Chapman theory for flat double layers (eq. 3.7) and for a 10^{-3} M solution at the i.e.p. amounts to 67.2 mF/m^2. C is found experimentally, but, unfortunately, the obtained value depends on the choice of the specific surface area. Adopting the capacitance area, one obtains 53 mF/m^2 (4). Then, according to eq. 7.5, the experimentally observed slope of 32 mV would correspond to an effective thickness of 3.6 nm for the layer between Stern- and slipping plane. Using the adsorption area, C would be 3 to 3.5 times larger. Then, for Δ one obtains a value of about 15 nm. However, when the adsorption area is chosen, specific adsorption near the i.e.p. has to be assumed (18). In that case $|d\sigma_d/d\sigma_o|$ is less than one, so that Δ is overestimated when using eq. 7.5. Anyway, this analysis shows that the discrepancy between the experimental and theoretical value of $(d\zeta/dpAg)_{i.e.p.}$ might be explained by the presence of a stagnant water layer at the silver iodide surface.

Additional information about the stagnant layer is obtained from the plateau value, at which ζ levels off at high pAg

(Fig. 7.10). Constancy of ζ upon increasing surface potential may result from the viscoelectric effect as well as from the presence of an adhering layer (due to structural influences of the surface) (7). In the former case the Lyklema-Overbeek (L-O) theory predicts a limiting zeta potential of about 130 mV (at 10^{-3} M), a value that exceeds the experimentally observed one. Since, moreover, indications exist that the L-O theory overestimates the viscoelectric effect (see section 7.3.2.1), it may be concluded that the constancy of ζ mainly stems from the presence of a layer of water molecules immobilized by structural influences of the surface. Viscoelectric effects play only a secondary role.

The Gouy-Chapman theory can be used to assess the thickness Δ of this stagnant layer from the limiting value of ζ. For flat double layers this theory relates ψ_d, ζ and Δ in the following way

$$\tanh(zF\zeta/4RT) = \tanh(zF\psi_d/4RT)\ \exp(-\kappa\Delta) \qquad [7.6]$$

In the absence of specific adsorption, ψ_d can be calculated from the data on σ_o presented in reference 1 by means of eq. 4.10. Adopting the adsorption area, in the region where ζ approaches a constant value ψ_d exceeds 200 mV. Then we may approximate

$$\tanh(zF\zeta/4RT) = \exp(-\kappa\Delta) \qquad [7.7]$$

Substituting the observed limiting value of ζ (101 mV), for Δ one obtains 2.7 nm. When specific adsorption occurs and/or when the capacitance area is chosen, for Δ a lower value is found.

In conclusion, the plateau in the ζ-pAg curve might also be accounted for by assuming the silver iodide surface to be covered with an immobilized layer. A quantitative estimate of the layer thickness from the limiting value of ζ as well as from the slope of the ζ-pAg curve near the i.e.p. awaits elucidation of the inconsistencies in the specific surface area and of the uncertainties about the extent of specific adsorption. In this connection, it may be worth-while considering possible effects of the stagnant water layer itself. More specifically, the high degree of ordening of the molecules could lower the permittivity. As a result, the specific area deduced from capacitance data would be overestimated.

Fig. 7.11 (dotted line) shows that surface conductance takes place at all pAg values. It increases with increasing charge density on the silver iodide. Surprisingly, the minimum in the κ_S^σ-pAg curve does not coincide with the i.e.p.. This is possibly due to small differences between the i.e.p. and point of zero charge. Another striking feature is that surface conductance occurs at the

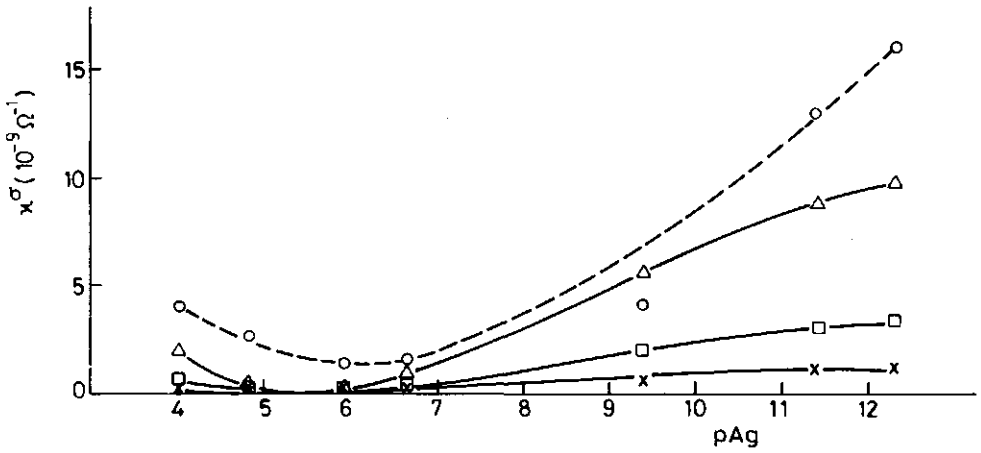

Fig. 7.11 - Experimental (o; Street, eq. 4.13) and theoretical (x = without anomalous conduction (eq. 4.21); □, Δ = including anomalous conduction (eq. 4.23), adopting the capacitance and adsorption surface area, respectively) values of the surface conductivity as a function of pAg; KNO_3 concentration = 10^{-3} M.

i.e.p., a phenomenon also noticed by Bijsterbosch (14). The following observations indicate that this excess conductance, as well as that observed at the i.e.p. of the $TBuA^+$-silver iodide system (section 7.3.2.2), stems from conductance within the solid silver iodide itself and not from tangential ionic transfer through the fixed layer near the wall

(i) at the i.e.p. of the $TBuA^+$-polystyrene system no anomalous conduction occurs in the fixed layer (chapter 6).

(ii) The excess conductances at the two i.e.p.'s (Figs. 7.9 and 7.11) are in close agreement. This correspondence is not to be expected when the conductance in the fixed layer contri-

butes significantly, since the composition of this layer strongly differs for the two i.e.p.'s.

(iii) Assessing the conductivity of silver iodide K_{AgI} from the excess conductances at the i.e.p., leads to values that are in reasonable accord with literature data. This can be illustrated as follows: assuming the electrical currents in the solid matrix and the pore liquid to be independent, and neglecting the tortuosity of the electrical streamlines, K_{AgI} can be obtained from the plug conductance at the i.e.p. $K_{i.e.p.}$ according to

$$K_{AgI} = (K_{i.e.p.} - K_o/C_p)\ (L/pA) \qquad [7.8]$$

Substituting the experimental values obtained with plug A at pAg = 5.92 (table 7.3) and with plug B at $pTBuA^+$ = 4.85 (table 7.2), one finds 8.3×10^{-4} and 7.5×10^{-4} Ω^{-1} m^{-1}, respectively. These values are in the order of those found in direct measurements (10^{-3} Ω^{-1} m^{-1} (19)).

It is emphasized that the slight conductance in the solid phase does not invalidate the inferred ζ-potentials. The extrapolation method enables determination of the streaming current under conditions of zero potential and, consequently, zero conductance. In addition, at 10^{-1} M the solid phase contribution to the overall conductance is only about 0.1 percent, so that its influence on the determination of the conductometric cell constant can be neglected.

The surface conductivity results presented in Figs. 7.7, 7.9 and 7.11 can be corrected for the conductivity of the silver iodide, by subtracting the value at the i.e.p. from all data. It can easily be seen that (except near the i.e.p.) all adjusted data still exceed the Bikerman predictions. This indicates conductance to take place behind the slipping plane, a phenomenon also observed for the polystyrene-solution interface (chapter 5). The contribution of anomalous conductance can be included in the theoretical predictions by means of the modified Bikerman equation 4.23. This has been done for the experiments at varying pAg. The required ψ_d values have been derived from the σ_o(pAg) curves in reference 1, using the $\sigma(\psi)$ relation for flat double layers (eq. 4.10) and

neglecting specific adsorption. In calculating ψ_d both the capacitance and the adsorption area (i.e. 3 times the capacitance surface area) have been considered. Assuming that the equivalent conductivities of the ions within as well as beyond the shear plane are identical to those in the bulk, the upper and middle drawn line in Fig. 7.11 were obtained on the basis of the adsorption and capacitance area, respectively. Despite the incorporation of anomalous conductance, the Bikerman theory still predicts surface conductivities far below the experimental ones when the capacitance surface area is chosen. When, on the contrary, the adsorption area is adopted the experimental and theoretical curves are in fair agreement. Irrespective of the choice of the specific surface area, however, it can be concluded that anomalous conductance occurs, which can be considered another proof of the presence of a specially structured layer at the silver iodide-solution interface.

7.3.3 CONDUCTANCE-FREQUENCY CHARACTERISTICS

For all electrolytes studied, the conductance of the silver iodide plug showed a frequency dependence towards the low frequency range. To illustrate this phenomenon, conductance-frequency spectra

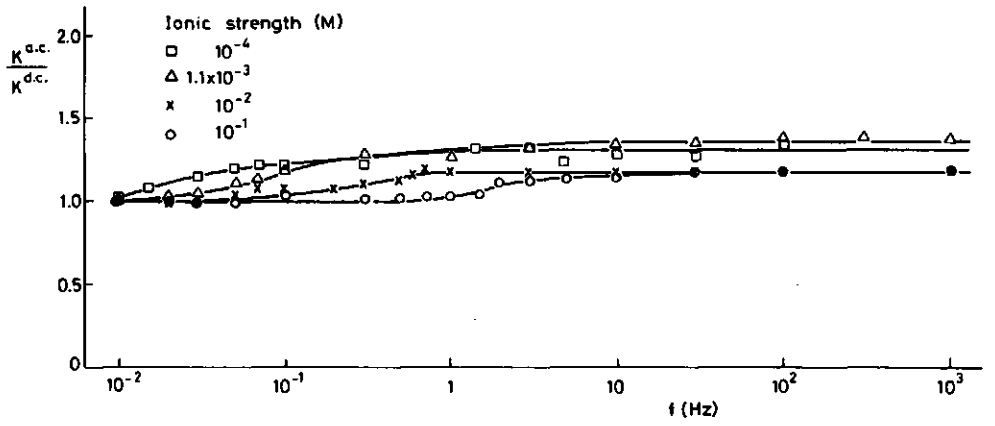

Fig. 7.12 - Dependence of the reduced plug conductance upon frequency for various ionic strengths; pI = 4.

of plug B for various ionic strengths at pI = 4 are shown in Fig. 7.12. Again the reduced cell conductance has been plotted ($K^{a.c.}/K^{d.c.}$). For electrolyte concentrations above 10^{-2} M the increment is independent of ionic strength and amounts to about 1.2. Identical results have been obtained for polystyrene, where these dispersions were shown to be related to polarization processes taking place at the electrodes (section 5.3.1.3). A similar situation will exist for silver iodide plugs above 10^{-2} M. For values of the ionic strength below 10^{-2} M, a small but significant increase of the increment is observed. This points to the occurrence of polarization phenomena in the silver iodide plug itself. However, these intrinsic processes are much less pronounced than those observed in polystyrene plugs (compare Figs. 5.8 and 7.12). The same conclusion was also arrived at on the basis of the I-V plots (section 7.3.2). No clear trend of the increment with respect to pAg and $TBuA^+$ concentration could be observed, which is also in accord with the conclusions drawn from the I-V plots.

No inference can be drawn as to the origin of the intrinsic processes.

7.4 CONCLUDING REMARKS

The results of this study demonstrate the general applicability of the electrokinetic techniques described in chapter 3. Compared with electrophoresis, these techniques yield considerably more accurate data, especially near the i.e.p.

The results obtained contribute to the elucidation of the interfacial properties of silver iodide. They indicate that the specific surface area obtained from the double layer capacitance near the point of zero charge at 10^{-3} M is incorrect. Furthermore, this study reveals the existence of a stagnant water layer on the silver iodide surface, implying ψ_d and ζ not to be identical. The thickness of this layer increases with decreasing ionic strength.

Despite the inferences made, it is felt that the silver iodide system should be subjected to further electrokinetic study before more general conclusions can be drawn. In particular, the determination of ζ-pAg curves at other salt concentrations is desirable.

Furthermore, the effect of temperature and of the age of the silver iodide sample (a gradual reduction of the slope of the mobility-pAg curve upon aging has been reported (20), indicating an outward shift of the shear plane) on the stagnant layer should be investigated.

Most importantly, the employed electrokinetic techniques may contribute to the solution of the ψ_d-ζ problem (2) for this colloidal system and also for other ones.

7.5 REFERENCES

1. Bijsterbosch, B.H. and Lyklema, J., Adv. Colloid Interface Sci. 9, 147 (1978).
2. Lyklema, J., J. Colloid Interface Sci. 58, 242 (1977).
3. De Keizer, A., Thesis, Agricultural University, Wageningen (1981).
4. Van den Hul, H.J., Thesis, State University, Utrecht (1966).
5. Bear, J., "Dynamics of Fluids in Porous Media", Elsevier, Amsterdam, 1972.
6. De Keizer, A., personal communication.
7. Lyklema, J. and Overbeek, J.Th.G., J. Colloid Sci. 16, 501 (1961).
8. Dukhin, S.S. and Derjaguin, B.V. in "Surface and Colloid Science" (E. Matijević, Ed.), Vol. 7, p. 145, Wiley, New York, 1974.
9. Reference 8, chapter 1.
10. Millero, F.J. in "Water and Aqueous Solutions" (R.A. Horne, Ed.), p. 545, Wiley, New York, 1972.
11. Parsons, R., "Handbook of Electrochemical Constants", Butterworths, London, 1959.
12. Jednacak-Biśćan, J., Mikac-Dadić, V., Pravdić, V. and Haller, W., J. Colloid Interface Sci. 70, 18 (1979).
13. Fridrikhsberg, D.A. and Barkovskii, V.Ya., Kolloidn. Zh. 26, 617 (1964).
14. Bijsterbosch, B.H., Thesis, State University, Utrecht (1965).
15. Troelstra, S.A., Thesis, State University, Utrecht (1941).
16. Billett, D.F., Hough, D.B. and Ottewill, R.H., J. Electroanal. Chem. 74, 107 (1976).

17. Koopal, L.K. and Lyklema, J., Faraday Discuss. Chem. Soc. 59, 230 (1975).
18. Van der Schee, H.A., Thesis, Agricultural University, Wageningen (1984).
19. Pieper, J.H.A. and de Vooys, D.A., J. Electroanal. Chem. 53, 243 (1974).
20. Ottewill, R.H. and Woodbridge, J., J. Colloid Sci. 19, 606 (1964).

LIST OF SYMBOLS

a	capillary radius
A	cross-sectional area of the plug
c	electrolyte concentration
c_t	ionic strength
C	overall capacitance of the double layer
C_d, C_s	capacitance of the diffuse double layer and of the Stern layer, respectively
C_i	input capacitance of measuring device
C_p, C_r	cell constant of the plug and plugholder, respectively
d	particle diameter
e	elementary charge
f	frequency of the applied field
f_d	dispersion frequency
F	Faraday constant
G	correction factor to the Helmholtz-Smoluchowski equation
$I(i,j)$	electrical current through the electrodes i and j
I_s	streaming current
J_v	volume flow rate
k	Boltzmann constant
K	conductance of the porous medium
$K^{d.c.}$, $K^{a.c.}$	conductance (admittance) at d.c. and a.c. conditions, respectively
K_o	conductivity of the bulk solution
K	conductivity of the dispersion
L	length of the plug
p	volume fraction of dispersed material
pX	negative logarithm of concentration of X
ΔP	hydrostatic pressure difference
r	radial distance from the axis
$\tilde{r}$	idem, in dimensionless form ($= \kappa r$)
R	gasconstant
R_i	input resistance of measuring device
R_p	resistance of the plug
S	overall surface area of the dispersed medium
t	time

T	absolute temperature
V	overall plug volume
$V(i,j)$	potential difference between electrode i and j
V_s	streaming potential
z	valency
Z	impedance
Γ	adsorbed amount
Δ	distance between the Outer Helmholtz Plane and the slipping plane
ε	dielectric permittivity
ζ	potential at the slipping plane
$\tilde{\zeta}$	idem, in dimensionless form (= $e\zeta/kT$)
η	viscosity of the solution
κ	reciprocal thickness of the double layer
κ^{σ}	surface conductivity
κ^{σ}_{ek}	surface conductivity beyond the slipping plane
κ^{σ}_{B}, κ^{σ}_{S}	surface conductivity calculated according to the Bruggeman and Street model, respectively
λ_c, λ_t	equivalent conductivity of co- and counterions, respectively
μ	dipole moment
ρ	density
σ_o	surface charge density
σ_{ek}	electrokinetic charge density
$\psi(r)$	double layer potential at r
ψ_d	potential at the boundary of the diffuse double layer

ABSTRACT

This thesis describes an experimental study on the electrokinetic and electrical properties of concentrated polystyrene and silver iodide dispersions. The purpose of the study is to obtain information on the structure of the electrical double layer at the solid-liquid interface. Special attention is paid to the various polarization phenomena that may interfere in electrokinetic and conductance measurements on condensed systems.

After a general introduction in chapter 1, in chapter 2 we discuss the preparation and characterization of the polystyrene latices. The geometry of these colloids is well-defined and easy to control, their surface properties, on the contrary, are not. The number and nature of the surface groups may change upon characterization, due to contact with a solution of high ionic strength as well as during storage. In order to preclude any effect of these phenomena on the electrokinetic experiments, after preparation the latices have been treated in a special way.

In chapter 3 the afore-mentioned polarization phenomena are studied with a four-electrode cell. The characteristics of this cell are investigated for both reversible and irreversible electrodes. In both cases electrode polarization phenomena considerably interfere with the streaming current measurements. Particularly disturbing are the polarizations that occur in the dispersed medium itself. The four-electrode method, however, enables correction for both forms of polarization. As a result, the electrokinetic data thus obtained are independent of the material of the measuring electrodes. When using reversible electrodes, another complication can be that electrolysis processes at the current-carrying electrodes disturb the system under investigation. When irreversible (platinum black) electrodes are incorporated in the cell, such processes do not occur. Another important advantage of the latter electrodes is that the four-electrode method is then most accurate and, moreover, generally applicable. Two independent experimental procedures (streaming potential and streaming current method) yield identical results, confirming the reliability of the four-electrode technique.

Chapter 4 deals with the choice of the theoretical models that

have been applied to infer double layer parameters from electrokinetic and conductance data. Zeta potentials are calculated by means of capillary models. In these the effect of double layer interaction has been taken into account, but not that of polarization of the double layer. For the inference of surface conductivities both capillary and cell models are considered. The latter take account of double layer and concentration polarization. The chapter concludes with a theoretical consideration of the relation between zeta potential and surface conductivity.

In chapter 5 the electrokinetic techniques described in chapter 3 are applied to polystyrene plugs. The results show the slipping plane to shift away from the solid surface upon decreasing the ionic strength. Considerable conductance takes place in the corresponding fixed layer. The relaxation phenomena, observed in the streaming current measurements, are also studied by measuring frequency-spectra of the plug conductance. In the low-frequency range dispersions occur, being the more pronounced the lower the salt concentration. At high salt concentrations the dispersions probably stem from processes taking place at the measuring electrodes. Below concentrations of 10^{-2} M relaxation processes in the plug itself contribute increasingly to the dispersions. These intrinsic processes as well as the electrokinetic data are accounted for by assuming the surface layer of polystyrene particles to consist of protruding, partly mobile polymer chains. The thickness of this "hairy" layer and, consequently, the position of the shear plane is controlled by the salt concentration.

In chapter 6 the techniques developed are used to investigate the influence of adsorbed charged species (tetraalkylammonium (TAA^+) ions) on the structure of the polystyrene-solution interface. To this end, adsorption isotherms are also determined. When the surface is (partially) covered with TAA^+ ions, the position of the slipping plane is independent of ionic strength. Between this plane and the solid surface under these circumstances only very little or no conductance takes place any more. The polarization phenomena in the plug practically disappear when TAA^+ ions adsorb. The conclusion is that TAA^+ adsorption largely eliminates the hairiness of the polystyrene particles.

Chapter 7 describes the measurements on silver iodide plugs.

These have been performed as a function of ionic strength and surface potential. Intrinsic polarizations do also occur in plugs of this material, but they are much less pronounced than those observed in polystyrene plugs. No satisfactory explanation for these polarization phenomena can be offered. The experiments reveal a number of peculiar features. For high salt concentrations the electrokinetically displaceable charge density considerably exceeds the surface charge densities reported in literature. This inconsistency is ascribed to the fact that the latter data is based on an improper value of the specific surface area. Upon decreasing the ionic strength, for this system the slipping plane also shifts outwardly. This phenomenon is interpreted in terms of water structuring due to influences of the silver iodide surface. The concept of a stagnant layer can also account for the results obtained at variable surface potential. Procedures to calculate the thickness of the adhering layer are indicated, but definite conclusions cannot be drawn, because of uncertainties as to the extent of specific adsorption. The layer behind the slipping plane substantially contributes to the conductance of the system. To a small extent this stems from ionic transfer in the solid phase.

It can be concluded that the electrokinetic and electrical techniques described in this thesis are useful tools to obtain insight into double layer structures. They have provided detailed information on the structure of the interface in aqueous polystyrene and silver iodide dispersions.

SAMENVATTING

Dit proefschrift beschrijft een experimenteel onderzoek naar de elektrokinetische eigenschappen en de elektrische geleiding van polystyreen- en zilverjodideproppen. Het onderzoek is erop gericht informatie te verkrijgen over de structuur van de elektrische dubbellaag aan het grensvlak tussen de vloeibare en vaste fase. Speciale aandacht wordt besteed aan de diverse polarisatieverschijnselen die elektrokinetische metingen aan geconcentreerde systemen kunnen verstoren.

De elektrokinetiek behandelt de verschijnselen die optreden wanneer twee fasen, op het grensvlak waarvan zich elektrische ladingen bevinden, ten opzichte van elkaar verplaatst worden. Doorgaans is één van deze fasen een vloeistof en de andere een vaste stof. De verplaatsing kan of door een elektrische of door een mechanische kracht teweeg gebracht worden. Een voorbeeld van de eerste soort is elektroforese, waarbij geladen deeltjes onder invloed van een aangelegd elektrisch veld door een vloeistof bewegen. Een voorbeeld van de tweede is de stromingspotentiaal die ontstaat wanneer een vloeistof ten gevolge van een drukverschil door een geladen capillair of poreus medium, zoals de bodem, geperst wordt.

Elektrokinetische technieken worden vaak gebruikt om informatie te verkrijgen over kolloidale dispersies. Dergelijke dispersies bestaan uit vloeibare of vaste deeltjes, meestal kleiner dan een duizendste van een millimeter, die homogeen over een vloeistof zijn verdeeld. Veel natuurlijke (melk, rubber) en industriële (verf, geneesmiddelen) produkten zijn kolloidale dispersies. Meestal zijn de deeltjes elektrisch geladen. Aan de hand van elektrokinetische verschijnselen kan men zich een beeld van de ladingstoestand vormen. Bepalend voor deze verschijnselen is de elektrische potentiaal, de zeta potentiaal, in het zogenaamde afschuifvlak. Dit is het denkbeeldige scheidingsvlak tussen de vloeistof die onbeweeglijk aan de vaste stof is gehecht en de vloeistof die vrij kan stromen. De literatuur overziende, blijken er grote onzekerheden te bestaan omtrent de ligging van dit afschuifvlak en daarmee over de betekenis van de zeta potentiaal. Het feit dat veel studies zijn uitgevoerd met slecht gedefinieerde systemen of onjuiste meettechnieken heeft

aan deze verwarring bijgedragen.

In dit proefschrift wordt een techniek beschreven, die het mogelijk maakt om te corrigeren voor de diverse polarisatieverschijnselen die optreden tijdens elektrokinetische metingen aan geconcentreerde systemen. Deze techniek wordt vervolgens toegepast op twee in de kolloidchemie veel gebruikte modelsystemen: polystyreen en zilverjodide.

Na een algemene inleiding in hoofdstuk 1, wordt in hoofdstuk 2 de bereiding en karakterisering van polystyreen latices besproken. De geometrie van deze kolloiden is goed gedefinieerd en hun afmetingen zijn eenvoudig in de hand te houden. Dit geldt niet voor de eigenschappen van het deeltjesoppervlak. Aantal en aard van de oppervlaktegroepen kunnen veranderen als gevolg van de karakterisering en als gevolg van contact met een oplossing met een hoge zoutconcentratie. Ook tijdens de bewaring kunnen dergelijke veranderingen optreden. Om dit soort invloeden op de elektrokinetische experimenten uit te sluiten, zijn de latices na hun bereiding op een speciale manier behandeld.

In hoofdstuk 3 worden de eerder genoemde polarisatieverschijnselen bestudeerd met behulp van een vier-elektroden cel. De karakteristieken van deze cel worden zowel voor reversibele als irreversibele elektroden onderzocht. In beide gevallen interfereren polarisatieprocessen aan de meetelektroden sterk met de stromingsstroommetingen. Bijzonder verstorend zijn de polarisaties die in de prop zelf kunnen optreden. De vier-elektroden techniek maakt het mogelijk om voor beide vormen van polarisatie te corrigeren. De aldus verkregen elektrokinetische gegevens zijn dan ook onafhankelijk van het type elektrode. Als gebruik wordt gemaakt van reversibele elektroden kan een extra complicatie optreden, namelijk dat elektrolyseprocessen aan de stroomvoerende elektroden het onderzochte systeem beïnvloeden. Worden irreversibele (platina zwart) elektroden gebruikt dan treden dergelijke processen niet op. Een ander belangrijk voordeel van deze elektroden is dat de vier-elektroden techniek dan zeer nauwkeurig en bovendien algemeen toepasbaar is. Twee onafhankelijke experimentele procedures (stromingspotentiaal- en stromingsstroommethode) leveren identieke resultaten, hetgeen de betrouwbaarheid van de vier-elektroden techniek onderstreept.

Hoofdstuk 4 behandelt de keuze van de theoretische modellen die zijn gebruikt om uit elektrokinetische gegevens de dubbellaag parameters te berekenen. Zeta potentialen zijn berekend met behulp van capillairmodellen. Het effect van dubbellaagoverlap is hierin in rekening gebracht, dat van polarisatie van de dubbellaag echter niet. Voor de berekening van de oppervlaktegeleiding zijn zowel capillair- als celmodellen in beschouwing genomen. In laatstgenoemde modellen is het effect van verschillende vormen van polarisatie verdisconteerd. Het hoofdstuk sluit af met een theoretische beschouwing van het verband tussen de zeta potentiaal en de oppervlaktegeleiding.

In hoofdstuk 5 worden de in hoofdstuk 3 beschreven elektrokinetische technieken toegepast op polystyreenproppen. De resultaten duiden erop dat het afschuifvlak verder van de vaste wand komt te liggen naarmate de zoutconcentratie daalt. Achter het afschuifvlak treedt aanzienlijke geleiding op. De relaxatieverschijnselen, die bij de stromingsstroommetingen werden waargenomen, worden tevens bestudeerd door frequentie-spectra van het geleidingsvermogen van de prop te meten. In het laag-frequente gebied treden dispersies op, die meer uitgesproken zijn naarmate de zoutconcentratie lager is. Bij hoge zoutconcentraties zijn de dispersies waarschijnlijk het gevolg van processen die aan de meetelektroden plaatsvinden. Beneden concentraties van 10^{-2} M dragen relaxatieprocessen in de prop zelf in toenemende mate aan de dispersies bij. Zowel deze intrinsieke processen als de elektrokinetische gegevens worden verklaard door aan te nemen dat de oppervlaktelaag van polystyreendeeltjes bestaat uit in het water uitstekende, gedeeltelijk beweeglijke polymeerketens. De dikte van deze "harige" laag, en daarmee de plaats van het afschuifvlak, wordt gecontroleerd door de zoutconcentratie.

In hoofdstuk 6 worden de ontwikkelde technieken gebruikt om de invloed van geadsorbeerde geladen stoffen (tetraalkylammonium (TAA^+) ionen) op de structuur van het polystyreen-water grensvlak te onderzoeken. Daartoe worden ook adsorptie-isothermen gemeten. Als het oppervlak (gedeeltelijk) met TAA^+ ionen is bedekt, is de plaats van het afschuifvlak onafhankelijk van de zoutconcentratie. Tussen dit vlak en de wand treedt dan ook nauwelijks of geen geleiding meer op. De polarisatieverschijnselen in de prop verdwijnen

nagenoeg door de adsorptie. Geconcludeerd wordt dat de adsorptie van TAA^+ ionen het harige karakter van het polystyreenoppervlak grotendeels teniet doet.

Hoofdstuk 7 beschrijft de experimenten met de zilverjodideproppen. Deze zijn uitgevoerd als functie van de zoutconcentratie en van de wandpotentiaal. Ook in deze proppen treden intrinsieke polarisaties op, maar deze zijn veel minder uitgesproken dan die welke in de polystyreenproppen werden waargenomen. Voor deze polarisatieverschijnselen kan geen bevredigende verklaring worden gegeven. De experimenten onthullen verder een aantal opmerkelijke feiten. Bij hoge zoutconcentraties is de elektrokinetische lading veel groter dan de in de literatuur vermelde wandlading. Deze inconsistentie wordt toegeschreven aan het feit dat laatstgenoemde gegevens gebaseerd zijn op een onjuiste waarde voor het specifiek oppervlak. Als de zoutconcentratie daalt, verplaatst ook in dit systeem het afschuifvlak zich naar buiten. Dit verschijnsel wordt verklaard in termen van waterstructurering onder invloed van het zilverjodide oppervlak. Het idee van een aanhangende waterlaag kan ook de resultaten van de experimenten bij variërende wandpotentiaal verklaren. Procedures om de dikte van deze laag te berekenen worden aangegeven, maar verregaande conclusies kunnen niet getrokken worden, vanwege de onzekerheden in de mate van specifieke adsorptie. De vaste laag achter het afschuifvlak levert een aanzienlijke bijdrage aan de geleiding van het systeem. Voor een klein deel vindt dit zijn oorsprong in geleiding in de vaste fase.

Geconcludeerd kan worden dat de in dit proefschrift beschreven elektrokinetische en elektrische technieken nuttige instrumenten zijn om inzicht in dubbellaagstructuren te verkrijgen. Ze hebben gedetailleerde informatie opgeleverd over de structuur van het vast-vloeistofgrensvlak in waterige polystyreen en zilverjodide dispersies.

CURRICULUM VITAE

Op 2 januari 1952 ben ik geboren te Eemnes, waar ik ook opgroeide. In 1970 behaalde ik het diploma Gymnasium β aan het "Alberthinck Thym" College te Hilversum. In hetzelfde jaar begon ik mijn scheikundestudie aan de Rijksuniversiteit van Utrecht. Het kandidaatsexamen S_3 (scheikunde en natuurkunde met wiskunde) werd in november 1973 afgelegd. Het doctoraalexamen, met als hoofdvak fysische en kolloïdchemie en als bijvak bedrijfskunde (Technische Hogeschool te Eindhoven), volgde in januari 1977. In deze periode werd ook de onderwijsbevoegdheid scheikunde behaald. Na het vervullen van de militaire dienstplicht was ik van januari 1978 tot en met december 1981 in dienst van de Landbouwhogeschool als medewerker van de vakgroep Fysische en Kolloïdchemie. Tijdens dit dienstverband werd, naast onderwijskundige taken, het in dit proefschrift beschreven onderzoek uitgevoerd. Sinds januari 1982 werk ik bij de Hoofdafdeling "Speurwerk" van het Keuringsinstituut voor Waterleidingartikelen, KIWA N.V., te Nieuwegein.

NAWOORD

Aan het eind van dit proefschrift bedank ik iedereen, die het tot stand komen ervan mede mogelijk heeft gemaakt. Enkelen wil ik hier noemen.

In de eerste plaats mijn ouders, die mij de gelegenheid geboden hebben te studeren. Elly, jouw belangstelling en steun zijn, met name in de periode dat het schrijven van dit proefschrift met een nieuwe baan gecombineerd moest worden, voor mij zeer waardevol geweest.

Bert Bijsterbosch, jou als promotor dank ik voor de verhelderende discussies over de resultaten van dit onderzoek en voor de kritische nauwgezetheid en de snelheid waarmee je het manuscript gecorrigeerd hebt. Ik bewaar plezierige herinneringen aan onze werkbesprekingen.

Arie de Keizer en Herman van Leeuwen, de nuttige discussies tijdens de uitvoering van dit onderzoek en jullie kritisch commentaar op delen van dit proefschrift heb ik zeer op prijs gesteld.

Maarten Bakkenes bedank ik voor de volharding, waarmee hij de polystyreen latices heeft gezuiverd en gekarakteriseerd en voor de nauwkeurigheid waarmee hij de adsorptiemetingen heeft uitgevoerd. Dank ook aan Hennie van Beek en Ronald Wegh voor de onmisbare technische hulp bij de propmetingen en aan Gert Buurman voor de creatieve wijze waarop hij de figuren heeft getekend.

Ik realiseer me dat, behalve de hulp van bovengenoemde personen, ook de prettige sfeer op de vakgroep Fysische en Kolloïdchemie voor mij een belangrijke stimulans is geweest.

Hulp heb ik ook van personen van buiten deze vakgroep gekregen. De heer Elerie van de Technische en Fysische Dienst voor de Landbouw heeft op kundige wijze de elektronenmicroscopie-opnamen gemaakt.

De afdeling Tekstverwerking van het Keuringsinstituut voor Waterleidingartikelen, KIWA N.V., in het bijzonder Yvonne van der Leeden, heeft op voortreffelijke wijze het typewerk verzorgd. Voor deze en ook andere dienstverleningen tijdens de afronding van dit proefschrift ben ik de directie van het KIWA zeer erkentelijk.

Ian Cunningham heeft met veel gevoel voor humor de engelse tekst gecorrigeerd.